17140 S. Avalon Blvd.
Carson, CA 90746

310-217-2411
www.westbasin.org

December 21, 2021

Mr. Warren Teitz
Metropolitan Water District
P.O. Box 54153
Los Angeles, CA 90054-0153

Subject: Final Report

Dear Mr. Warren Teitz,

Enclosed is West Basin Municipal Water District's (West Basin) Final report as required under the Future Supply Actions Program. I am informed and believe that the information contained in this report is true and that the supporting data is accurate and complete.

The submittal report includes a general overview of West Basin's project, results of the study, as well as a summary budget cost and schedule as outlined in the agreement.

Attachments

1. Attachment A: West Basin Final Report
2. Attachment B: Summary Budget Cost of the Study and Schedule Information

Should you have any questions or concerns, please do not hesitate to reach out to me at (562) 505-7541 or at alejandrac@westbasin.org.

Sincerely,

Alejandra Cano
Study Manager

Attachment A

Prepared for:

West Basin Municipal Water District
17140 South Avalon Blvd
Carson, CA 90746

Development of an Approach for the Evaluation of Brine Diffuser Shear Mortality

Al Preston, Ph.D., P.E. (CA)
December 20, 2021

Prepared by:

Al Preston, Ph.D., Geosyntec Consultants, Inc.
Mine Berg, Ph.D., Environmental Science Associates
Philip Roberts, Ph.D., Consultant
Brian Gaylord, Ph.D., Consultant
Alex Wesner, SPI Engineering
Eric Zigas, Environmental Science Associates

Geosyntec Project Number: LA0587

December 2021

ACKNOWLEDGEMENTS

This research was sponsored by Metropolitan Water District under the Future Supply Actions and the Desalination and Water Purification Research and Development Program, Bureau of Reclamation.

The authors acknowledge Alejandra Cano of West Basin Municipal Water District for managing the project, coordinating with Metropolitan Water District and Bureau of Reclamation, and extensive review of the work and reports. Additionally, we acknowledge both Veronica Govea and Uzi Daniels of West Basin Municipal Water District for providing internal review. The Project Team is immensely grateful to Daniel Ellis and Leslie Hart of the State Water Resource Control Board for providing review and perspective from a regulatory view and contributing to numerous virtual meetings with the team.

Although this was a joint report with input and review by the entire team, it is noted that Mine Berg of Environmental Science Associates was lead author for Chapters 2 and 5 and Al Preston of Geosyntec Consultants was the lead author for Chapters 3 and 4. Al Preston acknowledges Jai Panthail and Rica Enriquez of Geosyntec Consultants for performing the computational fluid dynamics and visualization/post-processing, respectively.

TABLE OF CONTENTS

TABLE OF CONTENTS (Continued)

Page

TABLE OF CONTENTS (Continued)

Page

TABLE OF CONTENTS (Continued)

LIST OF TABLES

TABLE OF CONTENTS (Continued)

LIST OF FIGURES

TABLE OF CONTENTS (Continued)

TABLE OF CONTENTS (Continued)

LIST OF APPENDICES

ACRONYMS AND ABBREVIATIONS

ADV	acoustic Doppler velocimeter
APF	area production foregone
CFD	computational fluid dynamics
CWIS	cooling water intake structure
DNS	Direct Numerical Simulation
DPR	Direct Potable Reuse
EIR	Environmental Impact Report
ESGS	El Segundo Generating Station
ETM	Empirical Transport Modeling
h	hour(s)
HBDP	Huntington Beach Desalination Plant
HBGS	Huntington Beach Generating Station
IPR	Indirect Potable Reuse
LA	light attenuation
LES	Large Eddy Simulations
LIF	Laser-induced fluorescence
MGD	million gallons per day
microV	micro-optical velocimeter
PIV	particle image velocimetry
OWDP	Ocean Water Desalination Project
ppt	parts per thousand
RANS	Reynolds-Averaged Navier-Stokes
RNG	re-normalized group
rpm	revolutions per minute
RSM	Reynolds Stress Model
SGS	sub-grid scale
SST	Shear Stress Transport
SWRCB	State Water Resources Control Board
USEPA	U.S. Environmental Protection Agency
ZFE	zone of flow establishment

EXECUTIVE SUMMARY

Ocean water desalination requires discharge of brine into the ocean via multi-port diffusers which can potentially result in mortality of marine organisms entrained into the discharge plume. Appropriate diffuser design requires striking the right balance between the competing goals of achieving adequate mixing and dilution through high velocity discharge and minimizing the mortality of small organisms that may be entrained into the plume of the discharge jet. While it is conceptually understood that higher discharge velocities will result in increased turbulence, higher shear stresses, and increased mortality of entrained organisms, our understanding of what levels of turbulence will induce mortality across a broad group of organisms is limited.

The goal of this project was to characterize realistic mortality levels of small marine organisms from exposure to turbulence to aid the estimation of impacts from ocean desalination discharges. Specifically, the objectives of the project were to 1) Summarize the understanding of the relationship between turbulence characteristics and shear mortality of organism groups based on peer-reviewed literature, 2) Improve the characterization of shear and turbulence properties in a negatively buoyant (i.e., sinking) brine discharge jet plume, and 3) Provide an approach for estimating larval population losses resulting from exposure to turbulence in a brine discharge plume.

Key findings of each objective, based on the full analyses presented herein, are summarized below:

Objective 1: Relationship between discharge jet plume turbulence characteristics and shear mortality of organism groups

- Organism mortality is greatest when the size of the organism is comparable to that of the smallest turbulent eddies, i.e., eddies at the Kolmogorov length scale, η.

- Mortality increases sharply below Kolmogorov length scale of 0.5 mm for all taxonomic groups including copepods and larvae of bivalves, gastropods, bryozoans, polychaetes, and barnacles.

- Based on the available data, organism mortality increased from 9 to 70% with increasing energy dissipation rates that varied from 10^{-5} to 10^{-1} m^2/s^3.

- The maximum adjusted mortality of 70% was observed for mussel veligers exposed to intense turbulence for a duration of 24 hours. Mussel veliger mortality associated with experimental conditions where turbulence duration was more

comparable to that expected to occur due to entrainment into a brine discharge plume was 56% and below.

- Experimental mortalities for exposure durations of less than 5 minutes were less than 50%.

Objective 2: Characterization of turbulence properties in a brine discharge jet plume

Microscale turbulence was characterized using computational fluid dynamics (CFD) modeling. Key insights from the CFD modeling for practically designed diffusers are that:

- The order of magnitude estimate of η developed by Roberts (2018) is appropriate for a neutrally buoyant jet and the rising portion of a negatively buoyant jet.

- Negative buoyancy moderates turbulence in the rising portion of the plume, resulting in larger values of η.

- This increase in η is relatively small, and values of η along the jet plume centerline up to the apex remain substantially less than 1 mm.

- The value of η throughout the entire rising portion of the plume is less than 1 mm.

Objective 3: Provide an approach for estimating larval population losses resulting from exposure to turbulence in brine discharge jet plume

The approach developed herein is based on applying scaling factors to the empirical transport modeling (ETM) method currently used to calculate mortality for seawater intakes. Key differences from the seawater intake calculations include scaling factors based upon:

- Using estimated volumes for entrainment into the rising portion of the discharge jet plume (i.e., up to the apex).

- Excluding larvae greater than 1 mm in size.

- Adjusting the mortality of the 1 mm and smaller larvae to 50% based on the available data for shorter duration turbulence exposures.

The method is applicable for negatively buoyant (i.e., sinking) discharges and is illustrated by applying it to the West Basin Ocean Water Desalination Project and the Huntington Beach Desalination Plant Project.

Challenges and Recommendations

Two principal challenges were identified in terms of applying the information from the literature review to the assessment of environmental impacts for the discharge of brine into the ocean. One was that the studies in the literature review covered mainly freshwater larvae and, as such, were not representative of oceanic species. Moreover, species typically used for estimating population losses (i.e., target species) such as larvae of special status or commercially important fish and shellfish species were not identified in this review.

The second challenge was that the mechanisms of generating turbulence in the literature were typically using grids or paddles. By contrast, the turbulence in a brine jet plume discharge is caused by the free shear layer at the edges of the jet stream. This distinction may be important as the mortality of organisms was found to partially vary depending on the mechanism used to generate the turbulence. In particular, it is likely that some of the mortality in the literature experiments may have been caused by mechanical damage due to physical contact with the grids or paddles.

For future experimental studies, it is recommended target species are used to test vulnerability of larvae to turbulence, and that turbulence is generated using a jet stream.

1. INTRODUCTION

1.1 Overview and Project Goals

Ocean water desalination, brackish groundwater desalination, and indirect/direct potable reuse of recycled water represent potentially important and reliable sources of water for coastal regions across California. Of these sources, desalination requires the discharge of brine back into the ocean. This entails minimizing damage to, and mortality of, marine life that is entrained into the discharge plume in accordance with the water quality objectives and guidelines outlined by the State Water Resources Control Board (SWRCB) in the California Ocean Plan (Ocean Plan; SWRCB 2015). One of the barriers to increasing production from existing or new desalination projects is the difficulty in characterizing and quantifying the potential damage to marine organisms associated with the discharge of brine through multi-port diffusers. Appropriate diffuser design requires striking the right balance between the competing goals of achieving adequate mixing and dilution through a high velocity turbulent discharge and minimizing the mortality of small organisms that may be entrained into the discharge jet plume.

The mixing and dilution of brine discharges has been well studied, primarily through experimental approaches and integral models that have enabled plume trajectory, entrainment, and dilution to be parameterized and used for diffuser design (i.e., Roberts 2018). Far less research has been done on the mortality of small marine organisms that may be entrained into the diffuser jet plume. It is conceptually understood that higher discharge velocities will result in increased turbulence, higher shear stresses, and increased mortality of entrained organisms, but few scientific studies have directly quantified these effects. The SWRCB previously consulted with Dr. Philip Roberts to develop an approach to characterize jet turbulence properties and to compare these with results from biological studies. As described in more detail in the following chapters, this project builds upon and extends the previous approach of Roberts (2018). Specifically, the goals and objectives of the project are to:

- Summarize the understanding of the relationship between turbulence characteristics and mortality of small marine organism such as larvae based on peer-reviewed literature.
- Improve the characterization of shear and turbulence properties in a brine discharge jet plume.
- Provide an approach for estimating vulnerability of larvae entrained in a brine discharge jet plume to turbulence-induced mortality.

1.2 Research Approach

The approach for the analysis in this project consists of a detailed literature search and review of mortality experiments (Chapter 2), CFD simulations to characterize shear and turbulence properties of dense jets/plumes (Chapter 3 and Chapter 4), and the development of the approach for estimating mortality of larvae and application to two potential desalination projects (Chapter 5). Project conclusions are presented in Chapter 6. Additional details on the research approach are summarized below.

1.2.1 Mortality Literature Review (Chapter 2)

More than 30 studies addressing the impacts of turbulence on planktonic organisms were initially identified for this review. Of those studies, 11 provided information on turbulence allowing for comparisons across studies and that enabled characterization of mortality of small aquatic organisms exposed to strong turbulence. These studies were a mix of measurements in natural systems (marine and freshwater) and laboratory experiments. The studies addressed various life stages (egg, larval, adult) of aquatic organisms from a range of taxonomic groups (bivalves, gastropods, copepods, barnacles, and others), and were critically reviewed to include the turbulence properties to which the organisms were exposed. To facilitate comparisons across publications, turbulence was quantified in terms of the turbulent kinetic energy dissipation rate, ε, from which the microscale energy dissipation length scale (hereafter the Kolmogorov length scale), η, was calculated. This was only possible for nine of the 11 studies. Mortality of small organisms in the reviewed studies was adjusted by subtracting mortality that occurred in the absence of turbulence. This adjusted mortality was related to the Kolmogorov length scale.

1.2.2 CFD Validation (Chapter 3)

A CFD model was developed to model negatively buoyant plumes at 60° vertical angles using the freely available and open-source OpenFOAM software. The model was validated through comparisons to numerous experiments for both simple jets (i.e., neutrally buoyant) and negatively buoyant jets, and was benchmarked against other CFD models.

1.2.3 CFD Results (Chapter 4)

The CFD model (as validated in Chapter 3) was used to evaluate turbulence quantities for a range of diffuser port sizes and variances in salinity relevant for California conditions. The goal of the modeling was to refine the estimates for turbulence intensity, and

particularly the Kolmogorov scale, η, developed by Roberts (2018). It was anticipated that the turbulence in the rising portion of the jet plume would be moderated by the negative buoyancy, resulting in larger values of η than those estimated by Roberts (2018), and the CFD model would enable these differences to be quantified.

1.2.4 Methodology and Case Studies (Chapter 5)

Using findings from previous chapters an approach for estimating turbulence-induced mortality resulting from entrainment of larvae into a brine discharge jet plume was developed. The approach considered 1) the volume of water entrained into the plume, 2) the turbulence intensity that the entrained water is subjected to, and 3) the vulnerability of the entrained larvae to a certain level of turbulence intensity. The proposed evaluation of the vulnerability of entrained larvae produced estimates of larval population losses (P_M) that differed from estimates based on empirical transport modeling (ETM) in accordance with Appendix E of the Substitute Environmental Documentation for the California Ocean Plan Seawater Desalination provisions (SWRCB 2015).

The approach was applied to calculate P_M values for two proposed desalination projects: the West Basin Ocean Desalination Project and the Huntington Beach Desalination Project. In addition, the adjusted P_M values were combined with areas over which the larvae are distributed to arrive at estimates of the area production foregone (APF) specific to each project.

2. MORTALITY LITERATURE REVIEW

2.1 Background

The discharge of water resulting from an industrial process into the ocean requires minimizing mortality to all forms of marine life in accordance with the water quality objectives and guidelines outlined by the SWRCB in the California Ocean Plan (SWRCB 2015). One of the barriers to the construction of new, or increasing production from existing, seawater desalination projects is the difficulty in quantifying potential mortality of organisms associated with the discharge of brine through diffusers. The discharge from a diffuser port results in a high velocity jet flow entering a relatively still ambient environment, resulting in high velocity flow adjacent to a low velocity flow, termed shear flow. This shear flow causes entrainment (i.e., drawing in of and mixing with ambient water) which in the case of desalination projects serves to dilute the brine (Figure 2-1). Shear flow also leads to shear stresses and deformations that can result in organism mortality. Appropriate diffuser designs require striking the right balance between the competing goals of achieving adequate mixing and dilution through a high velocity discharge and minimizing the turbulence-induced mortality of marine organisms resulting from that discharge. Although the Ocean Plan requires protection of all forms of marine life, the emphasis in this review is on small planktonic organisms (mainly larvae) that may be entrained into the diffuser jets. Evidence from existing diffuser jets indicate that larger, motile organisms, such as adult fish, simply swim away from the jets.

The mixing and dilution of negatively buoyant brine discharges have been well studied, primarily through experimental approaches and integral models[1] that have enabled brine plume trajectory, dilution, and entrainment of surrounding water, to be parameterized and used for diffuser design (Roberts 2018). Far less research has been done on the potential mortality of marine organisms present in the water that are entrained into the diffuser jet/plume. It is conceptually understood that higher discharge volumes and velocities will result in more turbulent discharges, higher shear stresses, and increased mortality of entrained organisms, but there are limited scientific studies to directly quantify these effects. With respect to the evaluation of desalination facilities, the SWRCB currently assumes 100% mortality of the organisms that are entrained into the rising portion of a brine plume where the entire flow is assumed to behave like a jet (Figure 2-1) and its properties are determined by the source momentum flux. However, jet flow created by the high velocity discharge (i.e., momentum) is moderated by effects of negative

[1] Integral models attempt to solve for the trajectory and dilution of plumes in one-dimensional numerical calculations including entrainment and buoyancy effects. Commonly used computer programs include UM3 and CORMIX.

buoyancy, which decelerates the upward component of the jet flow, resulting in subsequent descending flow and a limit to the terminal rise height (Figure 2-1). The purpose of this review is to assess the relationship between turbulence properties, particularly the energy dissipation rate, and mortality of small-scale planktonic organisms.

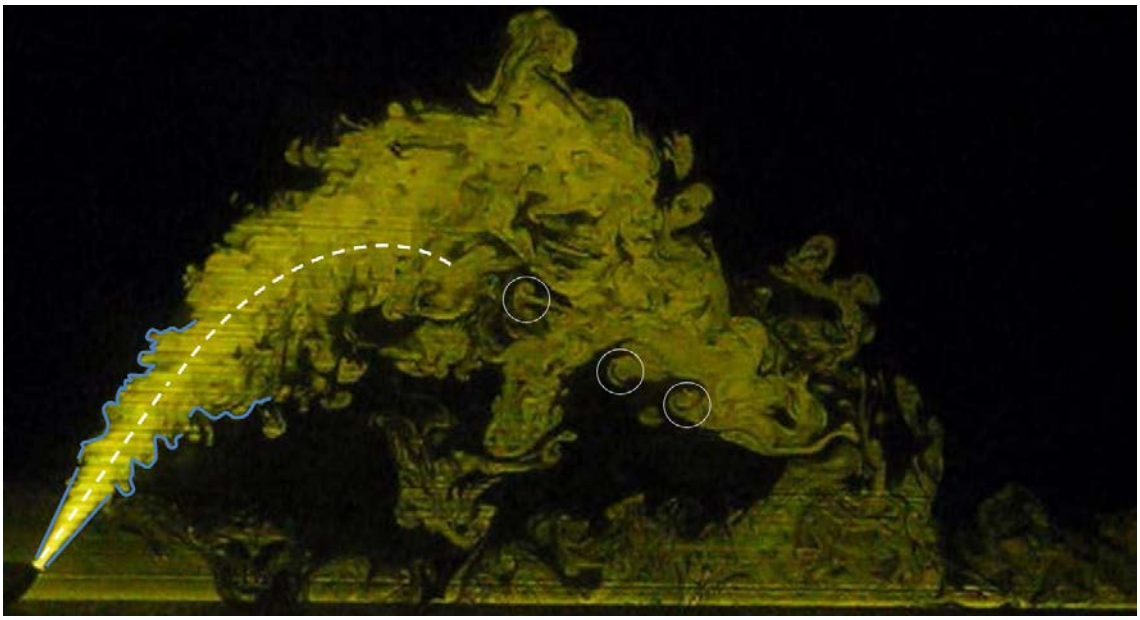

Figure 2-1. Laboratory image of high velocity brine jet/plume flow entraining surrounding water. Blue lines at edges of the jet indicate regions of strong shear flow where the difference in flow speed between ambient background water (black) and jet water (yellow) is large. The strong shear flow results in the formation of eddies and entrainment of ambient water into the jet. The dashed white line represents the centerline of the rising jet/plume where eddy sizes are smallest and viscous shear stresses are potentially damaging to marine organisms. Circles indicate larger eddies forming at the edges of the descending plume where background water continues to become entrained into the plume and dilute it. Image courtesy of Dr. Philip Roberts.

2.2 Turbulent Energy Dissipation and Damage Mechanisms

"Big whirls have little whirls,
That feed on their velocity;
And little whirls have lesser whirls,
And so on to viscosity."

- **Lewis Fry Richardson**

Shear flows created by a jet in ocean water produce whirls of water, or turbulent eddies. As conveyed in the above ditty of Lewis Richardson, these eddies in turn produce smaller eddies in a cascading fashion until the eddies are dissipated by viscosity (Lazier and Mann 1989). In a jet, such as from a brine diffuser, the eddy sizes are minimum on the jet

centerline and increase with distance from the centerline and along the jet plume trajectory (Roberts 2018). Viscous shear stress increases as the eddy size decreases and is maximum at the smallest scale. Smaller planktonic organisms that become entrained into the jet can be adversely affected by these shear stresses.

Larger organisms such as adult fish could also potentially be impacted by the shear stresses; however, video recordings of diffusers demonstrate that fish and other large motile organisms avoid the jet stream entirely by swimming away (Roberts 2018).

Experiments indicate that damage to small marine organisms increases sharply when their size is comparable to that of the smallest eddies (Rehmann et al. 2003, Zhang et al. 2017, Kozarek et al. 2018). Therefore, to measure the potentially negative impact of turbulence on organism growth and survival, it is useful to calculate the smallest size scale of eddies (i.e., the microscale) generated in a turbulent velocity field. The approximate diameter of microscale eddies is called the Kolmogorov length scale, η (m), and can be calculated from the energy dissipation rate, ε (m^2/s^3), of a turbulent velocity field and the kinematic viscosity of seawater (or freshwater), ν (m^2/s), according to Tennekes and Lumley (1972):

$$\eta = (\nu^3/\varepsilon)^{1/4} \qquad \text{Eq. 2-1}$$

Negative impacts from shear stresses range from increased energy expenditures, reduced growth rates, and reduced fecundity (Peters and Marrase 2000) to physical damage to the organism and death (e.g., Morgan et al. 1976, Horvath and Lamberti 1999, Zhu et al. 2016, Zhang et al. 2017). According to Rehmann et al. (2003), the potential for shear stresses to kill an organism increases as the diameter, d (m), becomes comparable to η. This ratio is typically represented as d^*:

$$d^* = d/\eta \qquad \text{Eq. 2-2}$$

The potential for physical damage to an organism is relatively small when it is much smaller than the smallest eddy ($d^* \ll 1$), as shear stresses are small at this scale; the main role of the turbulence at this scale is to transport the organism with little deformation (Figure 2-2A). Maximum damage may be experienced by organisms similar in size to the smallest eddy ($d^* \sim 1$) where shear stresses and the potential deformation are maximum (Figure 2-2B). For example, fluid forces acting in opposite directions along the body of an organism result in strong shear stress and increase the potential for damage and mortality. Kolmogorov length scale eddies typically do not impact larger organisms ($d^* \gg 1$) such as juvenile fish, several centimeters in size, that can simply swim away or are not affected by the much smaller scale flow field (Figure 2-2C).

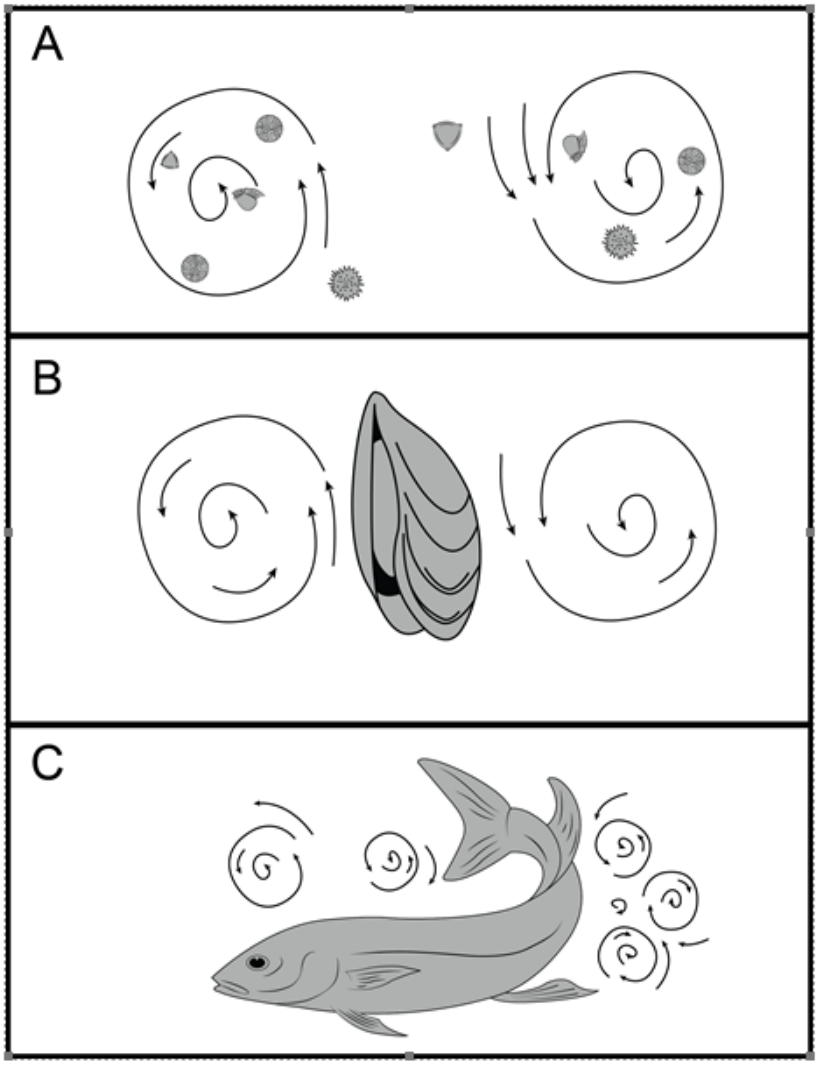

Figure 2-2. Size of eddy compared to size of organism. A) Kolmogorov scale length eddies (~0.2 mm) relative to phytoplankton sized organisms (~0.01 mm) ($d^* \ll 1$). Fluid forces act approximately uniformly on the organism resulting in advection with the flow. B) Kolmogorov scale length eddies (~0.2 mm) relative to mussel veliger sized organism (~0.2 mm) ($d^* \sim 1$). Fluid forces in opposite directions result in shearing on the organism increasing potential for damage and mortality. C) Kolmogorov scale length (~0.2 mm) eddies relative to larger organisms such as juvenile fish (several centimeters) ($d^* \gg 1$). These organisms can swim away or are not impacted by the much smaller scale flow field.

In accordance with the Ocean Plan, mortality to marine organisms resulting from desalination projects is calculated based on the entrainment of their larvae by the project. This calculation, termed the area production foregone (APF), was originally developed to estimate the impact of entrainment of larvae with water used to cool coastal power plants, and assumes 100% mortality of all entrained larvae (Boreman et al. 1981, Ehrler et al. 2002). With an eye toward calculating the APF due to the entrainment of larvae into

the brine discharge plume of a desalination project, this literature review focused specifically on studies emphasizing mortality as a function of turbulence intensity.

2.3 Organism Mortality as a Function of Turbulence

More than 30 studies addressing the impacts of turbulence on planktonic organisms were initially identified for this review. However, of those studies, only 11 provided quantitative information on turbulence allowing for comparisons among studies. These studies were a mix of measurements in natural systems (marine and freshwater) and laboratory experiments. Several methods were used to generate turbulence in the laboratory experiments, such as using a Couette cell, rotating vessels on an orbital shaker table, or bubbling vessels with air. Although this review applies to the marine environment, studies using freshwater species were also included as most of these species have marine counterparts and provide valuable insights. The metrics used to characterize turbulence in the studies differed widely, limiting direct comparisons and efforts to gain general insights from the combined dataset. To facilitate comparisons across the studies, and to facilitate the calculation of η, measurements of turbulence were converted where possible into ε as detailed in Appendix A. Of the 11 studies investigated for this review, ε could be approximated or calculated from nine studies, which are summarized in Table 2-1.

Table 2-1. Summary of investigations of mortality as a function of turbulence emphasized in this review, including experimental systems, sources of turbulence, turbulence exposure duration, organism(s) examined, life stage, and approximate organism size.

Reference	Experimental System	Turbulence Source	Turbulence Exposure Duration	Organism	Common Name	Organism Life Stage	Approx. Organism Size (µm)
Mead and Denny 1995	Couette cell	Opposing rotation of cylinders	2 min	*Strongylo-centrotus purpuratus*	Purple sea urchin	eggs	125
Denny et al. 2002	Couette cell	Opposing rotation of cylinders	2 min	*Strongylo-centrotus purpuratus*	Purple sea urchin	eggs	125
Rehmann et al. 2003	Glass beaker	Air flow	24 h	*Dreissena polymorpha*	Zebra mussel	larvae	84–126
Jessopp 2007	Natural channel	Tidal flow	2 min	Barnacle Nauplii	Barnacle	larvae	340
			2 min	Barnacle Cyprids	Barnacle	larvae	500
			2 min	*Littorina littorea*	Periwinkle	larvae	200
			2 min	*Turitella communis*	Tower shell	larvae	200
			2 min	*Aporrhais pespelicant*	Pelican's foot	larvae	200
			2 min	*Lamellaria perspicua*	Sea snail	larvae	200
			2 min	*Mytilus edulis*	Blue mussel	larvae	200
			2 min	*Membranipora membranacea*	Lacy crust bryozoan	larvae	500
			2 min	*Electra pilosa*	Colonial bryozoan	larvae	440
			2 min	*Polychaete trochophores*	Bristle worms	larvae	300

Reference	Experimental System	Turbulence Source	Turbulence Exposure Duration	Organism	Common Name	Organism Life Stage	Approx. Organism Size (µm)
Horvath and Crane 2010	Glass flask	Orbital shaker	1 h, 24 h, 48 h	*Dreissena polymorpha*	Zebra mussel	larvae	200
Bickel et al. 2011	Plexiglass container	Mixing paddle	0.5 min	*Acartia tonsa*	Copepod	adult	1,000
Zhang et al. 2017	PVC pipe	Water flow through grid	1 min, 5 min, 10 min, 15 min	*Limnoperna fortunei*	Golden mussel	larvae	200
Kozarek et al. 2018	Plastic jar	Rotating paddles	1 h, 24 h	*Dreissena polymorpha*	Zebra mussel	larvae	53–210
Prada et al. 2020	Plexiglass container	Vertically oscillating grid	1 min	*Ctenopharyng-odon idella*	Grass carp	eggs	3,000

The two studies that were not included either presented too large a challenge in terms of converting the shear measurement into ε (i.e., Morgan et al. 1976), or had conditions where turbulence varied in both space and time and was not directly measured and it was difficult to estimate adjusted mortality (i.e., Horvath and Lamberti 1999). Levels of turbulence used in the nine studies ranged over eight orders of magnitude, from an energy dissipation rate of 10^{-6} to 10^{1} m^2/s^3 (Figure 2-3A). This large range is comparable to the range in energy dissipation rates evidenced under natural conditions in the marine environment which varies from 10^{-9} to 10^{-3} m^2/s^3 in the offshore ocean mixed layer (Oakey and Elliott 1982, Terray et al. 1996), to 10^{-1} m^2/s^3 in the surf zone (George et al. 1994), to 1 m^2/s^3 in the rocky intertidal zone (Gaylord et al. 2013).

To facilitate comparison of mortalities across studies, natural mortality at zero turbulence was subtracted from the mortality associated with increasing levels of turbulence for each species. This produced mortality associated with turbulence only, termed adjusted mortality. Mortality was normalized in this manner for varying levels of non-turbulent mortalities associated with different species, life stages, and experimental set-ups (e.g., Sprung 1989). This normalization also allowed positive effects of turbulence on changes in population numbers (or egg fertilizations) to be displayed as negative adjusted mortality values (Figure 2-3A). Of the various organisms reviewed, purple sea urchin eggs (Mead and Denny 1995), grass carp eggs (Prada et al. 2020), and zebra mussel late stage larvae (hereafter veligers) (Rehmann et al. 2003) demonstrated positive impacts (e.g., increases in egg fertilization or population number) under low intensity turbulence (Figure 2-3A). In addition to normalizing mortality, replicate mortality measurements were averaged by energy dissipation level.

The above-referenced turbulence studies examined the effects on multiple life stages of marine organisms including adults, larvae, and eggs. Findings from the subset of studies that examined the consequences of turbulence exposure for egg fertilization success in broadcast spawning species (e.g., for purple sea urchins) were less applicable to brine discharges from desalination plants. This is because sperm-egg contact and subsequent fertilization likely occur only in the immediate vicinity of adults where plumes of gametes remain in high concentration. Once eggs are swept away from adults into locations where a desalination plant's diffuser might be positioned, the probability of fertilization becomes very small, rendering any other impact, such as from turbulence, irrelevant. Consequently, this review focused on life stages (such as larvae) that were viable in the vicinity of the brine discharge plume and more likely to be negatively impacted by entrainment into the plume. Excluding egg data, the maximum adjusted mortalities generally increased with increasing energy dissipation rates, varying from around 9% at ~10^{-5} m^2/s^3 to 70% at ~10^{-1} m^2/s^3 (Figure 2-3B).

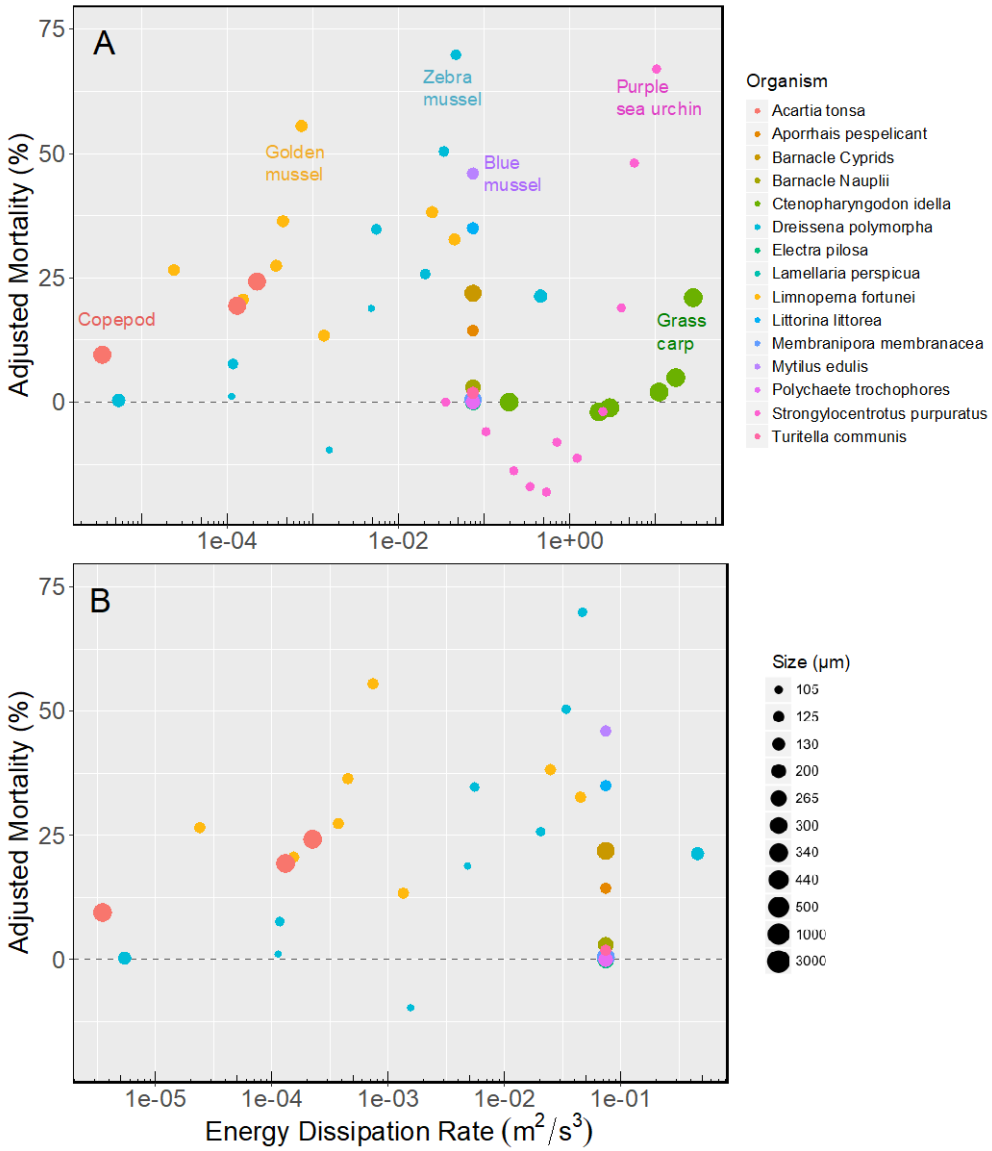

Figure 2-3. Adjusted mortality as a function of energy dissipation rate. A) Data aggregated from nine different studies summarized in Table 2-1. Where available, replicate data points were averaged across energy dissipation levels. Symbols plotted below zero on the y-axis, denoted by the grey dashed line indicate turbulence levels promoting growth of the population or fertilization of eggs. B) Same as in A but not including grass carp (*Ctenopharyngodon idella*) and purple sea urchin (*Strongylocentrotus purpuratus*) egg data. Color of symbol represents species of organism, and size of symbol represents size of organism varying from 105–3,000 µm.

2.4 Impact of Microscale Turbulence

Across all the studies reviewed here, adjusted mortalities increased sharply for $\eta \leq 0.5$ mm, reaching a maximum of 70% in zebra mussel veligers (Figure 2-4). For $\eta \geq 0.5$ mm,

adjusted mortalities remained below an average of 10% and were only notable for copepods (Figure 2-4). In the open ocean, η generally varies from approximately 0.2 mm to 6 mm, commensurate with variation in energy dissipation rates (i.e., 10^{-9} to 10^{-3} m^2/s^3) associated with the motion of currents and offshore breaking waves (Oakey and Elliott 1982, Terray et al. 1996). Direct measurements of η are few in the ocean, but Walter et al. (2014) found that it often exceeds 1 mm off the coast of California. In the region of the jets created by the discharge of brine, mortality of entrained organisms occurring below η of 1 mm is primarily associated with the diffuser jet and not natural turbulence (Roberts 2018). Given that Rehmann et al. (2003) demonstrated that mortality was greatest when η is roughly the same size as the organism (i.e., $d^* \sim 1$), this review focused on larvae less than about 1 mm in size. However, studies subsequent to Rehmann et al. (2003) have demonstrated that adjusted mortalities continue to increase even when $d^* > 1$, suggesting that organisms slightly larger than η may also be negatively impacted (Zhang et al. 2017, Kozarek et al. 2018). This raises the possibility that larger larvae belonging to a number of different organisms, including pelagic fish species, may be susceptible to the microscale turbulence associated with the jets. Although a study of mortality of fish larvae in response to turbulence was identified as part of this literature review (i.e., Morgan et al. 1976), the data were not included in this review because measurements of mean shear in a laminar flow were presented (rather than turbulence), precluding the calculation of ε and comparison with the other studies.

Based on the current review of data, the mortality of larval organisms would most likely be limited to the region of the jet where η < 0.5 mm (Figure 2-4). Even under the most severe rate of energy dissipation imposed and the smallest η, mortality of the larvae investigated here did not reach 100%, which is the current assumption made when calculating the APF for desalination projects. In our dataset (n=31), the median adjusted mortality was 20% and the maximum adjusted mortality was 70%. The maximum mortality was only achieved in an experiment where turbulence exposure duration lasted 24 hours (Kozarek et al. 2018). Such a long exposure scenario does not compare with durations of exposure to damaging turbulence, on the order of tens of seconds, that larvae entrained in a brine discharge plume would experience. Lower levels of mortality, e.g. ≤ 56%, were associated with experimental conditions where turbulence durations were more comparable to those expected to occur due to entrainment into a brine discharge plume. Additional discussion of duration of exposure is provided in the following section.

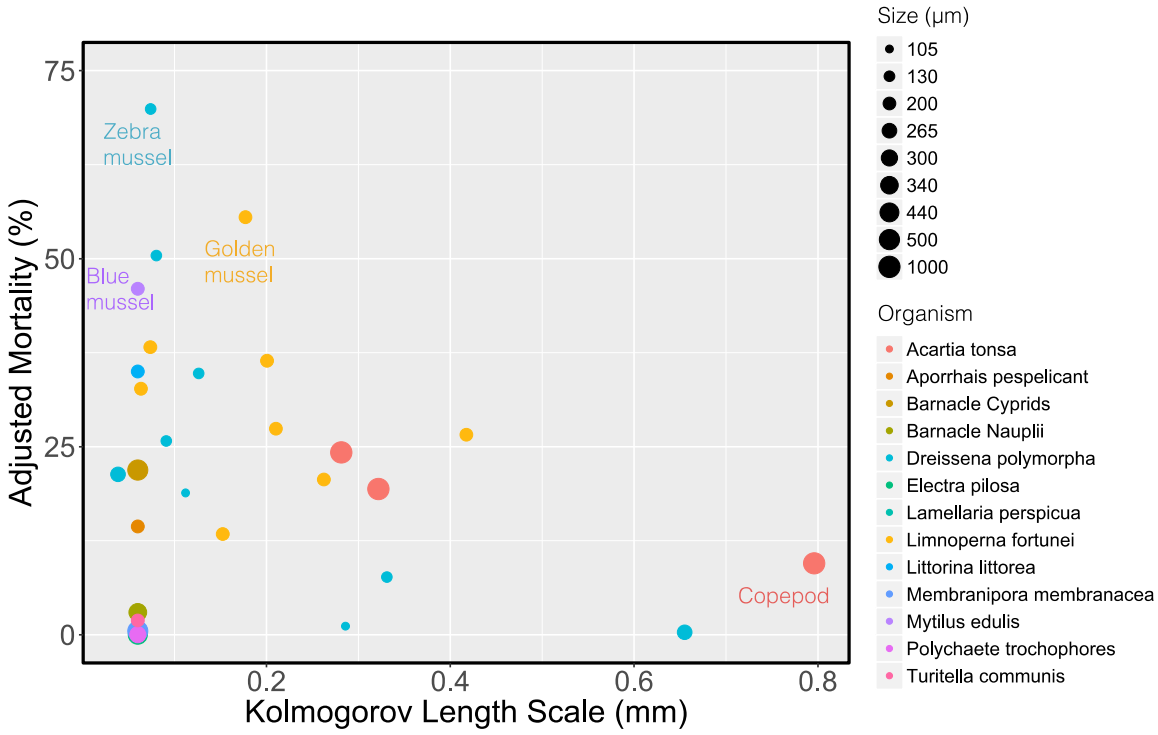

Figure 2-4. Adjusted mortality as a function of Kolmogorov length scale. Only means above zero are included. Data, coloring, and size of symbols as in Figure 2-3B.

2.5 Duration of Turbulence Exposure

Larval organisms caught in the plume of a jet discharging from a brine diffuser may be exposed to strong turbulence for tens of seconds before being expelled from the jet (Roberts 2018). However, data for assessing the impacts of turbulence duration over timescales of seconds to minutes are limited. Some studies have assessed the impact of turbulence duration over hours rather than seconds. For example, Kozarek et al. (2018) demonstrated an increase in adjusted mortality of zebra mussel veligers from 15% to 19% over a period of 24 h at a turbulence level of 1.7×10^{-4} m^2/s^3. At a turbulence level of 2×10^{-2} m^2/s^3, adjusted mortality increased from 15% up to 38%, depending on the size of the veligers, as exposure times increased from 1 to 24 h. With an increase in turbulence to 5×10^{-2} m^2/s^3, average adjusted mortality (for all size classes) increased to 70% at 24 h. At this latter turbulence level, however, mortality was measured only after 24 h (Kozarek et al. 2018). Similarly, Horvath and Crane (2010) demonstrated a 6% increase in adjusted mortality of zebra mussel veligers at 24 h compared with 1 h, and an additional 48% increase in adjusted mortality after 48 h.

In contrast with the above-mentioned studies, Zhang et al. (2017) demonstrated that adjusted mortalities in golden mussel veligers increased with turbulence duration only within the first 1–5 minutes of exposure, and then leveled out beyond that duration. This has important implications for entrained larvae with exposure durations on the order of tens of seconds since it is likely that the longer duration experiments result in higher mortalities. Notably, all experimental mortalities for exposure durations of less than 5 minutes were less than 50% (Figure 2-5).

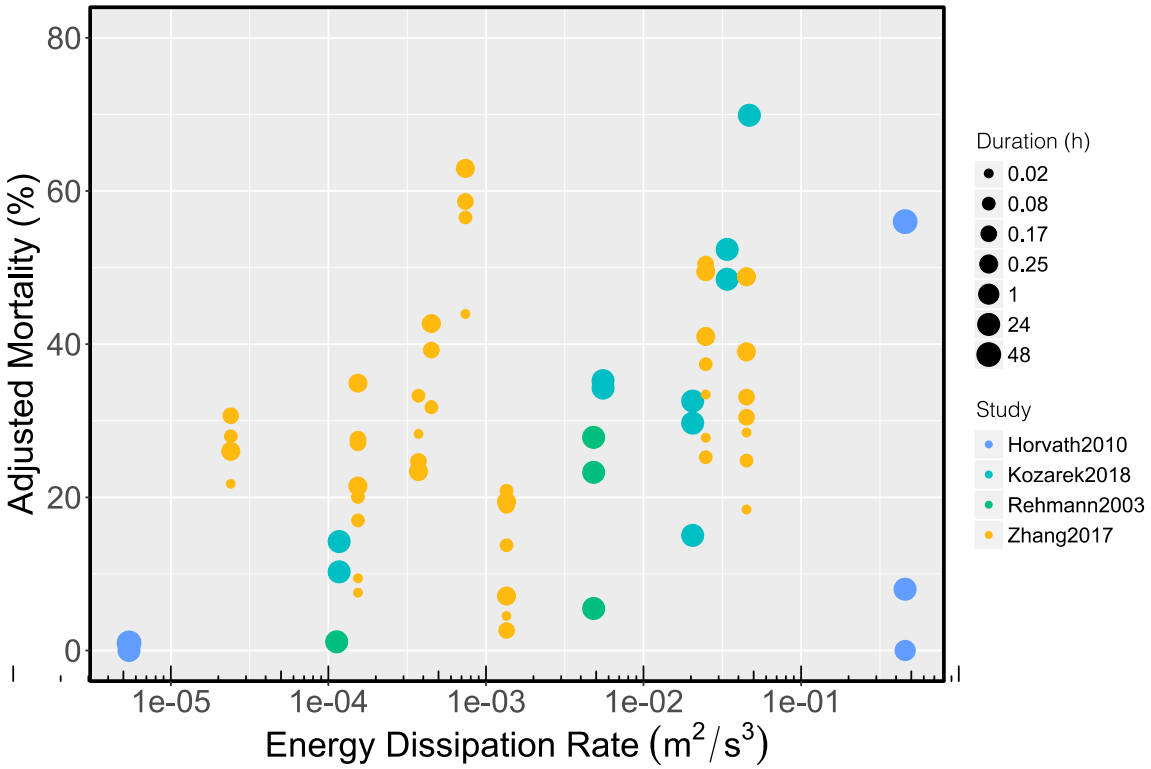

Figure 2-5. Adjusted mortality as a function of energy dissipation rate in studies of mussel veligers only. Yellow symbols represent golden mussel veliger data from Zhang et al. (2017), blue-green symbols represent zebra mussel veliger data from Rehmann et al. (2003), Horvath and Crane (2010), and Kozarek et al. (2018). Size of symbol represents turbulence duration in hours (0.02 to 48 h).

Zhang et al. (2017) further showed that there was no systematic increase in mortality with turbulence intensity across different experiments; rather, mortalities increased within each experiment with time (Figure 2-5). The greatest levels of mortality were attained in an experiment where the turbulence was generated using perforated plates with holes of 3 mm size, despite a relatively low overall turbulence intensity of 1.4×10^{-3} m^2/s^3. Despite the substantial overlap in energy dissipation rates among the aforementioned studies (Figure 2-5), the impact of duration of exposure to turbulence could not be extrapolated

beyond each individual study. The differences across studies could be associated with turbulence properties and distributions unique to each experimental set-up. That maximum mortalities were observed only after 24 and 48 h in the Kozarek et al. (2018) and Horvath and Crane (2010) studies could be due to a number of different factors; these may include a lack of measurements within the first few minutes of turbulence exposure, turbulence properties unique to each study, mechanical damage from contact of larvae with moving parts in the experimental apparatus, and/or increases in energy dissipation rates confounding the results of the impact of time. Damage to larvae in the above experiments, illustrated by photographs of larvae with broken shells taken during the experiments (Figure 2-6), could have resulted from shear forces as well as mechanical contact with the turbulence-generating apparatus.

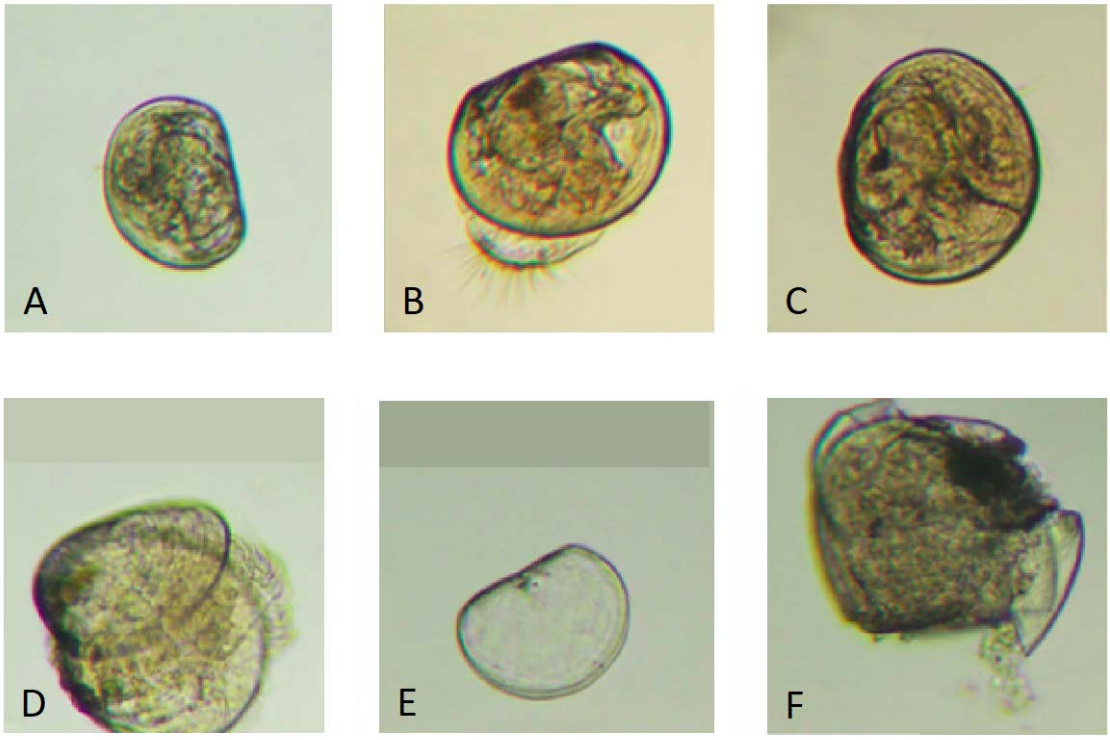

Figure 2-6. Photographs of larvae with broken shells. Top row: different stages of golden mussel (Limnoperna fortunei) veligers undamaged by turbulence, A) D-shape veliger, B) umboned veliger, and C) pediveliger. Bottom row: L. fortunei veligers damaged by turbulence exhibiting signs of shear stress, D) unhinged shell exposing tissue, E) empty shell, and F) damaged shell with tissue still remaining in the shell. Figures from Zhang et al. (2017).

2.6 Role of Organism Robustness

Turbulence-induced mortality, through the generation of shear stresses at the scale of the organism, can also be expected to depend on the robustness of the larvae entrained into the turbulence field. Based on the data in this review, zebra mussel veligers appeared particularly sensitive to turbulence-induced mortality, as evidenced by the positive relationship between adjusted mortality rate and d^* (Figure 2-7). A similar analysis of d^* for golden mussel veligers was less clear despite the susceptibility of these veligers to turbulence-induced effects (Figures 2-6 and 2-7). Although the studies on mussel veligers included in this literature review describe freshwater species, the information on susceptibility to turbulence-induced mortality could translate to marine mussel species such as *Mytilus californianus* inhabiting the coastline of California. *M. californianus* is broadly distributed along the middle intertidal zone and spends on average 2 to 3 weeks in the planktonic veliger stage before settling out of the water column (Haderlie and Abbott 1980).

Consistent with the results on susceptibility to shear mortality of freshwater mussel veligers, Jessopp (2007) demonstrated that blue mussel veligers entrained into turbulent tidal flow through a narrow channel in the North Sea experienced the greatest adjusted mortality compared with other larval classes. Mortality of samples taken at the end of the channel minus mortality at the beginning of the channel was 46%. The energy dissipation rate in the channel (7.4×10^{-2} m^2/s^3) compared well with the highest energy dissipation rates in Kozarek et al. (2018) and Zhang et al. (2017), 4.7×10^{-2} and 8.7×10^{-2} m^2/s^3, respectively, where similar mussel veliger adjusted morality rates were observed. A wide range of adjusted mortalities were observed for gastropod veligers such as *Littorina littorea* (35%), *Aporrhais pespelicant* (14%), *Turitella communis* (2%) and *Lamellaria perspicua* (0%). In comparison, larvae of Bryozoans and polychaetes had zero adjusted mortality, suggesting that these larvae were robust and relatively insensitive to shear mortality (Jessopp 2007).

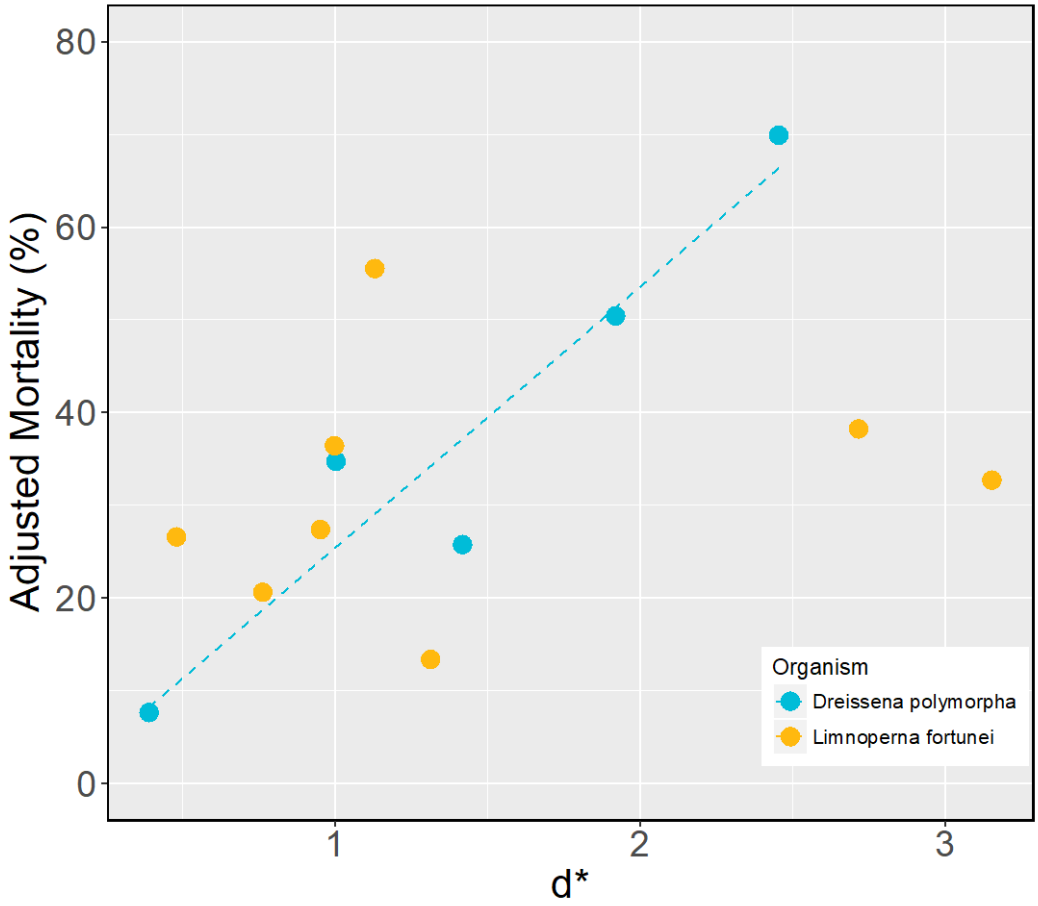

Figure 2-7. Adjusted mortality of mussel veligers as a function of d^*, the ratio of organism length to Kolmogorov length scale. Teal symbols represent zebra mussel veliger data and yellow symbols represent golden mussel veliger data. Regression line fit to zebra mussel veliger data (Adjusted Mortality=0.328(d^*)-0.128, r^2=0.85, p=0.0012, df=6).

Based on the characterizations in studies available to date, the susceptibility of larvae to turbulence-induced mortality appears to be decreasing in order from mussel veligers to polychaete trochophores (Table 2-2). However, insufficient data exist to assert general trends in turbulence sensitivity across most taxonomic groups. Nevertheless, apparent differences in susceptibility to turbulence-induced mortality suggest that the composition of invertebrate communities where desalination project discharges are located could play a role in determining the environmental impact (and thus the required mitigation) of the project. In addition, many organisms have larvae with long pelagic larval durations (weeks to months), which means those larvae could potentially experience negative impacts even some distance from adult populations (Gaylord and Gaines 2000). This latter group may include larvae of various fish species that are greater than 1 mm (e.g.,

Morgan et al. 1976) but are still small enough to be impacted (depending on their robustness) by shear stresses at the Kolmogorov scale of roughly 1 mm.

Table 2-2. Maximum adjusted mortalities of taxonomic groups as a function of dissipation rate (ε) ranges examined in this literature review.

Taxonomic Grouping	Maximum Adjusted Mortality (%)	ε_{min} (m^2/s^3)	ε_{max} (m^2/s^3)	Species examined
Bivalves	70	5.4×10^{-6}	4.7×10^{-2}	*Dreissena polymorpha, Limnoperna fortunei, Mytilus edulis*
Gastropods	35	3.1×10^{-4}	7.4×10^{-2}	*Littorina littorea, Aporrhais pespelicant, Turitella communis, Lamellaria perspicua*
Copepods	24	3.5×10^{-6}	2.2×10^{-4}	*Acartia tonsa*
Barnacles	22	3.1×10^{-4}	7.4×10^{-2}	*Barnacle nauplii* and *cyprids*
Bryozoans	0.5	3.1×10^{-4}	7.4×10^{-2}	*Membranipora membranacea, Electra pilosa*
Polychaetes	0.0	3.1×10^{-4}	7.4×10^{-2}	*Polychaete trochophores*

2.7 Summary

Turbulence-induced mortality, thought to derive from shear stresses, increased sharply for flows with Kolmogorov length scale less than 0.5 mm for all species and taxonomic groups reviewed here. Although there were large variations in adjusted mortalities as a function of energy dissipation rate across the different species of organisms, maximum adjusted mortalities generally increased from 9 to 70% with increasing energy dissipation rates that varied from 10^{-5} to 10^{-1} m^2/s^3. Within individual species, the relationship between adjusted mortality and energy dissipation rate was more consistent. Greater variability in the relationship across species could be related to differences in size as well as the robustness of the organisms. Not enough data currently exist to specify turbulence-induced mortality ranges for individual species, genera, or even taxonomic groups of organisms. However, based on the small subset of organisms whose response to turbulence has been examined, the greatest negative impact of turbulence was evident in mussel veliger populations at Kolmogorov length scales of 0.07 to 0.17 mm. The maximum adjusted mortality of 70% was observed for mussel veligers exposed to intense turbulence for a duration of 24 hours. Mussel veliger mortality associated with

experimental conditions where turbulence duration was more comparable to that expected to occur due to entrainment into a brine discharge plume was 56% and below. All experimental mortalities for exposure durations of less than 5 minutes were less than 50%.

3. CFD MODEL DEVELOPMENT AND VALIDATION

3.1 Background

This chapter summarizes the development of the computational fluid dynamics (CFD) model and presents validations against several sets of laboratory experiments. The focus of the current research project is on "negatively buoyant" discharges, where the density of the discharge is greater than that of the ambient receiving water, and will ultimately sink (e.g., Figure 2-1). This applies to many desalination facilities where the brine may typically have twice the salinity of the ambient ocean water and therefore has greater density. If the desalination plant is treating lower salinity water (e.g., brackish water) and/or if the waste stream is blended with other sources that have lower salinity (e.g., waste streams from traditional wastewater treatment plants) and/or higher temperature (e.g., rejected cooling water from electricity generation), then the discharge may become "positively buoyant" and ultimately continue to rise in the ambient receiving water. Positively buoyant discharges, or the intermediate case of "neutrally buoyant" discharges (where the discharge and ambient water have the same density) are not addressed directly in this research. However, the general research approach may be able to be adapted in future efforts to better address these situations. It is the moderating effect of the negative buoyancy on the jet flow and the associated turbulence properties that the current project aims to quantify through CFD simulations.

As illustrated in Figure 2-1, a turbulent jet generates shear (spatial variations in velocity) over a wide range of scales. Large-scale mean shear, that occurs mostly near the jet edges, would be mostly injurious to larger organisms such as fish, since smaller organisms will simply be advected with the larger scale flow that acts relatively uniformly over the smaller organism. Evidence from existing brine diffusers indicates that fish and other motile organisms simply swim away from the jets. As a result, impacts of large-scale mean shear are not considered in this report. Large-scale mean shear is important, however, in generating large eddies that entrain ambient water as the major mechanism in diluting the brine effluent. These large eddies break down to smaller and smaller eddies until the kinetic energy is dissipated by viscous friction as heat. These smallest eddies, known as Kolmogorov eddies or scales, generate high shear stresses that are potentially injurious to small planktonic organisms that cannot readily avoid entrainment into the jets. Although the Ocean Plan requires minimizing mortality of all forms of marine life, the emphasis in this research is therefore on small planktonic organisms, and this report emphasizes prediction of the turbulence properties that dictate the small-scale dynamics and Kolmogorov scales of turbulent brine jets.

While the approach of Roberts (2018) represents the best available methodology given the current state of research and understanding, it makes several simplifying assumptions

that likely result in an over-estimation of turbulence-associated mortality rates. In the first phase of this project (see Chapter 2), a literature review was conducted to assess the relationship between turbulence properties, particularly the turbulent kinetic energy dissipation rate, and mortality of small-scale planktonic organisms, and whether the 100% mortality assumption may be refined. In this Chapter 3, a CFD model of a negatively buoyant jet was developed that was later used to better quantify the turbulence properties throughout the jet and plume (with results presented in Chapter 4). Specifically, the effects of negative buoyancy that decelerate the upward component of the jet flow resulting in a terminal rise height and subsequent descending flow (Figure 2-1) are included in the CFD analyses.

As noted above, this chapter summarizes the development of the CFD model and presents validations against several sets of laboratory experiments. A brief summary of experimental studies is provided first, followed by a discussion of different CFD approaches that were reviewed to inform the approach selected for the current work. The CFD results are then validated by comparisons to experiments, including a discussion of limitations and noted issues. Finally, conclusions are summarized. Chapter 4 describes the scaling-up of the simulations to represent full-scale conditions, and quantification of the turbulence properties.

3.2 Experimental Studies

The following presents a summary of results from several sets of experiments for negatively buoyant jets. This summary is not intended to be an exhaustive review of past experiments, but rather has the primary goal of providing a means of validating the CFD model. For additional information on analyses and experiments, the reader is referred to, for example, Roberts et al. (1997), Besalduch et al. (2013), and Abessi and Roberts (2015).

The discussion herein is limited to jets with vertical angles[2] of 60°, which is the preferred angle to maximize dilutions at the impact point and the end of the near field (Roberts 2018). First, some basic terms of a negatively buoyant jet/plume are defined, including key non-dimensional parameters, and how the plume trajectory and dilutions scale with them. Then, results of experiments are tabulated and summarized statistically.

[2] Vertical angle refers to the angle of the diffuser port above the horizontal.

3.2.1 Terminology and Parameters

Figure 3-1 presents a schematic of a negatively buoyant discharge illustrating the dimensions that define the plume trajectory and dilutions[3] at key locations. This schematic represents time-averaged and not instantaneous conditions. The dilution at the end of the near field, S_n, is used in the methodology proposed by Roberts (2018) to meet the Ocean Plan criteria of a maximum 2 parts per thousand (ppt) increase above natural background salinity (SWRCB 2015). However, the current work focuses only on the turbulence in the jet and plume portions through to the impact point, and not in the horizontally spreading bottom layer where turbulence intensities are generally lower.

A key parameter to define the turbulence and behavior of jets is the Reynolds number, *Re*, based on velocity, *u*, a port diameter, *d*, and the kinematic viscosity of water, *v:*

$$Re = \frac{ud}{\nu} \qquad \text{Eq. 3-1}$$

A jet is typically considered to be fully turbulent when *Re* > 2,000, although sometimes a threshold as high as 4,000 is adopted[4]. Turbulent energy dissipation in a jet increases with *Re*, which has implications when scaling from experimental laboratory studies (*Re* values typically range from 2,000 to 5,000) to full-scale ocean implementation where *Re* values may be two orders of magnitude greater. This scale-up is assessed through additional CFD simulations, as presented in Chapter 4.

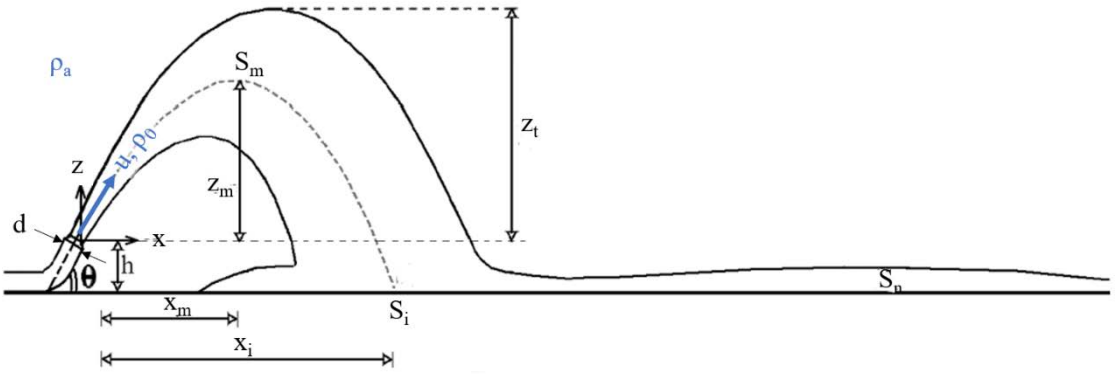

Figure 3-1. Schematic of a negatively buoyant discharge, with velocity, u, and density, ρ_0, through a port with diameter, d, at a vertical angle, θ, distance, h, above the seabed into ambient waters of density, $\rho_a <$

[3] Dilution, *S*, at a location is defined as $S = c_0/c$, where c_0 is the concentration of a tracer in the discharge and *c* is the local concentration of the tracer.
[4] See Section 9.2 of Fischer et al. (1979) for discussion.

ρ_0. Key horizontal dimensions, x, and vertical dimensions, z, are illustrated for the location of the plume centerline at the peak (subscript m), the plume top (subscript t), and impact point (subscript i). The dilutions, S, are also illustrated, including at the end of the near field in the spreading bottom flow (subscript n). Figure adapted from Abessi and Roberts (2015).

For a fully turbulent (i.e., $Re \gtrsim 2{,}000$) negatively buoyant jet, the trajectory and dilution characteristics are independent of *Re,* and for a fixed vertical angle θ, dimensional analyses[5] indicate that they are solely defined by the densimetric Froude number, *Fr*:

$$Fr = \frac{u}{\sqrt{g_0' d}} \qquad \text{Eq. 3-2}$$

Where $g_0' = g(\rho_0 - \rho_a)/\rho_a$ is the reduced gravity, g is the acceleration due to gravity, ρ_0 is the density of the discharge and ρ_a is the density of ambient water. Specifically, the dimensions x and z scale with the product of *d* and *Fr*, and the dilutions scale by *Fr*. Therefore:

$$\frac{x_m}{dFr} = c_1$$
$$\frac{z_m}{dFr} = c_2$$
$$\frac{z_t}{dFr} = c_3$$
$$\frac{x_i}{dFr} = c_4$$
$$\frac{S_m}{Fr} = c_5$$
$$\frac{S_i}{Fr} = c_6$$

where c_1 through c_6 are constants that can be determined through experiments. The values of the constants depend on the angle θ.

3.2.2 Experiments

Experimental studies have shown that a nozzle angle θ = 60° results in the longest jet plume trajectory and highest dilution, so this angle has become the de facto standard for brine diffusers and is emphasized in this report.

[5] See, e.g., Section 9.2 of Fischer et al. (1979) or Roberts et al. (1997) for additional details.

Eight studies of negatively buoyant jets with vertical angles of 60° published in the scientific literature were reviewed to extract estimates for the constants described above. This task typically involved obtaining values from the text or tables, or estimating values from graphs within the paper. Results are summarized in Table 3-1 and indicate some variability in the results among the experiments. The minimum and maximum values for trajectories and dilutions deviate from the mean values by approximately 10% to 20%.

The key experimental parameters (i.e., *Fr* and *Re*) and port diameter, *d*, are also provided in Table 3-1. Because most studies were conducted in the laboratory, the port diameters in the experiments are relatively small (less than 5 mm, or 0.2 inch), compared to practical full-scale diffusers, which may have port diameters ranging from a few inches to a few feet. Therefore, the Reynolds numbers of the experiments are much lower than those in full-scale diffusers. The densimetric Froude numbers in the experiments range from approximately 20 to 80. Based on the analyses of Roberts (2018) using the end of near field dilution, S_n, to meet the 2 ppt salinity increment required in the Ocean Plan, the value for *Fr* in most practical applications will be substantially lower than 20 (e.g., typically in the 5 to 10 range, depending upon the difference in salinity between the brine discharge and the ambient ocean water). These scale effects are assessed through additional CFD simulations with higher *Re* and lower *Fr*, with results presented in Chapter 4.

In addition to the parameters summarized in Table 3-1, figures from Roberts et al. (1997) and Abessi and Roberts (2015) were selected for validations of predictions of spatial variations by the CFD model. These are presented with other comparisons to CFD results in Section 3.4.

Table 3-1. Summary of experimental study results (θ = 60°).

Experimental Study		**Jet Plume Trajectory (x,z)**				**Dilutions, *S***		**Parameters**		
		$\frac{x_m}{dFr}$	$\frac{z_m}{dFr}$	$\frac{z_t}{dFr}$	$\frac{x_i}{dFr}$	$\frac{S_m}{Fr}$	$\frac{S_i}{Fr}$	d (mm)	Fr	Re
Roberts et al. 1997				2.2	2.4		1.6	4.29	20.5–27.6	3,300–4,400
Cipollina et al. 2005		1.42	1.77	2.32						
Nemlioglu and Roberts 2006				2.2	2.4		1.6			
Lai and Lee 2012		1.78	1.64	2.08		0.44				
Abessi and Roberts 2015a						0.6	1.6			
Abessi and Roberts 2015	min			2.2	2.7		1.5	3.17	21.4	1,700
	max			2.5	3.1		1.9	3.17	36.5	3,000
Palomar et al. 2015							1.41			
Kikkert et al. 2007	LA[1]	1.6	1.5	2.0				2.45	25 – 80	2,000–5,000
	LIF[2]	1.8	1.8	2.4				2.45	25 – 80	2,000–5,000
Statistics										
N		4	4	8	4	2	6			
min		1.4	1.5	2.0	2.4	0.4	1.4			
median		1.7	1.7	2.2	2.6	0.5	1.6			
mean		1.7	1.7	2.2	2.7	0.5	1.6			
max		1.8	1.8	2.5	3.1	0.6	1.9			

1. LA = light attenuation
2. LIF = laser induced fluorescence

3.3 CFD Approach

CFD modeling of negatively buoyant discharges is an active area of research. The goal of the current analysis is to utilize CFD to quantify the turbulence properties within a negatively buoyant jet, rather than to necessarily develop a better CFD model. With that goal in mind, this section presents a brief overview of CFD studies followed by a more quantitative evaluation that was conducted to inform the current approach. Finally, details of the current approach are provided. Results of the validation of the current CFD modeling are presented in Section 3.4.

3.3.1 Overview of CFD Studies

In recent years, several numerical modeling studies have been performed using a variety of CFD modeling tools to simulate the near-field kinematic and mixing behaviors for fully submerged negatively buoyant inclined jets. Brief summaries are provided below for both commercially developed CFD software and freely available OpenFOAM[6] software. CFD models traditionally fall into three main categories: Reynolds-Averaged Navier-Stokes (RANS), Large Eddy Simulations (LES), and Direct Numerical Simulation (DNS) (e.g., Ferziger and Peric 2002). DNS attempts to solve the full equations of motion (e.g., the Navier-Stokes equations) by fully resolving all aspects of the flow field, down to the smallest-sized turbulent eddies (i.e., the Kolmogorov scale). For most practical engineering problems with turbulent flow (i.e., high *Re*), DNS is not currently possible since too many computational grid points are required to resolve the Kolmogorov scale. Currently, DNS is mostly used in research settings to study complex phenomena and to improve the understanding of turbulence.

In contrast, RANS methods do not resolve the turbulent eddies. Rather, the Navier-Stokes equations are time-averaged to derive the RANS equations for the mean flow quantities. These equations also include terms for the unsteady turbulent fluctuations that are not solved directly but are rather modeled using a range of different approaches to close the equations. A commonly used closure model is the k-ε model, where k is the turbulent kinetic energy[7] and ε is the rate of dissipation of turbulent kinetic energy. Another often-used closure model is the k-ω model, where ω is the specific rate of dissipation[8] of turbulent kinetic energy. In both approaches, two additional partial differential equations are employed to directly solve for k and either ε or ω, and as such these are commonly referred to as "two-equation" models. Variations of these approaches have also been

[6] OpenFOAM is a freely available, open-source CFD software. https://www.openfoam.com/.

[7] $k = \frac{1}{2}|\boldsymbol{u}'|^2$, where $\boldsymbol{u}' = \boldsymbol{u} - \overline{\boldsymbol{u}}$ is the vector of turbulent velocity fluctuations, u is the vector flow velocity, and $\overline{\boldsymbol{u}}$ is the vector time-averaged flow velocity.

[8] The specific rate of dissipation is proportional to the rate of dissipation divided by k (i.e., $\omega \propto \varepsilon/k$).

developed. The choice of turbulence closure depends on the type of flow that is being solved as determined by comparisons to experiments and past applications. The RANS approach has the advantage of only requiring the computational grid to be small enough to model the time-averaged mean flow quantities but has the disadvantage of not providing the time-varying turbulent component of the flow field (since that has been averaged out).

The LES approach is intermediate to DNS and RANS in that the larger of the turbulent eddies are simulated directly (i.e., resolved by the computational grid), while sub-grid models (e.g., Smagorinsky model) are used to account for the effects of the smaller eddies. Typically, the goal is to directly simulate eddy sizes such that approximately 80% of the turbulent kinetic energy is captured, although different techniques are sometimes used that resolve lower fractions of the energy (particularly for higher *Re* flows). The benefit of the LES approach is that results include information on the time-varying turbulent component of the flow (i.e., the larger of the turbulent eddies), but the drawback is that additional computational resources are needed (i.e., finer grid resolutions are required compared to the RANS approach)

3.3.1.1 Commercial Software Studies

Vafeiadou et al. (2005) was perhaps the first to use CFD to evaluate the hydrodynamic processes of an inclined jet by employing the computational software CFX[9] with the RANS approach and the k-ε turbulence closure scheme. Other studies followed, such as Oliver et al. (2008 and 2013), which simulated similar conditions using CFX and modified integral models. Seil and Zhang (2010) employed FLUENT[10] with the RANS k-ω turbulence closure model and investigated both single- and multi-port diffusers. Robinson et al. (2016) employed Fluidity[11] with the RANS k-ε turbulence closure and a LES model to predict the trajectory and mixing characteristics of both positively and negatively buoyant plumes.

3.3.1.2 OpenFOAM Studies

The hydrodynamics of fully submerged inclined dense jets have been simulated extensively with OpenFOAM, with various turbulence closure models in quiescent ambient environments under a range of densimetric Froude numbers. Gildeh et al. (2014a,

[9] CFX is a commercially available CFD software now developed and maintained by ANSYS. https://www.ansys.com/products/fluids/ansys-cfx.
[10] FLUENT is a commercially available CFD software now developed and maintained by ANSYS. https://www.ansys.com/products/fluids/ansys-fluent.
[11] Fluidity is developed primarily by Imperial College, London, https://fluidityproject.github.io/.

2014b, and 2015) applied the RANS approach with the realizable k-ε, re-normalized group (RNG) k-ε, non-linear k-ε, and the Reynolds Stress Model (RSM) for a jet at inclinations ranging between 30° and 85°. Results indicated that the RSM and the realizable k-ε closures were more accurate than other approaches.

Zhang et al. (2015) evaluated the LES approach model with the standard Smagorinsky and dynamic Smagorinsky sub-grid scale (SGS) turbulence models for a 45° jet. They demonstrated that both model results were in reasonable agreement with the experimental data but pointed out the weaknesses of the SGS models, that a higher resolution mesh and longer computation time are required to resolve the convective mixing by buoyancy-induced instability in regions beyond the centerline peak. In a later study, Zhang et al. (2107) arrived at similar conclusions, when the LES dynamic Smagorinsky SGS and the RANS k-ε models were applied to simulate jets at 45° and 60° inclinations with the subsequent spreading of the plume on the bottom included in the model.

Yan and Mohammadian (2019) evaluated the performances of RANS standard and RNG k-ε turbulence closure models for a diffuser with moderately spaced multiple ports at a 60° angle. The study found that the RNG k-ε model produced more accurate results than the standard model without sacrificing computation time.

Baum and Gibbes (2017) used OpenFOAM with the RANS k-ω Shear Stress Transport (SST) turbulence closure to simulate a singular dense jet at 60° inclination subject to a range of ambient crossflow conditions. The method included an adaptive mesh refinement utility that adjusted the mesh during computation to better resolve both jet plume trajectory and mixing in the near field. Subsequently, Baum and Gibbes (2019) conducted a similar study but with multiple ports with alternating orientations. The study results indicated agreement with time-averaged field measurements of salinity increases.

3.3.2 Quantitative Evaluation of CFD Models

CFD studies that examined negatively buoyant jets for single ports with a vertical angle of 60° were reviewed to extract estimates for the constants described in Section 3.2.1. This review typically involved estimating values from graphs within the papers. Results are summarized in Table 3-2.

Table 3-2. Summary of CFD model results from the literature review (θ = 60°).

CFD Study		**Jet Plume Trajectory (x,z)**				**Dilutions, *S***		**Parameters**		
		$\frac{x_m}{dFr}$	$\frac{z_m}{dFr}$	$\frac{z_t}{dFr}$	$\frac{x_i}{dFr}$	$\frac{S_m}{Fr}$	$\frac{S_i}{Fr}$	d (mm)	Fr	Re
Oliver et al. 2008		1.4	1.4	1.9				5	48.66	10,458
Robinson et al. 2016			1.3		2.1		1.0	3.3	21.3	2,500
Gildeh et al. 2014a	min	1.4		1.8				10.65	12.6	6,300
	max	1.8		2.0				10.65	36.9	11,100
Zhang et al. 2017		1.75	1.70	2.00	2.67	0.35	1.10	6	11.4–40	2,200–7,800
Baum and Gibbes 2017				2.0	2.0	0.4	0.9	4.29	20	3,200
Statistics										
N		4	3	5	3	2	3			
min		1.4	1.3	1.8	2.0	0.35	0.9			
median		1.6	1.4	2.0	2.1	0.4	1.0			
mean		1.6	1.5	1.9	2.3	0.4	1.0			
max		1.8	1.7	2.0	2.67	0.4	1.1			

Compared to the experimental values in Table 3-1, the CFD studies generally slightly underestimated all of the plume trajectory dimensions (by between 6% and 15% when comparing mean values), with the exception of Zhang et al. (2017) that only underestimated z_t (by approximately 10% compared to experimental mean values). The dilutions at the centerline peak, S_m, were also slightly underestimated by all CFD approaches, although it is noted that only two papers provided these values in each of the CFD studies (Table 3-2) and the experiments (Table 3-1). The dilutions at the impact point, S_i, were substantially underestimated by all CFD approaches, although only three CFD studies provided these values.

In addition to accuracy, other considerations such as software cost (i.e., CFD software platform), computational requirements, and ability to extract relevant turbulence properties influence the current approach. These considerations are summarized in Table 3-3 and described further in the following sections.

Table 3-3. Summary of CFD model considerations ($\theta = 60°$),

CFD Study	Software	Trajectory Accuracy	Dilution Accuracy	Turbulence Model	Computer Resources	Software Cost
Oliver et al. 2008	CFX	moderate	unknown	k-ε	moderate	high
Robinson et al. 2016	Fluidity	moderate	moderate	k-ε	moderate	unknown
Gildeh et al. 2014a	Open FOAM	moderate	unknown	Realizable k-ε	moderate	free
Zhang et al. 2017	Open FOAM	high	moderate	LES	extremely high	free
Baum & Gibbes 2017	Open FOAM	moderate	moderate	k-ω SST	moderate (adaptive mesh)	free

3.3.2.1 Software

The models using the OpenFOAM platform (i.e., Gildeh et al. 2014a, Zhang et al. 2017, and Baum and Gibbes 2017) indicate comparable or better accuracy than the commercially available platforms. While there is some additional effort to use the OpenFOAM platform compared to commercially developed software, the free and open-source nature makes this a preferable choice in terms of current project budget and in terms of enabling subsequent researchers to utilize or expand on the current research. Additionally, numerous academic researchers are using OpenFOAM, as summarized in

Section 3.3.1.2, which facilitates staying current on new developments. Therefore, OpenFOAM is the preferred software option.

3.3.2.2 Turbulence Model

While the LES modeling approach used by Zhang et al. (2017) yields slightly improved predictions of trajectory and dilution parameters under quiescent conditions, the RANS approaches (e.g., variations of the k-ε and k-ω models) are more computationally feasible. For instance, the LES simulations required up to 20 days of simulation time on a 64- or 128-core parallel processor, while the equivalent RANS approach required only about 7 hours on a 16-core machine (Zhang et al. 2017). Additionally, the computational requirements for the LES simulations would become greater for the full-scale simulations, where higher Reynolds numbers result in smaller turbulent eddies that would require a finer computational mesh to resolve the same fraction of turbulent kinetic energy.

The RANS models also have the advantage of directly simulating the turbulence quantities of primary interest. The literature review of mortality studies conducted in the first phase of this project (Chapter 2) identified that the energy dissipation rate, ε, is a key parameter in informing mortality. The k-ε turbulence models (including the Realizable k-ε variation used by Gildeh et al. [2014a]) directly model and calculate the turbulent kinetic energy, k, and turbulent energy dissipation rate, ε, throughout the jet plume. Similarly, the k-ω turbulence models (including the k-ω SST variation used by Baum and Gibbes [2017]) directly model and calculate k and the specific turbulent energy dissipation, ω, which can be readily used to calculate ε[12].

Gopalakrishnan and Disimile (2017) investigated the effect of different turbulence models on the simulation of neutrally buoyant jets and found comparable results between the standard k-ε model, the realizable k-ε model, and the k-ω SST model. However, they found disparate and inaccurate results when the standard k-ω model was used, likely due to this model being more suitable to wall-bounded flows rather than free-shear flows. Therefore, due to accuracy, computational efficiency, and the directness of simulating the turbulence quantities of interest, the RANS approaches using variations of either k-ε or the k-ω SST turbulence models are preferred over the standard k-ω model in this application.

[12] $\varepsilon = C_{\mu}\omega k$, where C_{μ} is a constant equal to 0.09.
https://www.openfoam.com/documentation/guides/latest/doc/guide-turbulence-ras-k-omega-sst.html.

3.3.3 Current Approach

The current approach closely follows the method of Baum and Gibbes (2017), with some modification as described below. The adaptive meshing technique appealed in terms of being able to better resolve details of the jet plume with locally smaller mesh sizes while maintaining computational efficiency. We also greatly acknowledge the authors who shared their model input files and adaptive mesh utility. An overview of the model set-up is provided below, with more details available in Baum and Gibbes (2017).

Following Baum and Gibbes (2017), the OpenFOAM software with adaptive mesh utility was used to solve the unsteady RANS equations using the k-ω SST turbulence model. The simulations were run long enough to achieve steady state, which typically took 3,000 to 5,000 iterations. Simulations used a turbulent Schmidt number[13] of 0.7, a molecular diffusivity[14] of 1.4×10^{-8} m^2/s, and kinematic fluid viscosity[15] of 10^{-6} m^2/s.

The model domain was 0.81 m wide (y-direction), 0.61 m deep (z-direction), and 2.40 m long (x-direction). These dimensions were selected to match geometries of the laboratory experiments of Roberts et al. (1997)[16]; full-scale analyses suitable for real-world applications of brine diffusers in the field are described in Chapter 4. To represent the port, a cylinder with diameter, d = 4.29 mm, was placed at a 60° angle with the centroid of the face 0.025 m above the bottom of the domain and 0.5 m from the "left" (i.e., lowest x-value) boundary. The bottom of the domain, the port cylinder, and the "front" and "back" walls (i.e., the y-axis boundaries) were represented as solid no-slip (i.e., zero velocity) boundaries. A small inflow velocity of 0.0001 m/s was specified at the "left" boundary to assist with the numerical solution, while the "right" (i.e., highest x-value) boundary was represented as zero gradient (in both velocities and concentration) to allow outflow. The top boundary was represented with a "free-slip" condition to simulate the free surface. In most simulations, the main features of the jet plume were far enough from the top and side boundaries as to not be substantially affected.

---

[13] The turbulent Schmidt number is the ratio between the rates of turbulent transport of momentum and the turbulent transport of mass (or any passive scalar). It is set to less than 1.0 to account for the mean concentration profile being wider than the mean velocity profile in a turbulent jet (See Section 9.2.1 of Fischer et al. [1979] for discussion).

[14] The simulation results are not sensitive to molecular diffusivity since the mass transport process is dominated by the turbulent diffusion that is accounted for in the simulations with the turbulence closure and the turbulent Schmidt number.

[15] The simulation results are not sensitive to fluid viscosity since the turbulent diffusion dominates the molecular diffusion. A typical value representative for freshwater was used.

[16] The full length of the tank in the experiments in Roberts et al. (1997) was 6.1 m. The computational domain was truncated at 2.4 m for efficiency, and an outflow boundary condition was used instead of a wall boundary condition.

Velocities were prescribed on the face of the cylinder to represent the port inflow, with the same turbulent velocity profile used by Baum and Gibbes (2017). A turbulence intensity[17] of 5.8% was used to calculate the inflowing turbulent kinetic energy, k, that was specified at the port inflow, while ambient turbulence intensity was assumed to be 5% as an initial condition (see Baum and Gibbes 2017). The discharge density, ρ_0, was specified for the port inflow, and the ambient density, ρ_a, was specified as an initial condition. Additionally, a tracer was defined with port inflow concentration, $c_0 = 1$, and an ambient concentration of zero to enable the plume concentrations to be plotted and dilutions to be calculated.

Following Baum and Gibbes (2017), the domain was discretized using a uniform hexahedral mesh with 15 mm side dimensions, with additional refinement around the port to resolve the smaller and curved cylindrical geometry, as illustrated in the left panel of Figure 3-2. The adaptive mesh utility was executed every 200 iterations to sub-divide cells into smaller cells where needed as determined by evaluating the simulated concentrations. The parameters controlling the adaptive mesh utility included an absolute tolerance, a relative tolerance, and a limit on the number of levels of refinement. The mesh utility compared the difference between the minimum and maximum concentrations on the faces of each cell to these tolerances, and if they exceeded the thresholds, the cell was sub-divided. This protocol had the effect of reducing cell size in regions of high concentration gradients. Experiments with these parameters resulted in decreasing the relative concentration tolerance from 0.25 to 0.02, to result in smaller cells near the center of the jet plume close to the port. The absolute concentration tolerance was decreased from 0.03 to 0.02 to further refine regions away from the port. The limit on the number of levels of refinement was retained at eight.

[17] Turbulence intensity is defined as the root-mean-square of the turbulent velocity fluctuations normalized by the mean inflow velocity.[18] The turbulence intensity was calculated from the CFD simulations as $I = \sqrt{\frac{2}{3}k}/u$, where k is the turbulent kinetic energy that is extracted from the CFD results and u = 0.75 m/s is the average port velocity.

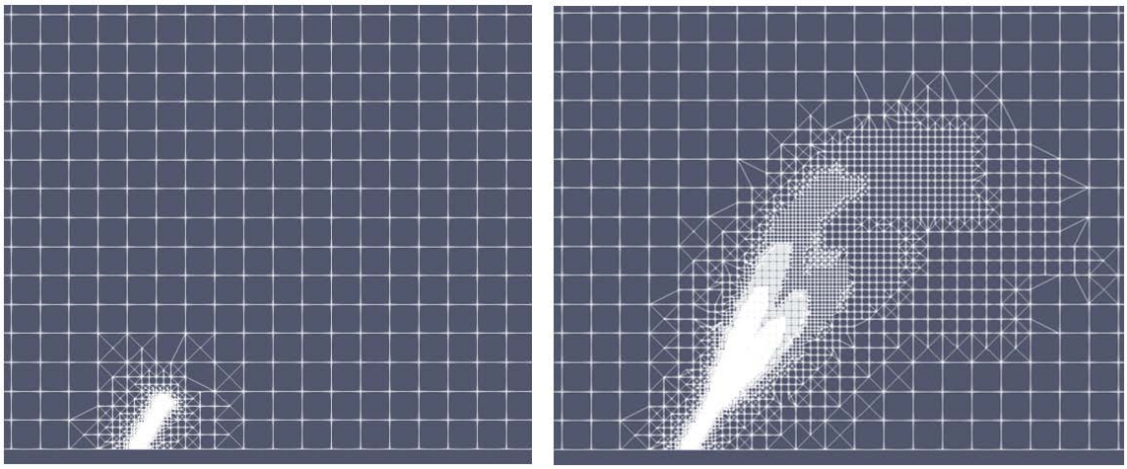

Figure 3-2. Slice of computational grid along plume center (y = 0) at beginning of simulation (left) and end of simulation (right). Initial mesh size is 15 mm with localized refinement around the cylindrical port geometry (left) and comprises ~400,000 cells. Final mesh size ranges from 15 mm far from the plume to as small as ~0.06 mm after eight levels of refinement (right) and comprises ~6,000,000 cells.

The adaptive mesh utility resulted in an initial ~400,000 cells increasing to ~6,000,000 cells by the end of the simulation, as illustrated in Figure 3-2. As a comparison, the Baum and Gibbes (2017) model resulted in ~1,100,000 cells. The modified mesh refinement resulted in slightly less spreading near the port and a slightly higher trajectory.

The same parameters used by Baum and Gibbes, and as summarized in Table 3-2, were used for initial testing and simulations. Additional simulations were performed to evaluate the effects of a higher Froude number and a neutrally buoyant jet. These parameters are defined in Section 3.4.

3.4 Validation Results

The CFD model was used to evaluate three different scenarios as presented in Table 3-4.

Table 3-4. CFD model scenarios ($\theta = 60°$).

Scenario	**Ambient Density,** ρ_a (kg/m^3)	**Discharge Density,** ρ_0 (kg/m^3)	**Froude Number,** *Fr*	**Mean Discharge Velocity,** u (m/s)	**Reynolds Number,** *Re*
Simple Jet	997	997	n/a	0.75	3,200
Fr = 20	997	1,030	20	0.75	3,200
Fr = 40	997	1,030	40	1.5	6,400

The "Simple Jet" scenario refers to a neutrally buoyant jet, i.e., without density effects ($\rho_0 = \rho_a$), and was included to validate the ability of the model to correctly capture momentum effects in the absence of buoyancy. For negatively buoyant jet CFS simulations the "*Fr* = 20" scenario is the same as used in Baum and Gibbes (2017), which was parameterized to match the experiments of Roberts et al. (1997). The "*Fr* = 40" scenario has a higher Froude number, discharge velocity, and Reynolds number, and was executed to better match the conditions in the experiments of Abessi and Roberts (2015). Additional discussions and comparisons to experiments are provided in the following sections.

3.4.1 Simple Jet Scenario

Simple jets have been studied for many decades (see, e.g., Section 9.2 of Fischer et al. [1979]). For round, fully turbulent simple jets, a wealth of experimental data are available that provide information on turbulence intensity, centerline velocity, and mixing and dilution. These processes are dominated by the momentum of the jet. To validate the CFD model in the absence of buoyancy, a simulation was conducted with the discharge density set equal to the ambient density (Table 3-4). Results from the CFD model, including turbulent kinetic energy, k, centerline velocity, u_c, and concentration, c_c, were extracted along the jet centerline and compared to previous studies, as described below.

3.4.1.1 Turbulence Intensity

The correct modeling of the turbulence is a critical part of the overall project, since it will ultimately be used to relate to the mortality of marine organisms using results of the first phase of this project (Chapter 2). The turbulence intensity, *I*, is defined as the root-mean-square of the turbulent velocity fluctuations normalized by the mean inflow velocity, and has been measured experimentally for round turbulent jets. Comparisons between the CFD results[18] and experimental results are presented in Figure 3-3.[19]

The CFD results indicate much higher turbulence on the centerline close to the jet orifice than the experiments. This is a result of applying a constant value of turbulent intensity

[18] The turbulence intensity was calculated from the CFD simulations as $I = \sqrt{\frac{2}{3}k}/u$, where k is the turbulent kinetic energy that is extracted from the CFD results and u = 0.75 m/s is the average port velocity.

[19] Results are plotted as a function of non-dimensional distance from the port orifice, Z/l_Q. Here uppercase Z represents the distance along the jet centerline, rather than the vertical z-axis of the computational domain. The characteristic length scale, l_Q, is defined as the square root of the port area, *A*. Viz, $l_Q = \sqrt{A} = \sqrt{\pi/4}d \approx 0.9d$, and l_Q is almost equivalent to the port diameter, *d* (Section 9.2 of Fischer et al. 1979).

of 5.8% (i.e., $I = 0.058$[20]) as an inflow boundary condition for the port (see Section 3.3.3), which is a reasonable value for fully developed flow from a pipe. However, the experimental results in Figure 3-3 are for flows through an orifice (i.e., a hole in a plate) and have much lower turbulent intensities at the center than flow from a pipe.

The region of lower turbulence near the port is known as the "potential jet core" or "zone of flow establishment" (ZFE), which typically extends approximately six port diameters (i.e., $6d$, or about $7l_Q$) from the jet orifice. At this distance, the locally higher intensity regions at the jet edges converge and meet, resulting in a peak intensity at the centerline. Beyond this distance, the turbulence intensity on the centerline decreases. Despite the differences in turbulence intensity within the ZFE, the modeled turbulence intensity agrees extremely well with the experimental data farther from the port, as illustrated in Figure 3-3. This finding provides confidence that the turbulence modeling is correct, despite the limitation of the boundary condition at the port inflow.

[20] Since the centerline velocity of the applied turbulent velocity profile (u_c = 0.97 m/s) is greater than the mean velocity (u = 0.75 m/s) with which the turbulence intensity in Figure 3-43 is defined, the turbulence intensity at the port center as plotted in Figure 3-4 (i.e., the asymptotic value that intersects the vertical axis) is greater than 0.058 and can be calculated as, $I_c = I\,u_c/u$ = 0.075.

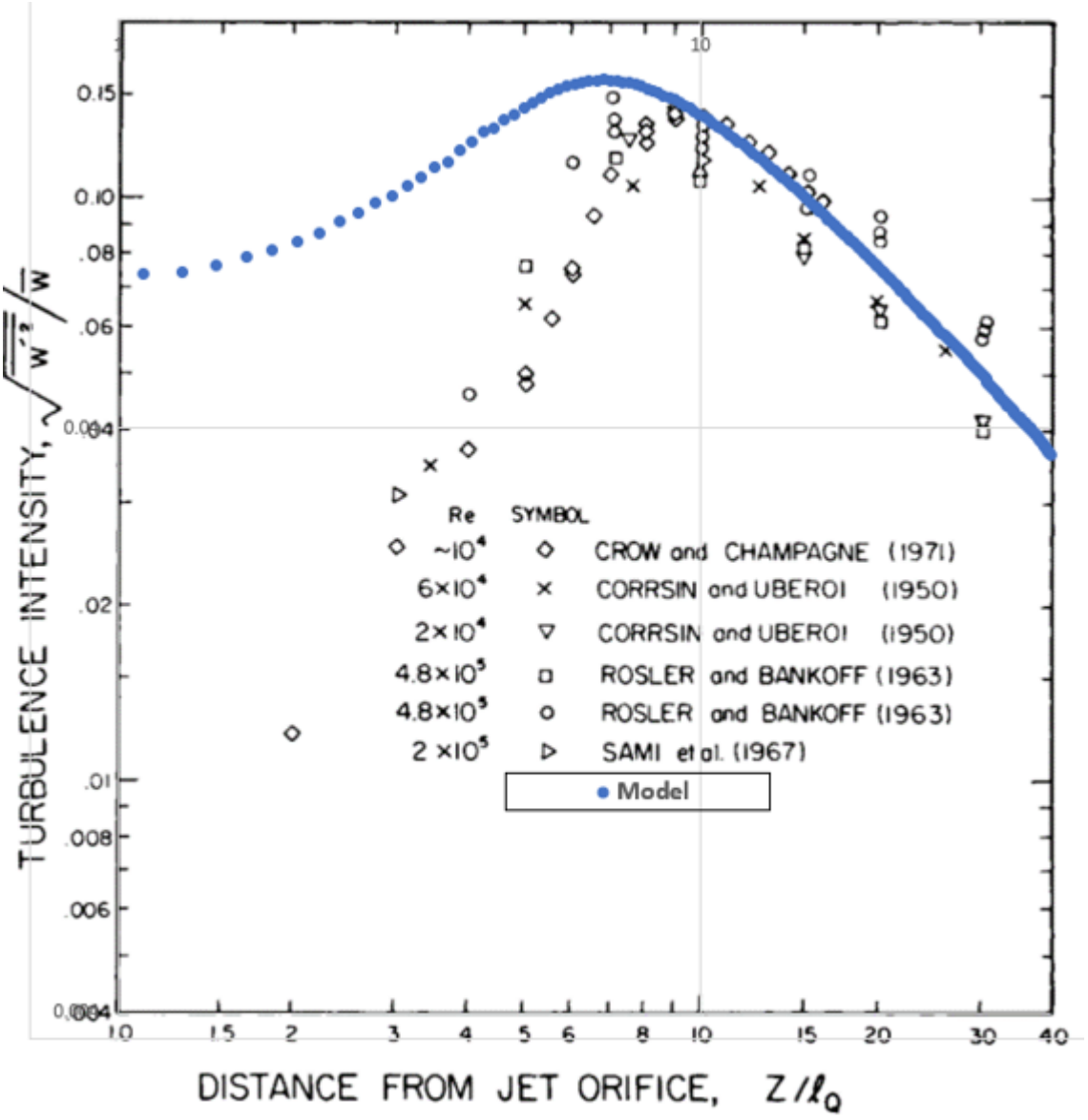

Figure 3-3. Turbulence intensity on the centerline of a round turbulent jet as a function of distance from the jet orifice. The background image is Figure 9.4 of Fischer et al. (1979). The results of the CFD model are superimposed in blue.

3.4.1.2 Centerline Velocity

The velocity along the jet centerline from the CFD model is compared to experimental measurements in Figure 3-4. The experimental measurements indicate a constant velocity within the ZFE (i.e., within about $7l_Q$), beyond which the centerline velocity decays inversely proportional to distance as the fully established jet flow spreads laterally. The CFD model results indicate normalized values within the ZFE that are higher than one due to the use of a turbulent velocity profile with a higher velocity on the centerline. The

values within the ZFE exhibit a slight decrease with distance from the port, compared to the constant values in the experiments. The "elbow" of the curve from the CFD results represents the end of the ZFE and occurs at approximately $5l_Q$ (or about 4.5d) from the jet orifice, compared with $7l_Q$ (or about 6.3d) for the experiments. The CFD results therefore underestimate the length of the ZFE by up to about two port diameters (i.e., 2d), and this manifests as a horizontal shift (rather than a vertical shift) in Figure 3-4. These differences may be a result of too much turbulent mixing in the ZFE (see Section 3.4.1.1), the use of non-uniform inflow velocity, or possibly inadequate grid resolution on the edges of the ZFE.

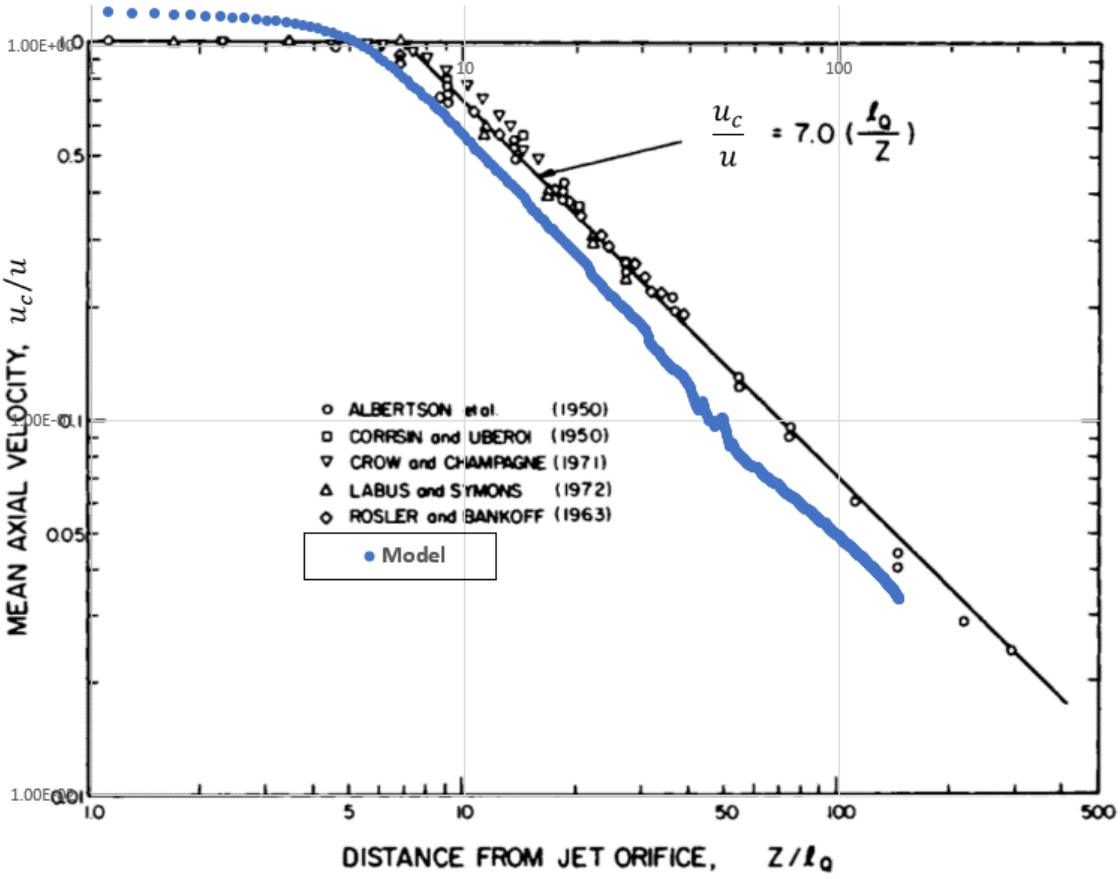

Figure 3-4. Time-averaged velocity on the centerline of a round turbulent jet as a function of distance from the jet orifice. The background image is adapted from Figure 9.5 of Fischer et al. (1979). The results of the current CFD model are superimposed in blue. Close to the jet orifice, the values exceed one due to the use of a turbulent velocity profile with centerline velocity (uc = 0.97 m/s) being greater than the mean velocity (u = 0.75 m/s). Plotting of the experiments assumes uniform outflow velocity across the port.

Beyond the ZFE, the decay rate of the centerline velocity closely matches that of the experiments, indicating that the far field spreading is accurately captured by the model.

This pattern is consistent with the good agreement of the turbulence modeling in that same region (Section 3.4.1.1).

3.4.1.3 Dilution

The relative volume flux within the jet from the CFD model is compared to experimental measurements in Figure 3-5. The relative volume flux represents the total volume flow rate of water within the jet, μ, normalized by the discharge volume flow rate, Q, and thus represents an average dilution within the plume. Results from the CFD model were calculated directly from the modeled centerline concentration, c_c, rather than attempting to perform an integral calculation across the plume.[21]

The CFD results indicate slightly higher volumes (i.e., more entrainment and dilution) within the initial stage of the ZFE (up to about $3l_Q$), which is consistent with the numerical findings on turbulence and velocity. Beyond this, the CFD results demonstrate excellent agreement with the experimental measurements, indicating that dilution is correctly modeled. Beyond about $50l_Q$, the CFD results begin to slightly underestimate the dilution, which may be a result of a lack of mesh refinement or interference from the top boundary.

[21] The centerline concentration, c_c, was converted to an average jet concentration, c_{av}, using $c_c/c_{av} \approx 1.4$ (Equation 9.26, Fischer et al. 1979). Then, equation 9.22 of Fischer et al. (1979) was re-written as $\mu/Q = c_0/c_{av}$ to calculate the relative volume flux, where $c_0 = 1$ is the discharge concentration.

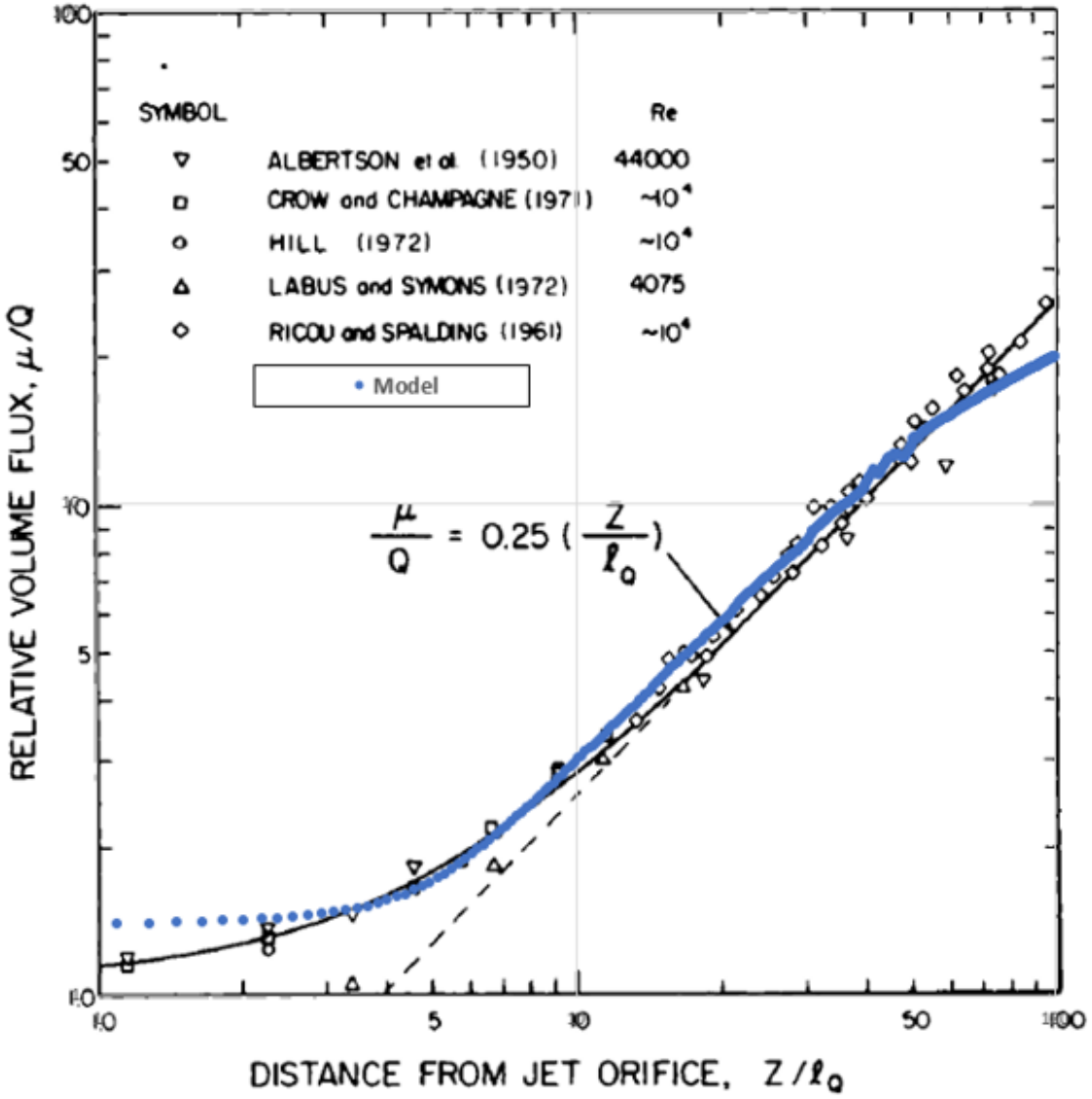

Figure 3-5. Average dilution for a round turbulent jet as a function of distance from the jet orifice. The background image is Figure 9.6 of Fischer et al. (1979). The results of the current CFD model are superimposed in blue.

3.4.2 Negatively Buoyant Jet Plume Scenarios

The results of the negatively buoyant jet CFD simulations (i.e., the *Fr* = 20 and *Fr* = 40 scenarios in Table 3-4) were validated by first benchmarking them against other CFD studies. Qualitative comparisons were then made to the experiments to confirm general trajectory and mixing characteristics, and importantly the ability of the model to replicate plume asymmetry that is driven by density differences.

3.4.2.1 Benchmark to CFD Studies

The simulated jet plume trajectory dimensions and dilutions were extracted from the CFD simulation and are presented in Table 3-5, together with the statistical summary (from Table 3-2).

Table 3-5. Summary of CFD model results (θ = 60°).

CFD Study	**Jet Plume Trajectory (x,z)**				**Dilutions, S**	
	$\frac{x_m}{dFr}$	$\frac{z_m}{dFr}$	$\frac{z_t}{dFr}$	$\frac{x_i}{dFr}$	$\frac{S_m}{Fr}$	$\frac{S_i}{Fr}$
Current study (Fr = 20)	1.3	1.2	1.7[22]	2.3	0.43	0.95
Statistics from Other CFD Studies (see Table 3-3)						
min	1.4	1.3	1.8	2.0	0.35	0.9
median	1.6	1.4	2.0	2.1	0.4	1.0
mean	1.6	1.5	1.9	2.3	0.4	1.0
max	1.8	1.7	2.0	2.67	0.4	1.1

The current CFD model results indicate slightly lower (<8%) trajectory dimensions for the plume centerline (x_m,z_m) than the minimums of other CFD studies.[23] This may be a direct result of underestimating the extent of the ZFE, as described in Section 3.4.1. Similarly, the height of the top of the plume, z_t, is underestimated (approximately 5% lower than the minimum of the other studies). The distance to the impact point, x_i, is close to the mean value of the other studies.

The modeled dilutions, S_m and S_i, are comparable to the other CFD studies, but it is noted that the CFD models substantially underestimated the dilution at the impact point, S_i (see Section 3.3.2).

Generally, the results of the current CFD model are acceptable when benchmarked against other CFD models, although the underestimation of the extent of the ZFE may lead to lower trajectory dimensions. This is further considered in Chapter 4, where the CFD model is used for lower values of *Fr*. This will have the effect of increasing the

[22] This value is lower than the value extracted from Figure 4 of Baum and Gibbes (2017), which may be due to measuring above the domain floor rather than the port.
[23] Note that Baum and Gibbes (2017) did not provide x_m or z_m, and as such those results are not included in the statistics (see Table 3-2).

portion of the jet/plume that is occupied by the ZFE, since the ZFE length scales with *d*, whereas the overall jet plume dimensions scale with *d Fr*.

3.4.2.2 Qualitative Comparisons to Experiments

There are generally less experimental data for negatively buoyant jets than for simple jets. Specifically, there appear to be no direct measurements of turbulence or velocity for 60° negatively buoyant jets. Instead, comparisons are limited to information based on concentrations within the jet plume, such as presented in experiments of Roberts et al. (1997).

3.4.2.2.1 General Trajectory and Mixing

The CFD model was developed to replicate the geometry of the experiments of Roberts et al. (1997). A qualitative comparison between the experiments and CFD simulation is made in Figure 3-6 and indicates general agreement of the plume shape. The CFD results do not resolve the details and thickness of the spreading layer (i.e., beyond the impact point) due to inadequate grid resolution.

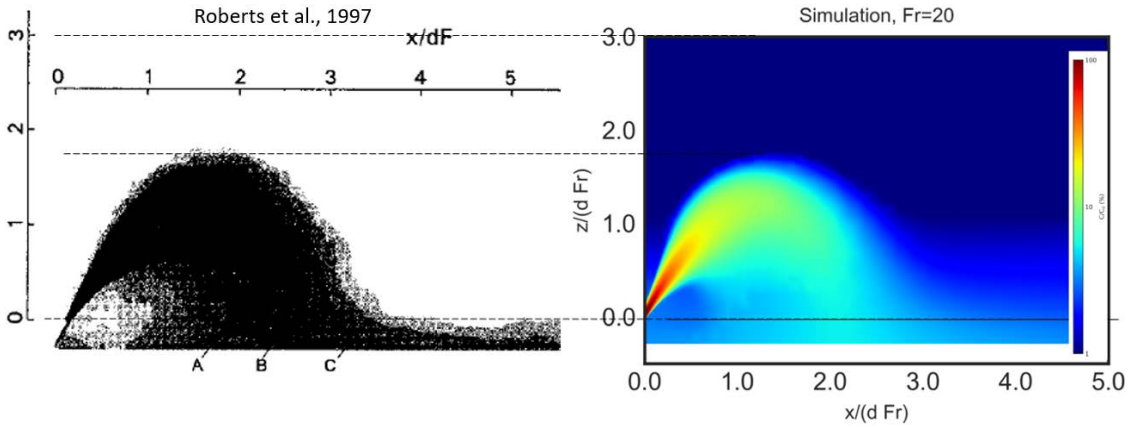

Figure 3-6. Comparison between experiments of Roberts et al. (1997) (left) and CFD simulation (right).

The experiments of Abessi and Roberts (2015) used a different port diameter and a different range of *Fr* and *Re* numbers (see Table 3-1). Results of the CFD model are compared to the experiments in Figure 3-7. The plume trajectory, and specifically the top of the plume, is underpredicted. This is consistent with the findings in Sections 3.3.2 and 3.4.2.1, and may be a result of underestimation of the extent of the ZFE. The spreading layer is not resolved by the simulation, but this is outside the region of interest. Despite the underprediction of the trajectories, the agreement of the simulated concentrations with the experiment is reasonable.

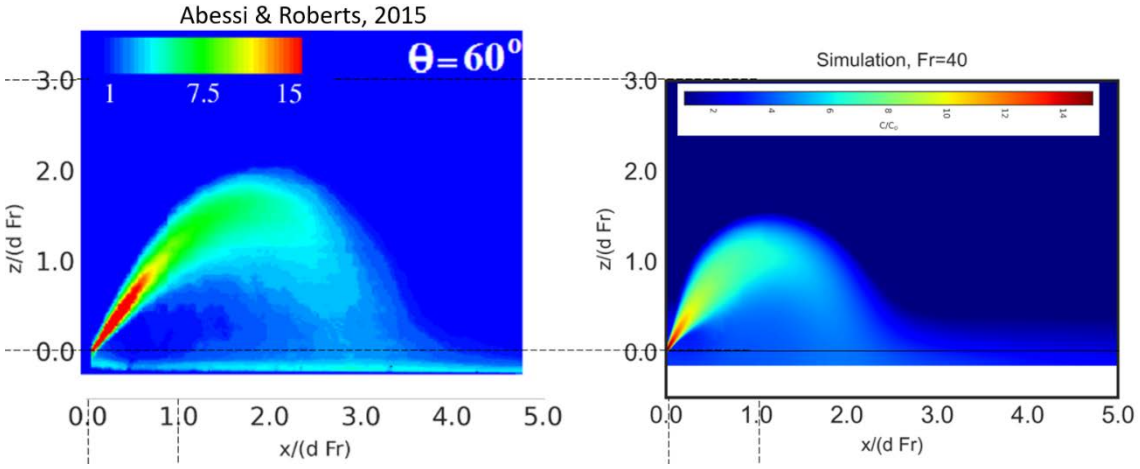

Figure 3-7. Comparison between experiments of Abessi and Roberts (2015) (left) and CFD simulation (right).

3.4.2.2.2 Plume Asymmetry

The asymmetry of a negatively buoyant plume is driven by the density differences, with additional mixing on the underside of the plume being enhanced by instabilities (Abessi and Roberts 2015). The ability of the model to replicate this feature was verified by comparisons to the experiments of Abessi and Roberts (2015) by extracting concentrations from the CFD simulation along three transects (Figure 3-8). The results are provided in Figure 3-9 and compare extremely well, with nearly symmetrical concentrations close to the port (left frames), and increasingly asymmetrical concentrations with higher concentrations on the underside of the plume farther from the port (center and right frames). This validates the ability of the CFD model to capture the mixing processes resulting from negative buoyancy.

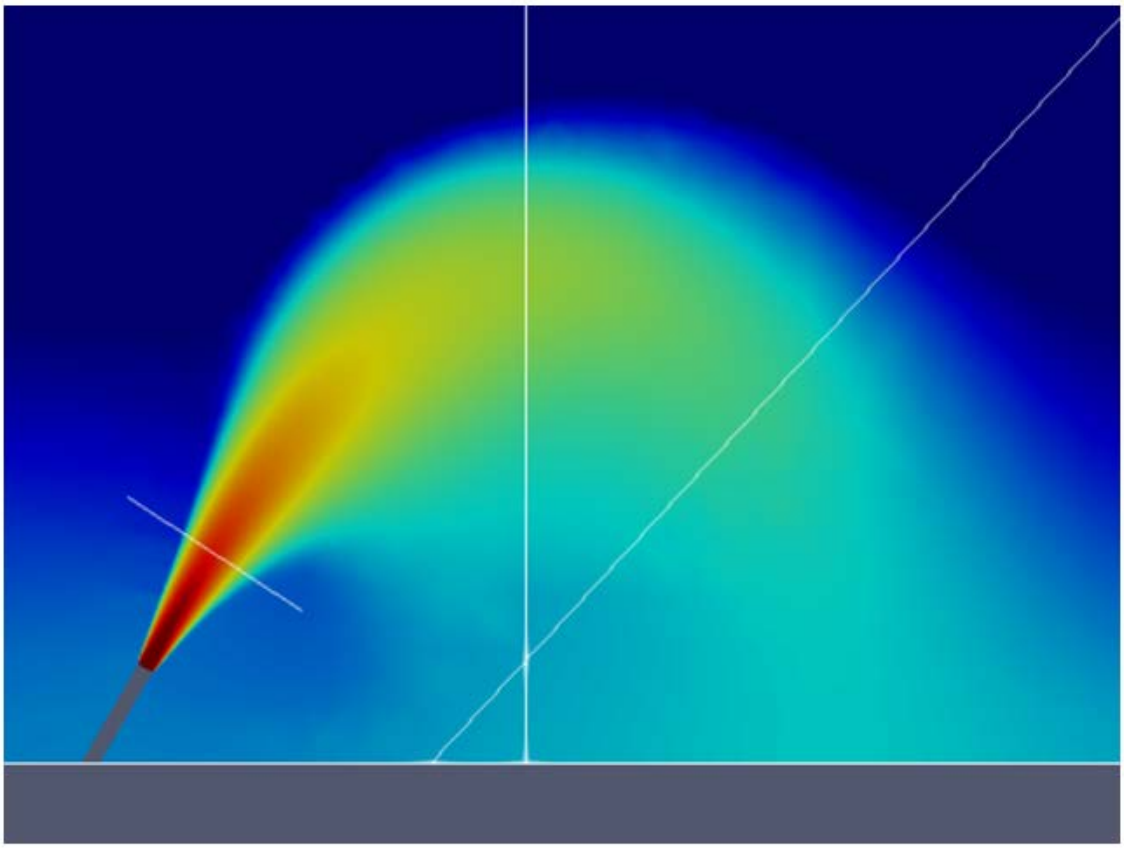

Figure 3-8. Locations of three transects sampled from the CFD simulation; near the port, through the location of maximum rise, and through the descending portion. Extracted concentrations are plotted in Figure 3-9.

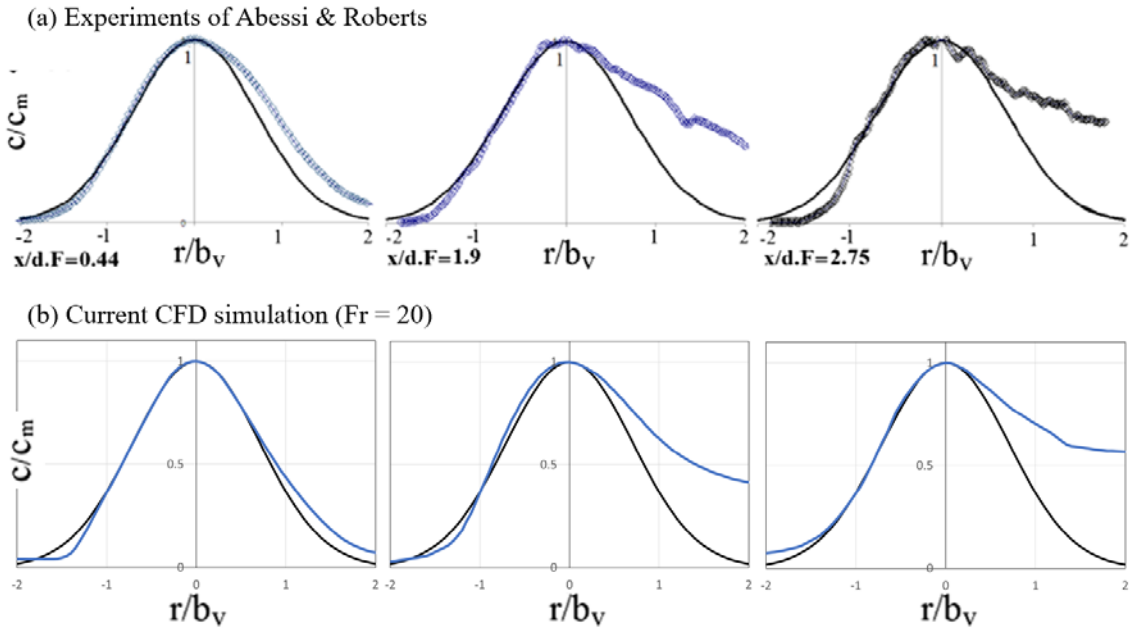

Figure 3-9. Comparison of concentration profiles taken at transects through the plume at close to the port (left frames), through the plume peak (center frames), and through the descending plume (right frames). Upper row is from experiments of Abessi and Roberts (2015), and lower row is from CFD model. Each frame includes a standard symmetrical Gaussian curve (in black) for reference.

3.5 Summary

A CFD model was developed to model negatively buoyant plumes at 60° vertical angles using the freely available and open-source OpenFOAM software. The model uses an adaptive mesh utility and a RANS k-ω SST turbulence model to enable efficient run-times (typically ~12 hours on a 16-core machine). Quantities relevant to turbulence can be extracted directly from the model or readily calculated, including the turbulent energy dissipation, ε.

The model was validated through comparisons to numerous experiments for both simple jets (i.e., neutrally buoyant) and negatively buoyant jets, as well as benchmarked against other CFD models.

Key results from the validation of the CFD model are:

- The model well replicates the simple jet, including:
  - Turbulence intensity on centerline.
  - Decay rate of centerline velocity.
  - Average dilution.

- The model underestimates the extent of the ZFE (i.e., the initial portion of the jet where the flow is developing).

- The model generally replicates the trajectory of a negatively buoyant jet/plume, but underestimates some dimensions:
    - Underestimation of trajectory dimensions may be due to underestimating the extent of ZFE.
    - This may have implications when the model is scaled for scenarios with lower densimetric Froude numbers.

- The model estimates of dilution for a negatively buoyant jet are comparable to other CFD studies but underestimate experimentally measured values.

- The model well replicates the asymmetry of concentrations within the plume.

4. CFD MODEL RESULTS

4.1 Background

Following the CFD model validation (as described in Chapter 3), this phase of the project re-evaluates the estimation of turbulence in the approach of Roberts (2018) that was based on a neutrally buoyant jet. Roberts derived the following estimate for the Kolmogorov length scale, η, along the centerline of a jet:

$$\eta = 0.24 Re^{\frac{3}{4}} x \qquad \text{Eq. 4-1}$$

where x is the distance from the port along the jet centerline and Re is the Reynolds number defined by Eq. 3-1.

Based on this analysis Roberts (2018) demonstrated that for practical ocean scale diffusers, the Kolmogorov length scale in the jet/plume up to the apex is likely to be substantially less than 1 mm, and potentially to be damaging to small scale organisms (see Chapter 2). The current research re-evaluates the estimate of the Kolmogorov length scale by using CFD to account for the negative buoyancy that may moderate the turbulence intensity (i.e., increase the Kolmogorov length scale) in the rising portion of the jet/plume. A previously developed and validated CFD model (see Chapter 3) is scaled-up from laboratory scale to ocean scale and used to quantify the turbulence and Kolmogorov length scale in the rising portion of the jet/plume.

This chapter summarizes the approach, results, and evaluation of turbulence properties.

4.2 Approach

A CFD model for negatively buoyant discharges was previously developed using OpenFOAM[24] software and based on RANS equations using the k-ω SST turbulence model (see Chapter 3). As described in Chapter 3, this model was validated against laboratory experiments that had comparatively small port diameters. Practical port diameters in ocean scale diffusers will typically be 10 to 100 times larger than those in the experiments, and therefore potentially have important scale effects (especially much larger Reynolds numbers). Therefore, the CFD model was required to be scaled-up from laboratory scale to ocean scale. Other changes to the model were also required, such as modifying the salinities, port velocities, and boundary conditions.

[24] https://www.openfoam.com/.

The scaled up CFD model is then used to evaluate the turbulence properties of the jet/plume for a range of port diameters and salinities to reflect ocean conditions that reflect conditions in California. The following sections present the simulation parameters, including discussion of how and why they were selected, followed by how they were implemented into the scaled-up CFD model.

4.2.1 Simulation Parameters

The parameters used in the simulation are defined in Table 4-1. Run 0 is the validation simulation described in detail in Chapter 3, with a small port diameter. Runs 1 through 9 are larger scale simulations developed to assess practical sized ocean diffusers with negatively buoyant discharges under a range of conditions, while Run 10 is a neutrally buoyant simulation used for comparison purposes only. Simulations were done only for nozzle angles of 60° as this is the optimum angle for dense jet diffusers (Roberts 2018).

For Runs 1 through 9, the primary parameters selected are the port diameter, d, ambient salinity, S_a (and corresponding density ρ_a), and discharge salinity, S_0 (and corresponding density, ρ_0). From these primary parameters, all other parameters are calculated under the assumption that the Ocean Plan requirement of meeting the 2 ppt increment is satisfied at the end of the near field (Roberts 2018). This determines the required densimetric Froude number[25], Fr, for the specified salinity increment, $\Delta S = S_0 - S_a$, and where Fr is defined by Eq. 3-2. The definition of Fr (i.e., Eq. 3-2) is then used to calculate the port velocity, u, required to meet the dilution requirements. The Reynolds number, Re, is then calculated from Eq. 3-1 using kinematic viscosity for water, $\nu = 10^{-6}$ m^2/s.

The port sizes and salinities in Table 4-1 were selected to represent a range of conditions appropriate to ocean-scale diffusers in California conditions. These are discussed briefly below.

4.2.1.1 Runs 1 through 4

These simulations were selected to evaluate the effect of port size, d, with ranges from 0.05 m (about 2 inches) to 0.4 m (about 16 inches) being approximately 10 to 100 times larger than that in the validation simulation (Run 0). The primary effect of varying this parameter is to substantially increase Re by up to three orders of magnitude compared

[25] The densimetric Froude number represents the ratio of momentum to buoyancy effects. Higher Fr results in higher momentum and a longer plume trajectory, resulting in more dilution (see, e.g., Roberts et al. 1997, Besalduch et al. 2013, and Abessi and Roberts 2015).

with the validation run, which is important for the turbulence properties given the dependence of η on *Re* (see Eq. 4-1).

4.2.1.2 Run 5

This simulation modified Run 2 to evaluate the effect of variations in ambient salinity. For most simulations, a typical ocean salinity, S_a = 33 ppt, was assumed for ambient ocean conditions. In Run 5, the ambient and discharge salinities were both increased by 1 ppt from the Run 2 values such that the salinity increment, ΔS = 33 ppt, was the same in both Run 5 and Run 2. This resulted in Run 5 having the same values of *Fr* and *Re* as Run 2 (Table 4-1). Based on dimensional analyses, it is anticipated that the results of Run 5 would be the same as for Run 2. The objective of this simulation is to confirm that hypothesis, which if true enables fewer simulations to fully evaluate variations in both ambient and discharge salinities, since only the salinity increment influences the results.

Table 4-1. Simulation parameters.

Run#	**Description**	**Port Diameter,** d (m)	**Ambient Salinity,** S_a (ppt)	**Discharge Salinity,** S_0 (ppt)	**Salinity Increment,** ΔS (ppt)	**Ambient Density,** ρ_a (kg/m^3)	**Discharge Density,** ρ_0 (kg/m^3)	**Froude Number,** Fr	**Port Velocity,** u (m/s)	**Reynolds Number,** Re
0	Validation	0.00429	0	33	33	997	1030	20	0.75	3,200
1	Vary Re – 1	0.05	33	66	33	1,023.2	1,048.6	6.35	0.70	33,000
2	Vary Re – 2	0.1	33	66	33	1,023.2	1,048.6	6.35	0.99	93,400
3	Vary Re – 3	0.2	33	66	33	1,023.2	1,048.6	6.35	1.40	264,300
4	Vary Re – 4	0.4	33	66	33	1,023.2	1,048.6	6.35	1.98	747,400
5	Vary S_a	0.1	34	67	33	1,024.0	1,049.4	6.35	0.99	93,400
6	Vary S_0 – 1	0.1	33	60	27	1,023.2	1,044.0	5.19	0.73	69,100
7	Vary S_0 – 2	0.1	33	72	39	1,023.2	1,053.3	7.50	1.27	120,200
8	Blended – 1	0.1	33	50	17	1,023.2	1,036.3	3.27	0.37	34,500
9	Blended – 2	0.1	33	40	7	1,023.2	1,028.6	1.35	0.10	9,100
10	Neutrally Buoyant*	0.1	33	33	0	1,023.2	1,023.2	undefined	0.99	93,400
* The neutrally buoyant simulation is used for comparison purposes only. The current project only considers negatively buoyant jet plumes.										

4.2.1.3 Runs 6 and 7

These simulations modified Run 2 to evaluate the effect of variations in discharge salinity, S_0. However, provided that Run 5 confirms the hypothesis described above, these simulations effectively evaluate variations in the salinity increment, ΔS, and as such can account for variations in both discharge salinity (e.g., different operations and concentration factors) and ambient salinity (e.g., naturally occurring variation). Run 6 had a lower salinity increment, and therefore requires a lower *Fr* to meet the 2 ppt dilution requirements, resulting in a lower velocity, *u*, and lower *Re* (Table 4-1). Conversely, Run 7 had a higher salinity increment and higher *Fr*, *u*, and *Re* (Table 4-1).

4.2.1.4 Runs 8 and 9

These simulations modified Run 2 to evaluate the effect of blending the discharge brine stream with a freshwater source (e.g., wastewater). This has the effect of substantially decreasing S_0 and ΔS.[26] This resulted in much lower *Fr* being required to meet the 2 ppt dilution requirement, resulting in much lower velocities, *u*, and lower *Re* (Table 4-1). These calculations assumed that the blending ratios are maintained throughout the entire operation range, whereas in practice a diffuser would typically need to accommodate both blended discharges and brine-only discharges. Since the required dilutions would be governed by the brine-only discharge, higher velocities would likely be required for practical diffuser designs. Therefore, the parameters for Runs 8 and 9 may not be realistic, but the simulations are included here for completeness and to enable an assessment of a wider parameter space (i.e., at low values of *Fr*).

4.2.1.5 Run 10

This simulation modified Run 2 by setting the discharge salinity to be the same as the ambient salinity to result in a neutrally buoyant discharge. The current project only considers negatively buoyant discharges, but this simulation was conducted for comparison purposes since it can be used to compare results to Eq. 4-1 and to contrast with the negatively buoyant simulations that are of interest (see Section 4.4.2).

4.2.2 Implementation into CFD Model

Runs 1 through 10 in Table 4-1 were implemented by modifying the CFD model used for the validation simulation (Run 0). The following summarizes the modifications that were

[26] In many blended scenarios, there may be enough freshwater such that the plume is positively buoyant when discharged into the ocean. However, this project only examines negatively buoyant discharges and therefore the salinity increment, ΔS, is always assumed positive.

made to the validation simulation. Additional details of the validation model (Run 0) set-up are available in Chapter 3.

4.2.2.1 Scaling up the Domain

Runs 1 through 4 evaluate a range of different port sizes that are 10 to 100 times larger than in Run 0. This was achieved in OpenFOAM by scaling up the entire computational domain, including the nozzle geometry and the grid, so that the desired port size was achieved. The resulting domains are illustrated in Figure 4-1 for Runs 2 and 4 as examples. The domain size for Run 2 has a length of 55.9 m, width of 18.9 m, and height of 14.2 m, with the domain for Run 4 being four times larger.

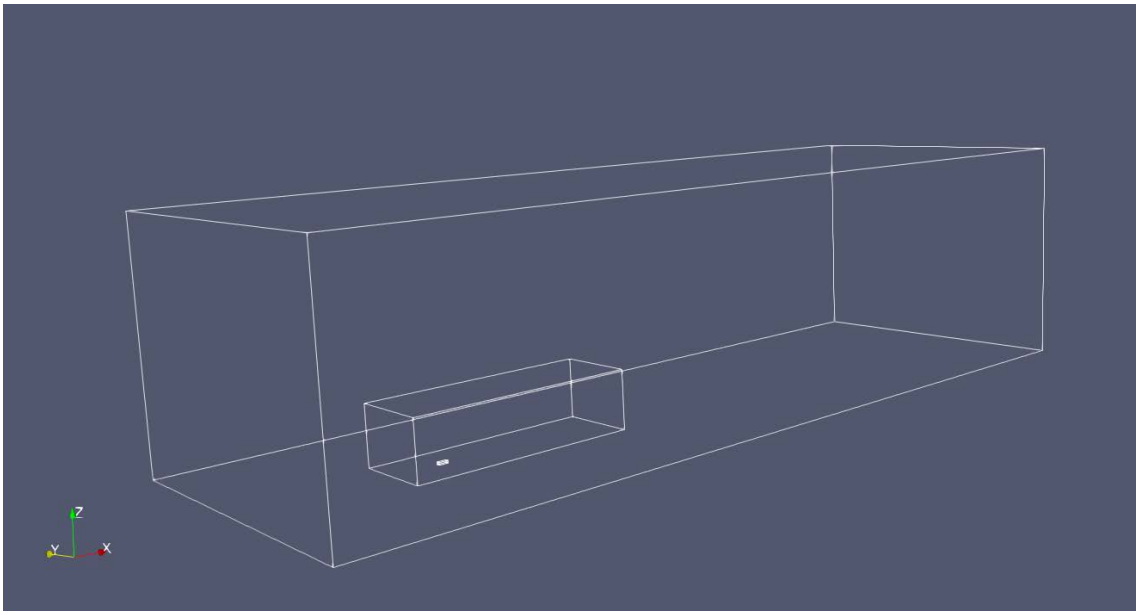

Figure 4-1. Computational domains for Run 0, Run 2, and Run 4. The domain for Run 2 was achieved by scaling up the Run 0 domain (with d = 0.00429 m) by 0.1/0.00429 = 23.3 times such that the port diameter of d = 0.1 m was obtained. The domain for Run 4 was scaled up by an additional factor of 4 (i.e., scaling Run 0 by 93.2 times) such that the port diameter of d = 0.4 m was obtained.

4.2.2.2 Port Inflow Velocity and Turbulence

The port velocities, *u*, in Table 4-1 and in Eqs. 3-1 and 3-2 are average velocities across the port area. Following Baum and Gibbes (2017) and being consistent with Run 0 (see Chapter 3), a turbulent velocity profile was implemented as a prescribed velocity boundary condition on the port face. This assumed a power-law profile, with the exponent (i.e., shape) being a function of *Re* (see Baum and Gibbes 2017). In addition, the turbulence intensity, *I*, of the port inflow is specified and is also a function of *Re* (see Baum and Gibbes 2017). Values for the turbulence intensity implemented in the simulations are provided in Table 4-2.

Table 4-2. Simulation port turbulence intensity.

Run #	Description	Port Diameter, d (m)	Port Velocity, u (m/s)	Reynolds Number, Re	Turbulence Intensity, I (%)
0	Validation	0.00429	0.75	3,200	5.8
1	Vary Re – 1	0.05	0.70	33,000	4.4
2	Vary Re – 2	0.1	0.99	93,400	3.8
3	Vary Re – 3	0.2	1.40	264,300	3.4
4	Vary Re – 4	0.4	1.98	747,400	3.0
5	Vary S_a	0.1	0.99	93,400	3.8
6	Vary S_0 – 1	0.1	0.73	69,100	4.0
7	Vary S_0 – 2	0.1	1.27	120,200	3.7
8	Blended – 1	0.1	0.37	34,500	4.3
9	Blended – 2	0.1	0.10	9,100	5.1
10	Neutrally Buoyant	0.1	0.99	93,400	3.8

4.2.2.3 External Boundary Conditions

Run 0 was set-up to model the laboratory experiments that were conducted in a tank and therefore included solid boundaries to represent the tank walls. Specifically, these walls were implemented on the “front” and “back” boundaries, while a small inflow velocity was implemented on the “left” boundary to improve the numerics (see Chapter 3). The “right” boundary used an outflow condition to account for the truncation of the computational domain (i.e., the full length of the experimental tank was not modeled).

To better represent open ocean conditions for Runs 1 through 10, the wall boundary conditions on the “front” and “back” were changed to zero gradient to allow flow through. The “left” and “right” boundaries were kept the same as for Run 0.

4.2.2.4 Mesh Refinement Parameters

Following Baum and Gibbes (2017), the CFD simulations used an adaptive mesh that added cells in regions of high concentration gradients. Validating the CFD model against experiments resulted in some adjustment of the parameters that control the adaptive meshing (see Chapter 3). It was found that additional adjustments of these parameters were required for the scaled-up simulations to avoid regions with too many cells.

Table 4-3. Mesh adjustment parameters.

Run #	Description	Port Diameter, d (m)	Relative Tolerance	Absolute Tolerance	Number of Refinement Levels
Baum and Gibbes (2017)		0.00429	0.25	0.03	8
0	Validation	0.00429	0.02	0.02	8
1	Vary *Re* – 1	0.05	0.06	0.06	8
2	Vary *Re* – 2	0.1	0.06	0.06	8
3	Vary *Re* – 3	0.2	0.08	0.08	8
4	Vary *Re* – 4	0.4	0.10	0.10	8
5	Vary S_a	0.1	0.06	0.06	8
6	Vary S_0 – 1	0.1	0.06	0.06	8
7	Vary S_0 – 2	0.1	0.06	0.06	8
8	Blended – 1	0.1	0.06	0.06	8
9	Blended – 2	0.1	0.06	0.06	8
10	Neutrally Buoyant	0.1	0.06	0.06	8

4.3 CFD Results

The following presents the CFD model results as plots of simulated time-averaged concentration and velocity on a slice through the plume center. The axes of the plots are normalized by *dFr*, which is the relevant length scale for the jet/plume geometry (e.g., Roberts et al. 1997, Besalduch et al. 2013, and Abessi and Roberts 2015), while the concentrations and velocities are normalized by the values at the port. Turbulence metrics are presented and described in Section 4.4.

4.3.1 Runs 1 through 4

Plots of simulated concentration and velocities for Runs 1 through 4 are presented in Figure 4-2 and Figure 4-3, respectively. Results indicate generally similar normalized trajectories, concentrations, and velocities among all the simulations[27], confirming that results are scaling as expected. Microscale turbulence properties are not anticipated to

[27] Run 4 (d = 0.4 m) results indicate slightly lower plume height than the other three simulations, which may in part be due to requiring less mesh refinement (see Section 4.2.2.4).

follow the same scalings as the trajectories, concentrations, and velocities and are instead anticipated to depend on *Re*. This is examined in Section 4.4.

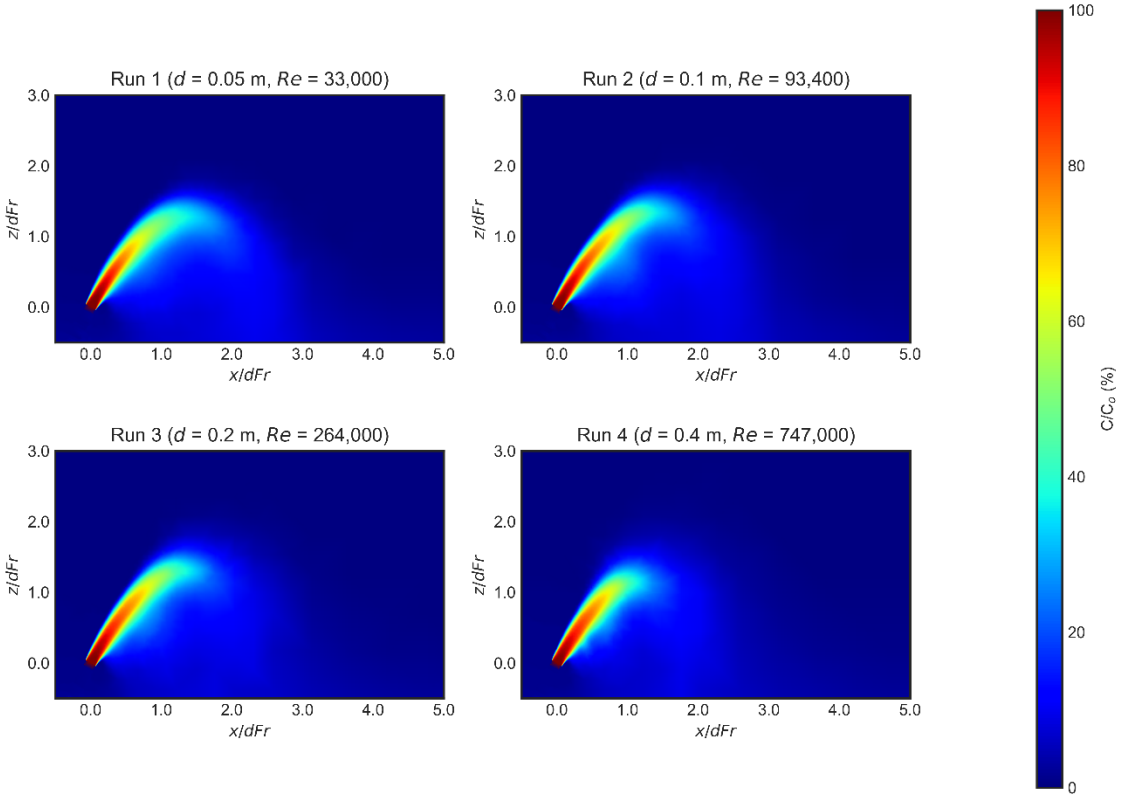

Figure 4-2. Simulated normalized concentrations for Run 1 (upper left), Run 2 (upper right), Run 3 (lower left), and Run 4 (lower right) plotted on a vertically oriented slice through the jet plume center with axes normalized by dFr. These simulations evaluate the effect of increasing the port diameter, d, which has the primary effect of increasing the Reynolds number, Re.

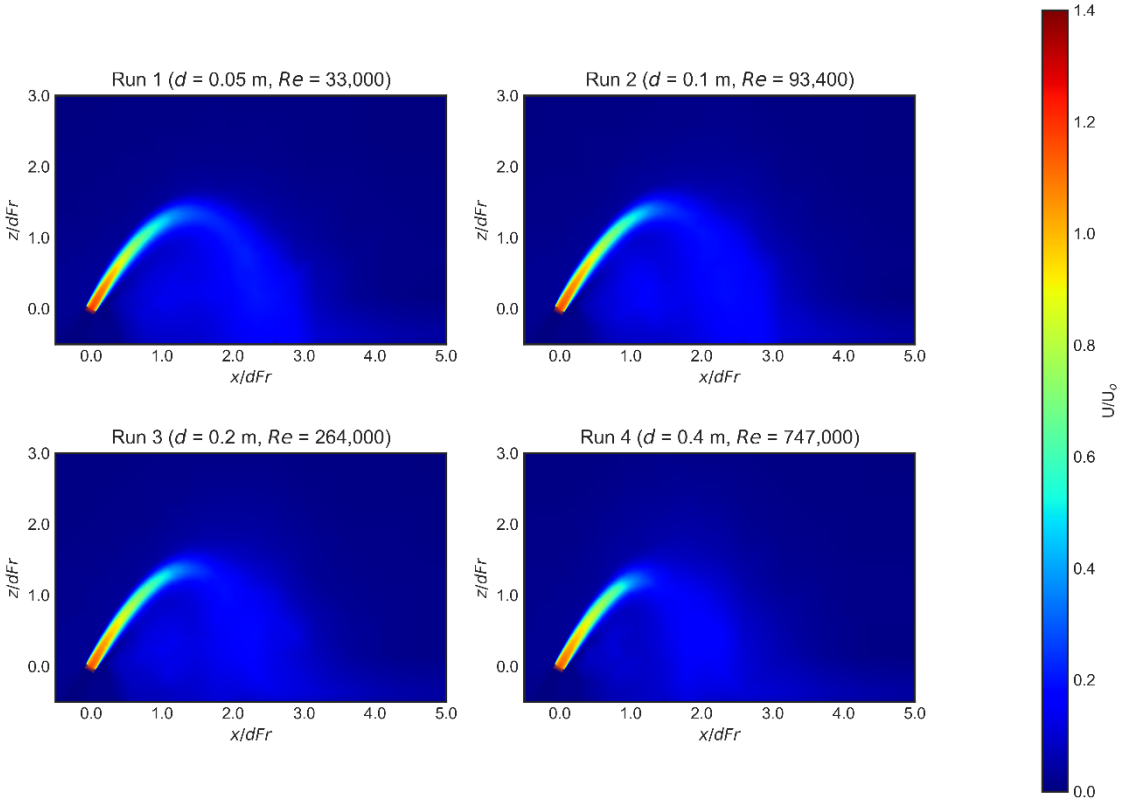

Figure 4-3. Simulated normalized velocities for Runs 1 through 4 (diameters as in Figure 4-2) plotted on a slice through the jet/plume center with axes normalized by dFr. These simulations evaluate the effect of increasing the port diameter, d, which has the primary effect of increasing the Reynolds number, Re.

4.3.2 Run 5

Plots of simulated normalized concentrations and velocities are presented in Figure 4-4 for Run 5. The figure also includes results for Run 2 for comparison purposes. Normalized trajectories, concentrations, and velocities of Run 5 and Run 2 appear almost identical in the figures, confirming the hypothesis that it is only the salinity increment, ΔS, and not independently the ambient or discharge salinities that govern behavior (see Section 4.2.1.2). Given the similarities between Run 5 and Run 2 (including identical *Re*), the turbulence properties for Run 5 are not evaluated.

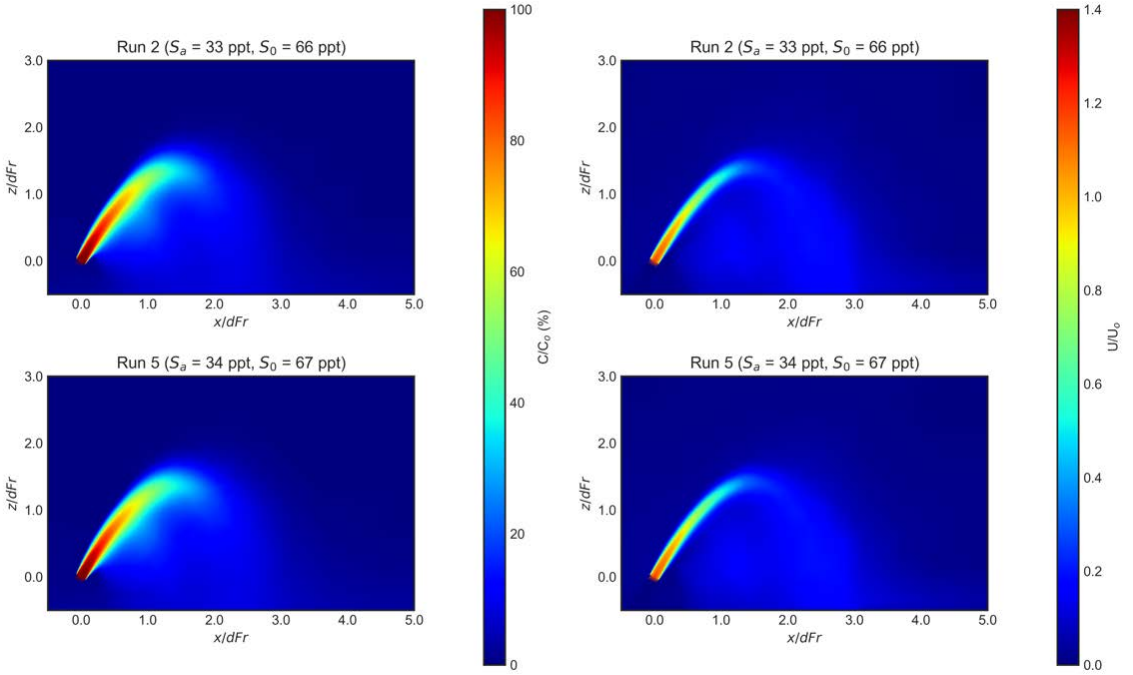

Figure 4-4. Simulated normalized concentrations (left) and velocities (right) for Run 2 (upper) and Run 5 (lower) plotted on a slice through the jet plume center with axes normalized by dFr. Run 5 is the same as Run 2, except for modified ambient and discharge salinities. The salinity increment is the same, ΔS = 33 ppt, for both simulations.

4.3.3 Runs 6 and 7

Plots of simulated normalized concentrations and velocities for Runs 2, 6, and 7 are presented in Figure 4-5. The jet plume normalized trajectories and normalized velocities are similar between the simulations, confirming that the results are scaling as expected. The normalized concentrations indicate differences between the simulations, with Run 6 (*Fr* = 5.19) having the highest concentrations, followed by Run 2 (*Fr* = 6.35) and then Run 7 (*Fr* = 7.50). This is a result of the dilution (i.e., the inverse of the concentration) at fixed points in the jet plume (e.g., the apex) being proportional to *Fr* (e.g., see Chapter 3). The result is that cases with lower *Fr* have higher concentrations, and vice-versa.

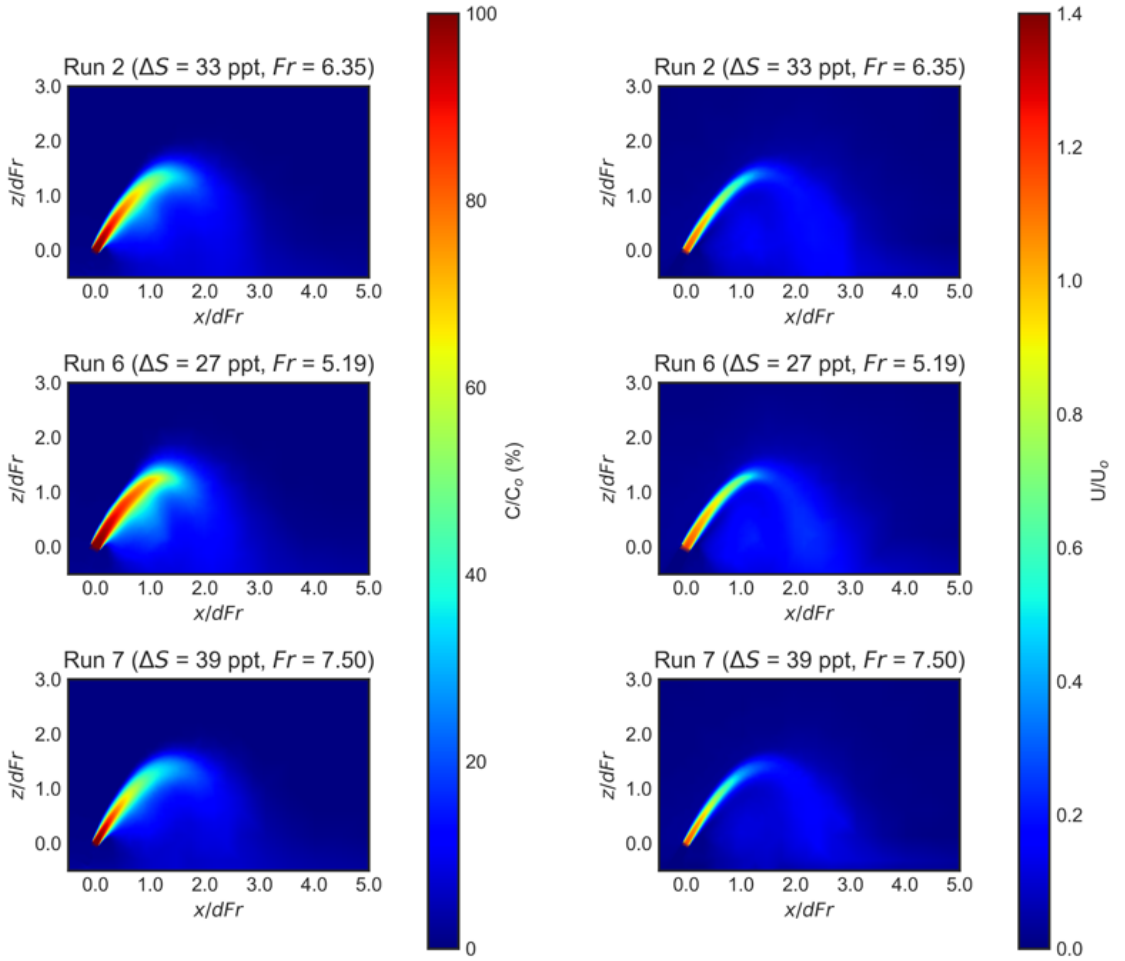

Figure 4-5. Simulated normalized concentrations (left) and velocities (right) plotted on a slice through the jet plume center with axes normalized by dFr for Runs 2 (upper), 6 (middle), and 7 (lower). The simulations have different salinity increments, ΔS, which results in different values of Fr.

4.3.4 Runs 8 and 9

Plots of simulated normalized concentrations and velocities for Runs 2, 8, and 9 are presented in Figure 4-6. In contrast to Runs 1 through 7, the normalized trajectories and velocities appear to be quite different in Runs 8 and 9. This indicates that the scaling laws do not hold true at low values of *Fr*, likely as a result of the plume trajectory dimensions becoming smaller and comparable to the port diameter.

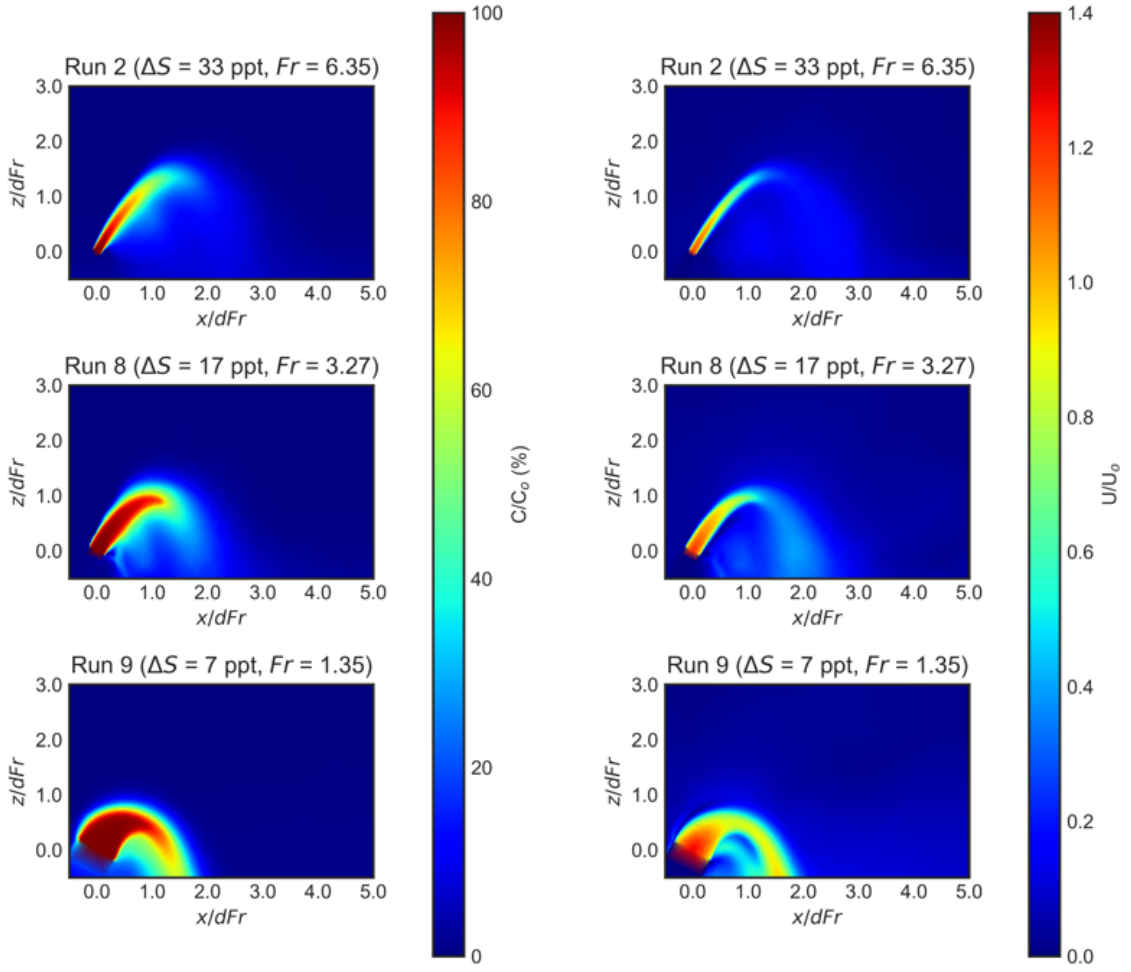

Figure 4-6. Simulated normalized concentrations (left) and velocities (right) plotted on a slice through the jet plume center with axes normalized by dFr for Runs 2 (upper), 8 (middle), and 9 (lower). The simulations have different blends, with freshwater resulting in much lower salinity increments, ΔS, and Froude numbers, Fr. Note that the normalization of the axes by dFr makes the port diameter appear larger in the figures as Fr is decreased. Each simulation has the same port diameter, d = 0.1 m, as is better illustrated in Figure 4-7.

The results are better visualized in Figure 4-7, where the axes are normalized by the port diameter, *d*, rather than *dFr*. Runs 8 and 9 have substantially smaller trajectories due to the lower port velocities (Table 4-1). In particular, Run 9 has a trajectory height and horizontal distance to the apex that are less than about one port diameter. As discussed in Section 4.2.1.4, the low port velocities of Runs 8 and 9 are not realistic for a practical diffuser design, and as such the turbulence properties are not evaluated.

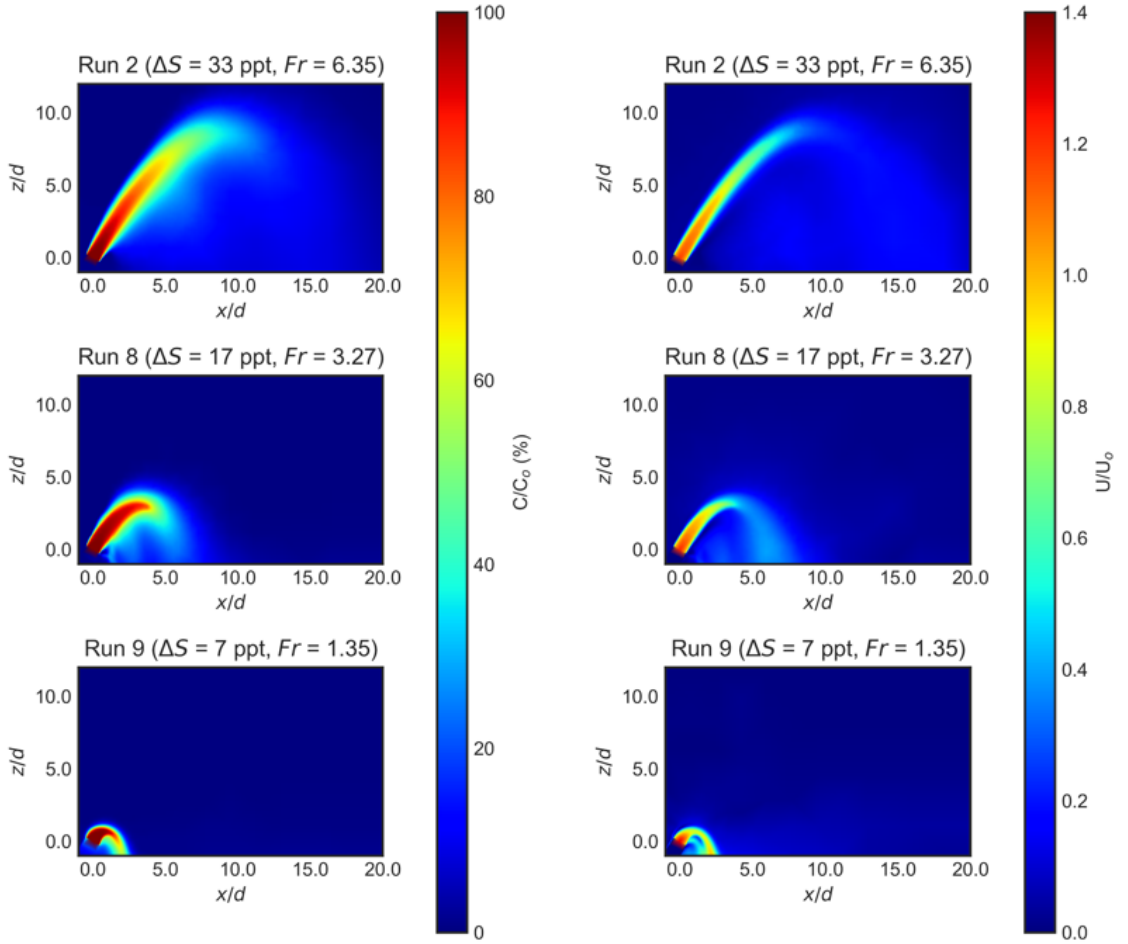

Figure 4-7. Same results as presented in Figure 4-6 except with axes normalized by d instead of dFr. This figure better illustrates the vastly different plume trajectories.

4.4 Turbulence Metrics

The previous section presented simulated concentrations and velocities. The goal of the current project is to quantify turbulence properties to refine previous estimates of the Kolmogorov length scale, η, (Roberts 2018) and potentially relate those refined estimates to previous biological studies (Chapter 2). This section summarizes how η may be calculated from the CFD results, and then presents results along the jet plume centerline, including comparisons to neutrally buoyant simulations and the estimate of Roberts (2018). Finally, results are provided along streamlines throughout the rising portion of the plume.

4.4.1 Calculating Kolmogorov Length Scale

The CFD simulations used the *k*-ω SST turbulence model (see Chapter 3), where *k* is the turbulent kinetic energy and ω is the specific dissipation (e.g., Ferziger and Peric 2002). Values for *k* and ω are available throughout the simulation and may be used to calculate η using relatively straightforward algebraic equations.

First, the dissipation, ε, is calculated as (e.g., Ferziger and Peric 2002):

$$\varepsilon = 0.09\,\omega k \qquad \text{Eq. 4-2}$$

From the dissipation, the Kolmogorov length scale is then calculated as (Tennekes and Lumley 1972):

$$\eta = \left(\frac{\nu^3}{\varepsilon}\right)^{0.25} \qquad \text{Eq. 4-3}$$

4.4.2 Results on Centerline

Results from the CFD simulations were extracted along the jet plume centerline and used to calculate η. This is plotted as a function of centerline distance from the port in Figure 4-8.

Included on Figure 4-8 is the relation from Eq. 4-1 as derived by Roberts (2018), with *Re* chosen to match Run 10 (neutrally buoyant). The growth rate of η with distance from the port in Run 10 is about two times greater than Roberts (2018), while the values of η near the port are considerably greater. These differences near the port are expected, since Roberts (2018) is derived for the far field, beyond the zone of flow establishment (ZFE) and potential core, which is less turbulent (i.e., has larger values of η). The difference in the far field is also not unexpected given other approximations and assumptions made in the "order of magnitude" analyses of Roberts (2018). In general, the CFD results for Run 10 agree with the approach of Roberts (2018) in predicting a linear growth of η with distance from the port in the far field (i.e., Eq. 4-1).

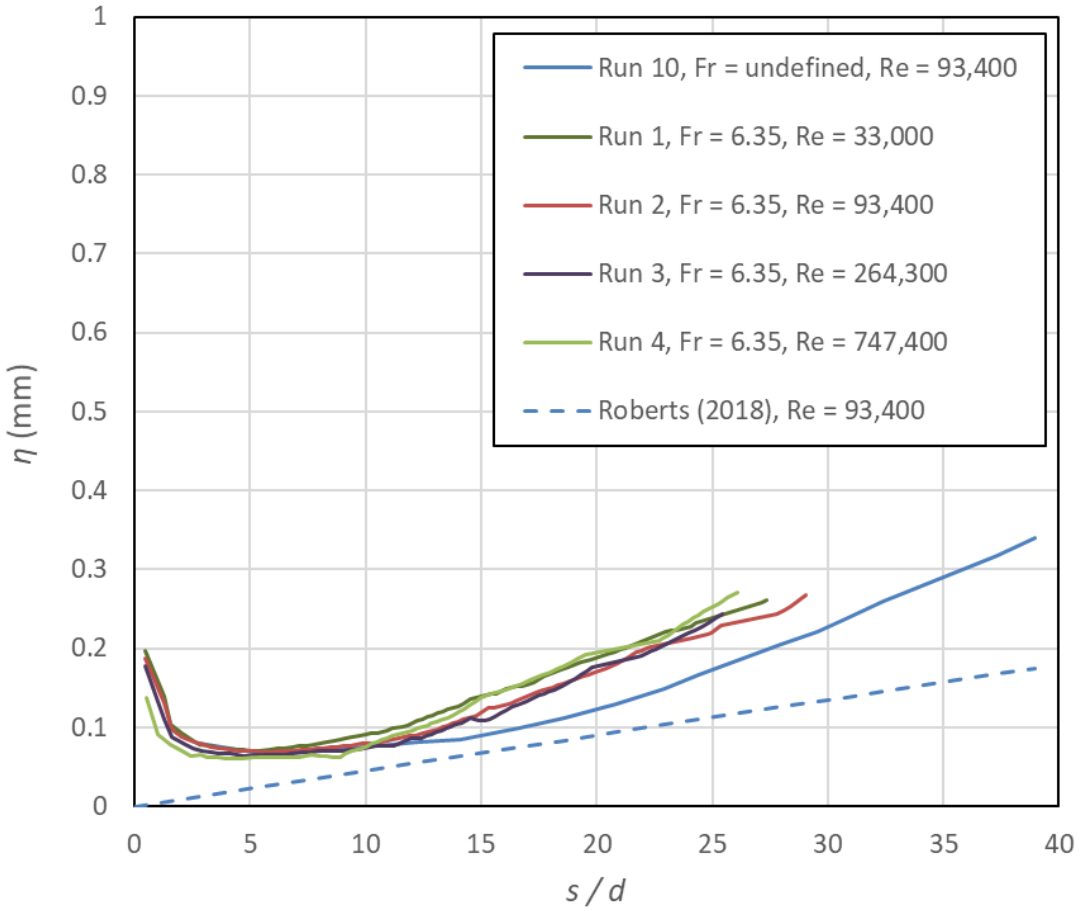

Figure 4-8. Calculated Kolmogorov scale, η, as a function or distance, s, along the jet plume centerline normalized by the port diameter, d.

Comparisons of Runs 1 through 4 with Run 10 in Figure 4-8 indicate that the negative buoyancy is moderating the turbulence as hypothesized, resulting in larger values of η. However, the values of η are still much smaller than the threshold for mortality of 1 mm suggested by Roberts (2018).

4.4.3 Results on Streamlines

The analyses of the centerline results were expanded by repeating the calculations along streamlines up to the apex of the jet plume. This accounts for organisms that are entrained only into the edges of the jet plume, which has larger values of η than the centerline.

Streamlines were created within ParaView[28] by integrating the velocity field backwards in time from a series of "seeds" placed near the jet plume apex. Relevant variables (including k and ω) were extracted from the CFD simulations along each of the streamlines, and Eqs. 4-2 and 2-1 were used to calculate η.

Results for Runs 1 through 4 are plotted in Figure 4-9 through Figure 4-12, respectively. The plots illustrate that the entrainment into the jet plume up to the apex is primarily from behind and above the port. Far from the jet plume, the values of η are larger and generally greater than 1 mm (as illustrated by the brown coloring). Within the plume, the values of η are smaller and less than 1 mm (as illustrated by the green coloring).

While the results for Runs 1 through 4 look similar, it is noted that the lengths of the axes are quite different (i.e., smallest for Run 1 and largest for Run 4) since the plume size scales with port diameter, d. Additionally, the 1 mm delineation (i.e., the delineation between the brown and green colors) is different for each of the simulations. Specifically, in Run 1 the green color is confined relatively closely to the jet/plume, while for Runs 2, 3, and 4 the green color progressively expands farther from the jet/plume. This is expected since values of *Re* increase progressively from Run 1 to Run 4 by more than 20 times (see Table 4-1). Higher *Re* results in more turbulence and therefore lower η is expected[29].

[28] ParaView is an open-source, multi-platform data analysis and visualization application (https://www.paraview.org/).
[29] This relation is supported by Eq. 4-1, which was derived for the centerline of a neutrally buoyant jet.

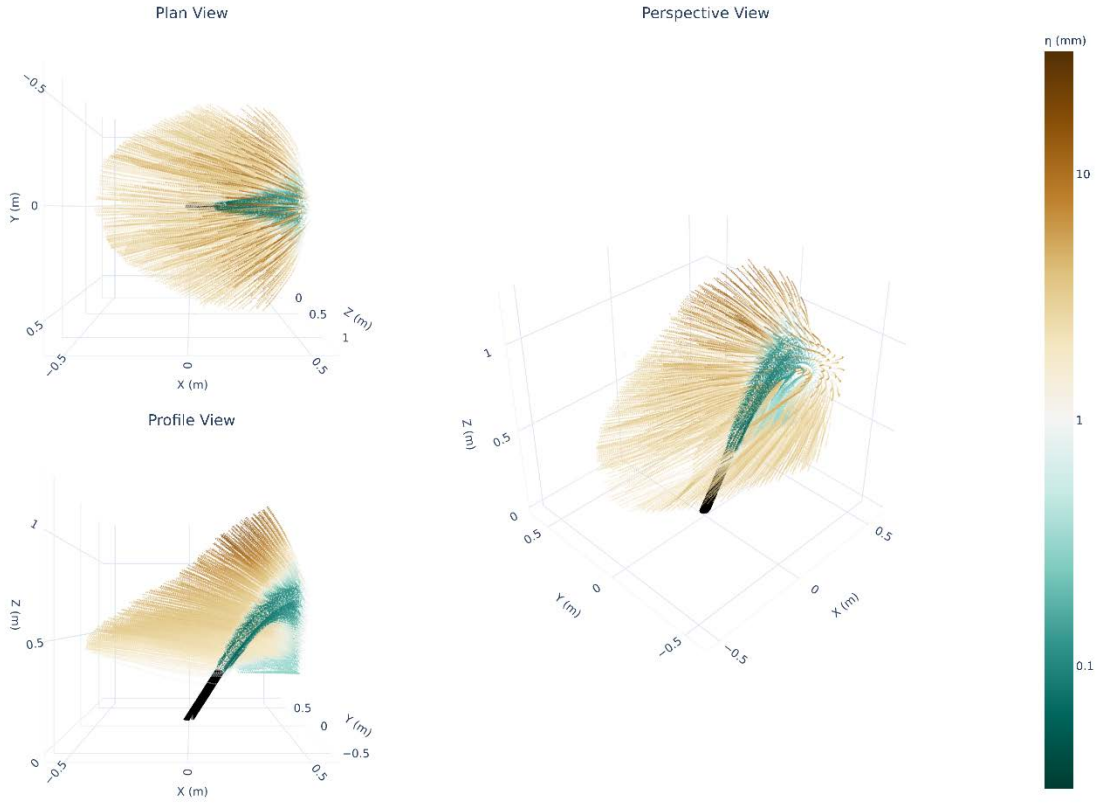

Figure 4-9. Three-dimensional streamlines up to the apex of the jet plume for Run 1 in plan view, profile view, and perspective view. Streamlines are colored by the value of η, with green shades indicating values less than 1 mm and brown shades indicating values greater than 1 mm. The port geometry is represented as a black cylinder.

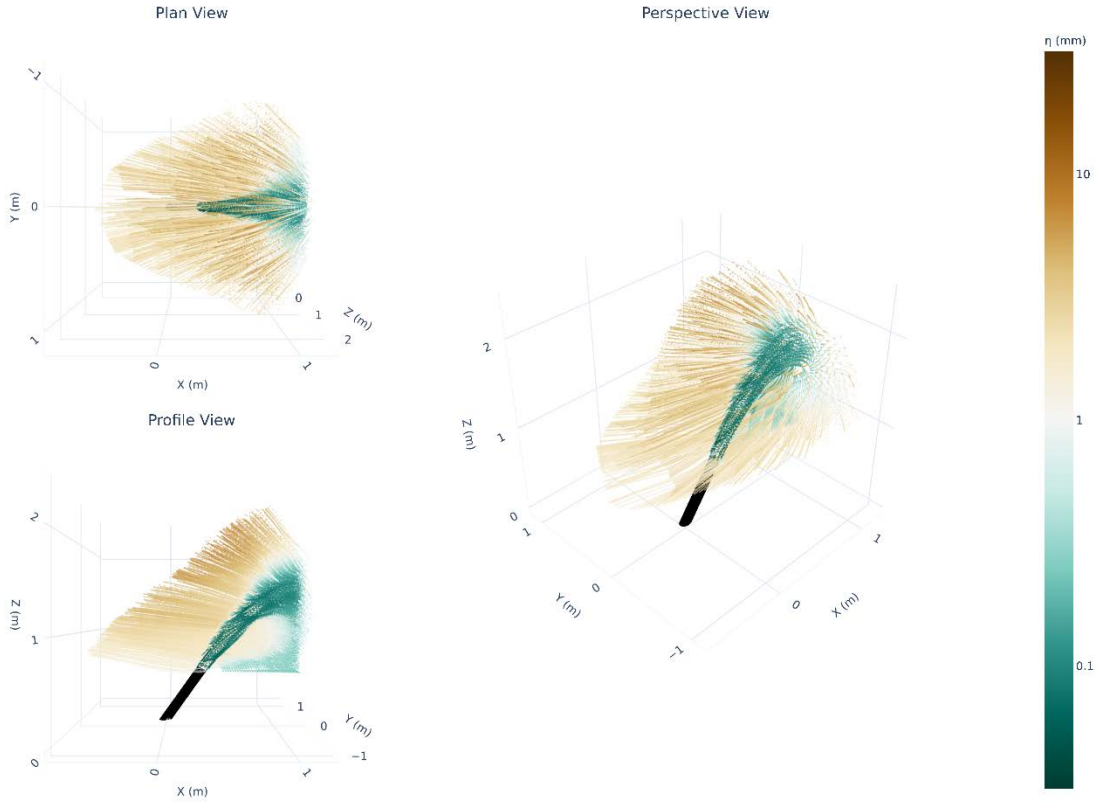

Figure 4-10. Three-dimensional streamlines up to the apex of the jet plume for Run 2 in plan view, profile view, and perspective view. Streamlines are colored by the value of η, with green shades indicating values less than 1 mm and brown shades indicating values greater than 1 mm. The port geometry is represented as a black cylinder.

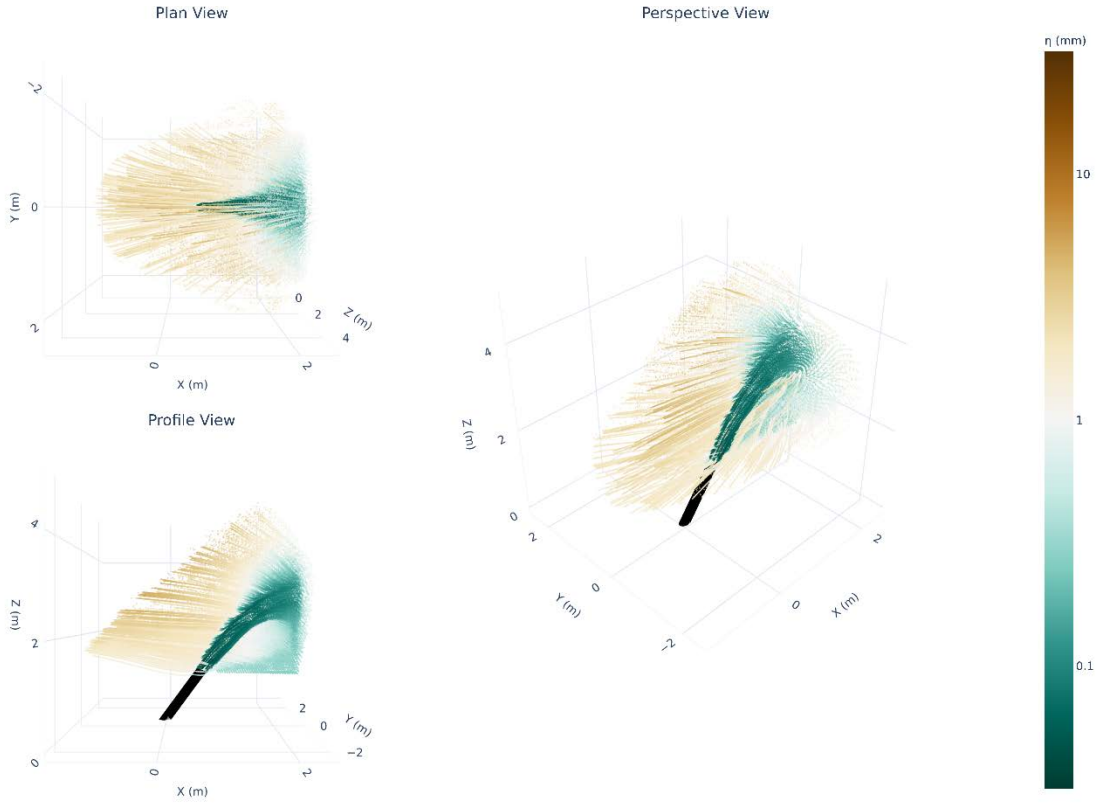

Figure 4-11. Three-dimensional streamlines up to the apex of the jet plume for Run 3 in plan view, profile view, and perspective view. Streamlines are colored by the value of η, with green shades indicating values less than 1 mm and brown shades indicating values greater than 1 mm. The port geometry is represented as a black cylinder.

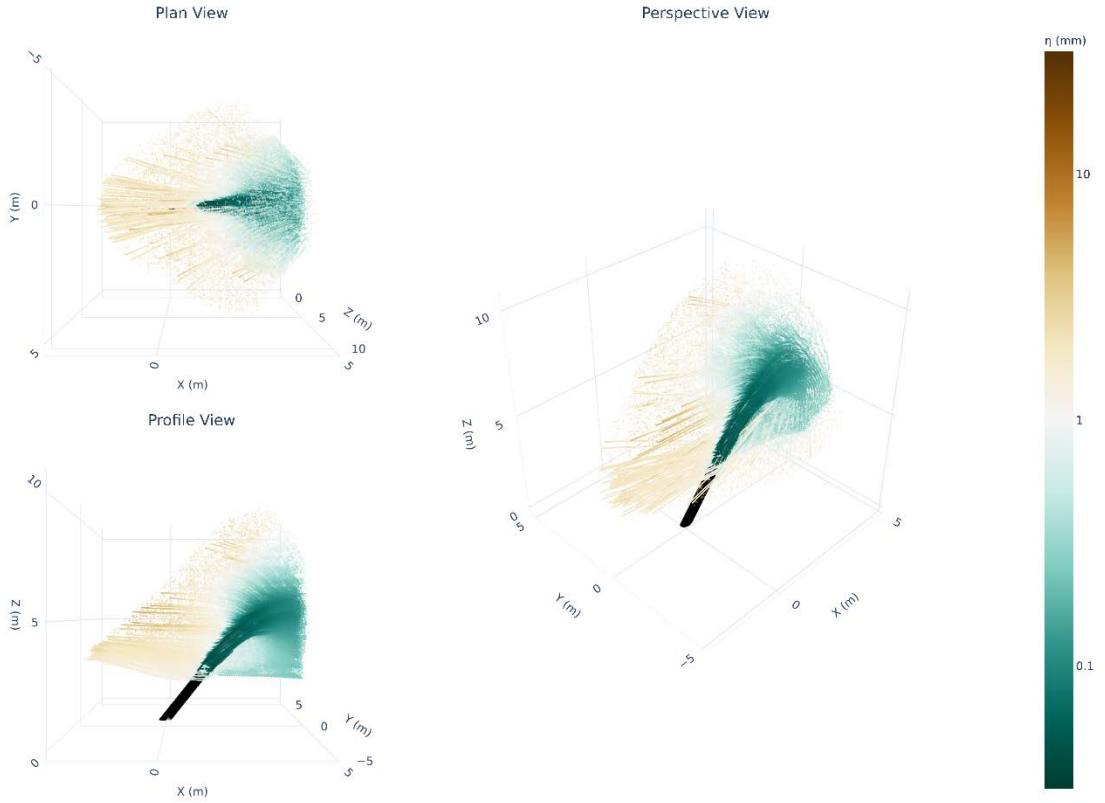

Figure 4-12. Three-dimensional streamlines up to the apex of the jet plume for Run 4 in plan view, profile view, and perspective view. Streamlines are colored by the value of η, with green shades indicating values less than 1 mm and brown shades indicating values greater than 1 mm. The port geometry is represented as a black cylinder.

Results for Runs 6 and 7 are presented in Figure 4-13 and Figure 4-14, respectively, and look substantially similar to each other and to Run 2. This is likely due to having relatively similar values of *Re* (i.e., differences less than a factor of two per Table 4-1).

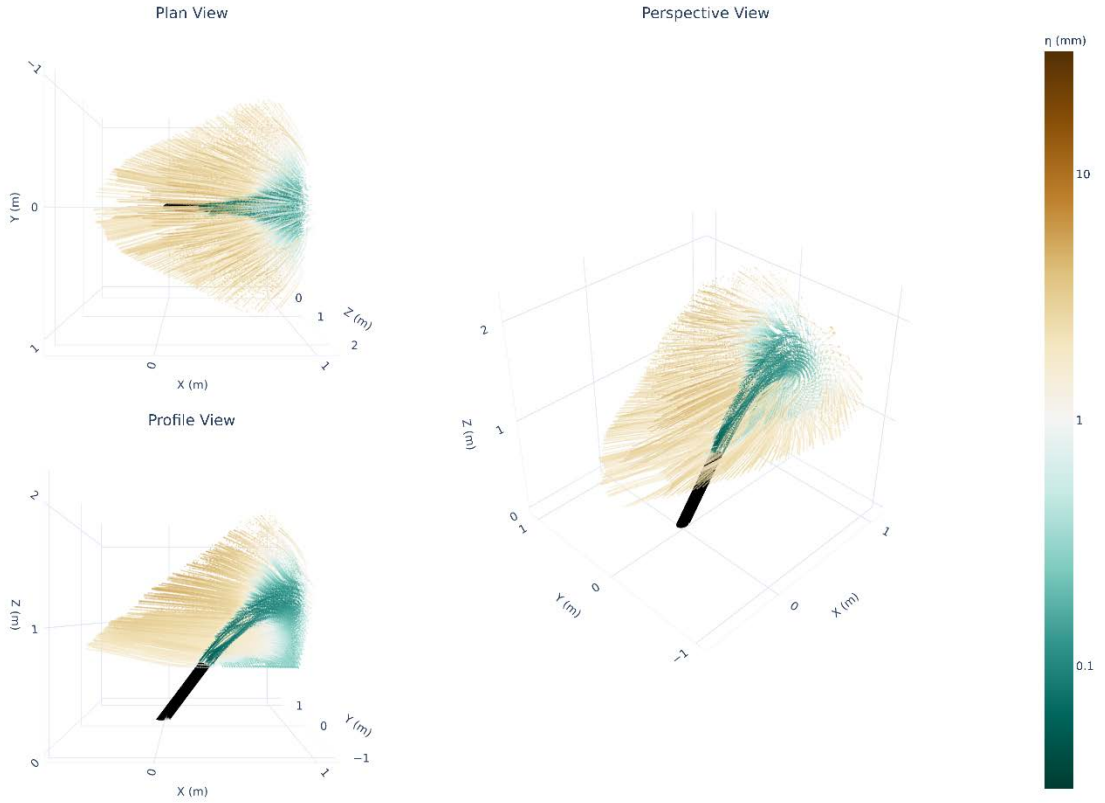

Figure 4-13. Three-dimensional streamlines up to the apex of the jet plume for Run 6 in plan view, profile view, and perspective view. Streamlines are colored by the value of η, with green shades indicating values less than 1 mm and brown shades indicating values greater than 1 mm. The port geometry is represented as a black cylinder.

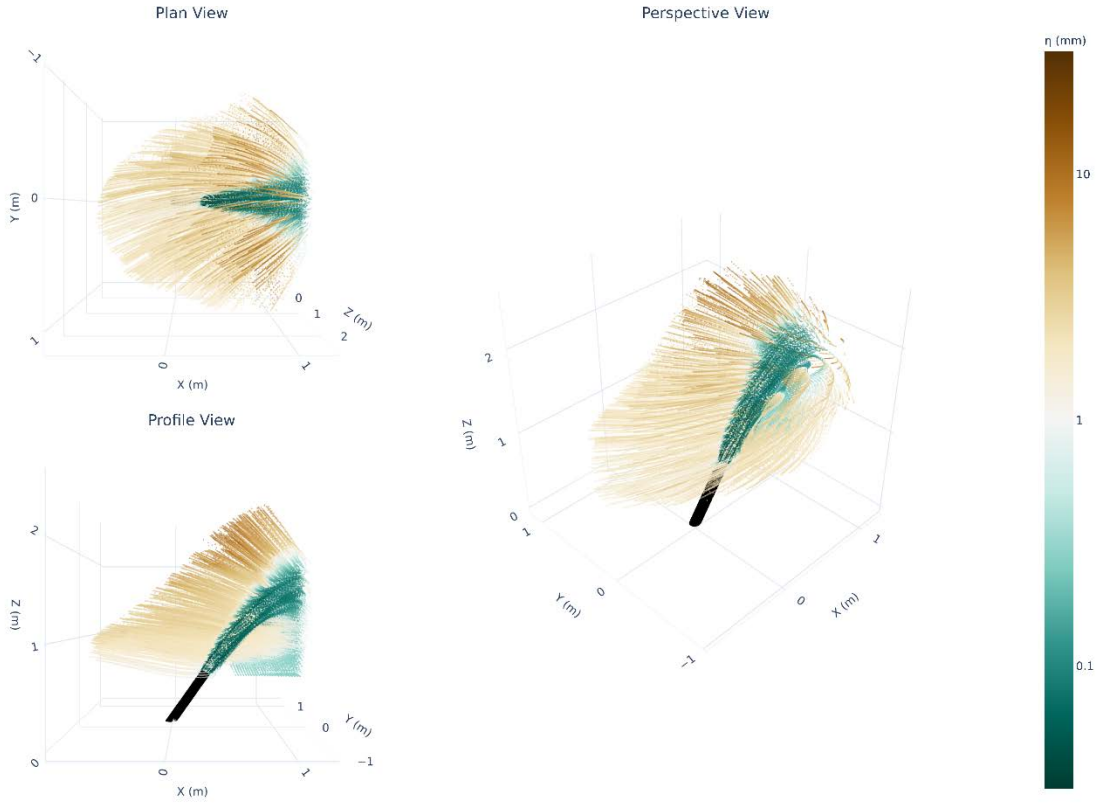

Figure 4-14. Three-dimensional streamlines up to the apex of the jet plume for Run 7 in plan view, profile view, and perspective view. Streamlines are colored by the value of η, with green shades indicating values less than 1 mm and brown shades indicating values greater than 1 mm. The port geometry is represented as a black cylinder.

Of critical interest is whether substantial portions within the jet plume (e.g., near the edges and/or near the apex) may have values of η that are greater than about 1 mm and, therefore, may be less damaging than estimated by the method of Roberts (2018). Close examination of the results indicate that η is less than 1 mm throughout the entire portion of the rising plume, confirming that the approach developed by Roberts (2018) to estimate η is reasonable.

The CFD results did not demonstrate values of η greater than 1 mm in any portion of the rising plume. However, there is a wealth of other turbulence information in the CFD results that may be useful to future additional studies. This information may include:

- Statistical summaries of the duration that organisms would be exposed to potentially damaging turbulence (e.g., Kolmogorov scales less than a critical value).
- Statistical summaries of dissipation thresholds and/or time integral of total dissipation.

- Estimates of entrainment velocities around the jet plume that may be used to evaluate the ability of motile organisms to avoid entrainment.
- Refined estimates of entrainment volumes.

4.5 Summary

A CFD model was developed to model negatively buoyant plumes at 60° vertical angles and used to evaluate turbulence quantities for a range of diffuser port sizes and variances in salinity relevant for California conditions. The goal of the modeling was to refine the estimates for turbulence intensity, and particularly the Kolmogorov scale, η, developed by Roberts (2018). It was anticipated that the turbulence in the rising portion of the jet plume would be moderated by the negative buoyancy, resulting in larger values of η than those estimated by Roberts (2018).

Key results from the CFD modeling for practically designed diffusers are:

- The estimate of Kolmogorov scale η developed by Roberts (2018) is appropriate for a neutrally buoyant jet, and the rising portion of a negatively buoyant jet plume.
- Negative buoyancy slightly moderates turbulence in the rising portion of the plume, resulting in larger values of η.
- This increase in η is relatively small, and values of η along the jet plume centerline up to the apex remain substantially less than 1 mm.
- The value of η throughout the entire rising portion of the plume is less than 1 mm:
    - This is consistent with the estimate developed by Roberts (2018).
    - Therefore, the use of the CFD results to refine the current estimates of η does not result in an increase in the size of η to above 1 mm.

5. DEVELOPMENT OF METHODOLOGY AND CASE STUDIES

The following sections provide discussion of the results presented in Chapters 2 and 4, and then develops a recommended approach for estimating mortality due to brine discharges based on scaling of existing methodology for open ocean intakes. The methodology is then illustrated through application to two case studies.

5.1 Estimating Mortality for Ocean Water Desalination

Entrainment and the subsequent mortality of small larval organisms associated with the operation of a desalination plant may occur both during the open ocean intake of seawater, and during discharge of brine back into the ocean. The estimation of the impact of entrainment resulting from an open ocean intake has been well described, modeled on entrainment impacts from power plant once-through cooling water intake structures (CWIS) (Boreman et al. 1981, Ehrler et al. 2002); however, the impact on larvae of being entrained into a turbulent jet plume emanating from the discharged brine has not been fully characterized. The purpose of the current study is to estimate the potential impact of entrainment of larval organisms into a plume associated with the discharge of brine, using computational fluid dynamics to describe turbulence intensity properties combined with a literature review of mortality of larval organisms subjected to turbulence intensities at the Kolmogorov length scale.

Impacts of entrainment are typically based on the fractional loss of a larval population (P_M), distributed over a certain source water area (A_{sw}) of the ocean, to arrive at a loss of adult population production, termed Area Production Foregone (APF). The estimation of P_M associated with the intake of seawater is commonly accomplished through Empirical Transport Modeling (ETM). It involves determining the number of larvae entrained as a fraction of the total number of larvae in a population. The total number of larvae in a population is characterized by the number of days a larval population is subjected to entrainment and the area over which the population would be distributed, given the strength of ocean currents, during those days (Appendix E of the Substitute Environmental Documentation for the California Ocean Plan Seawater Desalination provisions, SWRCB 2015). The calculation of P_M for an open ocean intake is straightforward because it rests on knowing the concentration of larvae in a certain volume of water to obtain total numbers of larvae (entrained and in the population). Mortality of the entrained fraction is assumed to be 100% given that larvae do not survive being entrained into a desalination plant where they would be subjected to water treatment.

There are three principal unknowns regarding the calculation of P_M for the discharge of brine from a diffuser. First is the volume of water that is entrained into the discharge

plume, second is the turbulence intensity that the entrained water is subjected to, and third is the vulnerability of the entrained organisms to a certain level of turbulence intensity. It is not known whether the turbulence intensities of the entrained water impact all larval size classes equally, and, of the size classes it impacts, whether it leads to 100% mortality of the organisms. Discussion of these unknowns are provided in the following sections. Based on the findings, recommendations for how to revise the estimation of P_M for brine discharge through use of scale factors is provided in Section 5.2.

5.1.1 Volume of Water Entrained into Jet Plume

The volume of water entrained by the jet plume that is potentially damaging to organisms is assumed to be the volume of water that is entrained up to the terminal rise height, as shown in Figure 2-1 (Roberts 2018). A recommendation for how to calculate this volume was described in Roberts (2018) and is used here in the revisions of the calculations of P_M. Briefly, the entrained volume (Q_e) can be calculated given the average dilution (S_{ta}) obtained from the UM3 model (Visual Plumes modeling suite) according to Roberts (2018) as:

$$Q_e = n(S_{ta} - 1)Q_j = (S_{ta} - 1)Q_T \qquad \text{Eq. 5-1}$$

where:

Qe = entrained volume up to the terminal rise height of jet
n = number of jet ports in the linear diffuser
S_{ta} = average dilution computed by UM3 at the terminal rise height
Q_j = the flow rate per jet
Q_T = the total flow rate of all jets combined

For example, the volume entrained by the West Basin Ocean Water Desalination Project (OWDP) 14 port linear diffuser, discharging approximately 25.4 million gallons per day (MGD) of brine, would be 116 MGD (Roberts 2019).

5.1.2 Turbulence Intensities of Water Entrained by Jet Plume

As described in Chapters 3 and 4, computational fluid dynamics (CFD) modeling was employed to characterize the turbulence intensities of the water entrained up to the terminal rise height. The CFD model was developed to determine whether turbulence intensities, particularly at the Kolmogorov length scale, were sufficient to result in damage to planktonic organisms. In general, calculated turbulence intensities were greatest, and therefore Kolmogorov length scales smallest, along the jet centerline. The

calculated Kolmogorov scale increased with distance from the jet port (i.e., point of exit of water, along the plume centerline up to the terminal rise height). For a typical diffuser design, however, the Kolmogorov length scale remained below 0.5 mm along the entire centerline distance up to the terminal rise height. Analysis of streamlines in the CFD model indicated that all water entrained into the rising portion of the plume was subject to turbulence intensities with Kolmogorov length scales < 0.5 mm (Figure 5-1). This confirms that the approach of Roberts (2018) is appropriate for estimating turbulence intensity in the rising portion of the jet plume. As a result, it is recommended that the entire volume of entrained water up to the terminal rise height be used, together with the concentration of organisms, to estimate the total number of organisms impacted by the discharge.

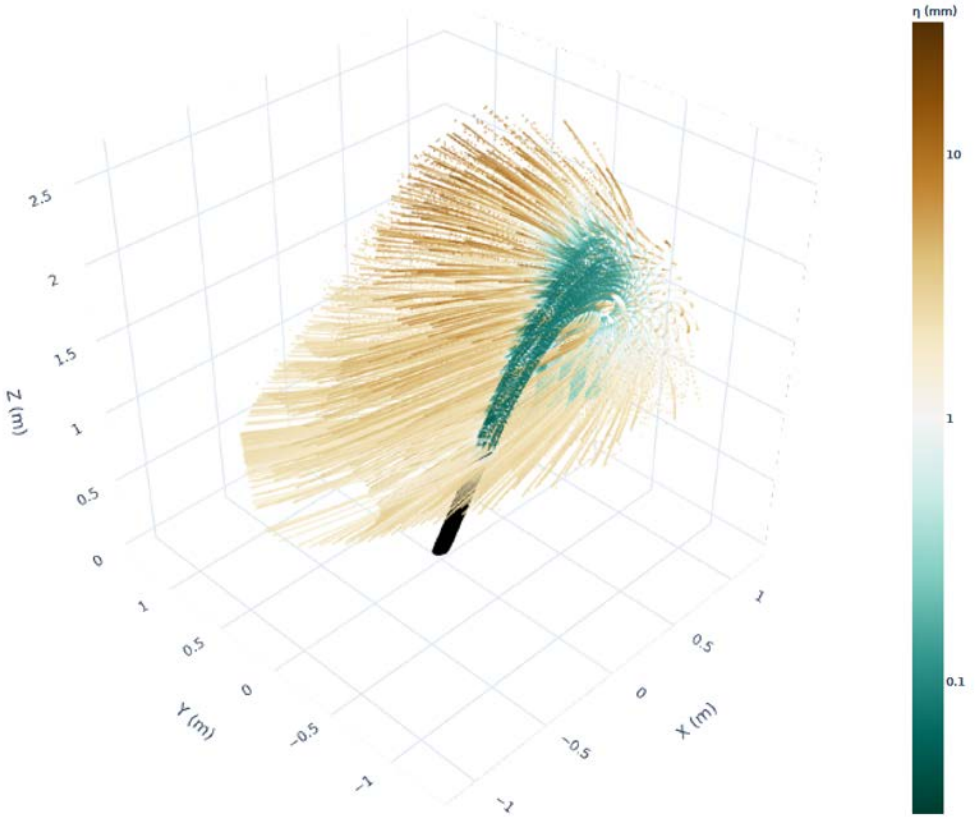

Figure 5-1. Streamlines from the CFD model illustrating the entrainment of water into the jet plume. Color scale indicates the Kolmogorov length scale, η, with brown tones having η > 1 mm and green tones having η < 1 mm. The Kolmogorov length scale decreases rapidly as the water is entrained into the jet and is below 0.5 mm throughout the rising portion of the jet. Results are presented here for a port diameter, d = 0.1 m, but are similar for other port diameters (see Chapter 3).

5.1.3 Turbulence Impact on Planktonic Species

As part of the literature review described in Chapter 2, more than 30 studies addressing the impacts of turbulence on planktonic organisms were initially identified. A subset of 11 studies characterized mortality of organisms as a function of turbulence energy dissipation rates, and 9 of these studies were used to develop statistical relationships as well as to calculate the Kolmogorov length scales that resulted in mortality (see Chapter 2). Three principal findings of the literature review were that: (1) mortality is greatest when the size of the organism is comparable to that of the smallest turbulent eddies, i.e., eddies at the Kolmogorov length scale; (2) mortality increases sharply above turbulence intensities corresponding to a Kolmogorov length scale < 0.5 mm; and (3) mortalities differ by taxonomic groupings, ranging from zero to a maximum of 70%. Key points from the literature review are summarized below, with more detailed information presented in Chapter 2.

5.1.3.1 Relationship Between Organism Size and Mortality

A number of the reviewed studies demonstrated that mortality of planktonic organisms is greatest when the length of the organism is comparable to the length of the Kolmogorov eddy scale. This is because when the size of the organism is similar to the size of the eddy, the organism may experience the greatest shear stresses resulting from flows at different speeds or in opposing directions across its body. For example, a bivalve caught between eddies rotating in opposite directions across its shell can result in the shell being pulled apart. The larger the organism size is compared with the size of Kolmogorov eddy, the smaller the impact of the eddy becomes.

5.1.3.2 Relationship Between Mortality and Kolmogorov Length Scale

Across all the planktonic organisms studied in this review, mortality due to turbulence increased above background mortalities when the Kolmogorov length scale was 0.5 mm and smaller. At Kolmogorov scales larger than 0.5 mm, mortalities were not distinguishable from background or control mortalities. This suggests that organisms with a length scale or diameter close to 0.5 mm would be impacted most in terms of mortality. However, even when organism size was close to the Kolmogorov eddy size (i.e., 0.5 to 2 times the Kolmogorov eddy size), it was not a given than an organism or taxonomic grouping would have a high mortality (Table 5-1).

Table 5-1. Larval mortalities by taxonomic group

Taxonomic Group	Approximate Size Range of Species in Group (µm)	Maximum Adjusted Mortality* (%)	Species Examined in Group
Bivalves	50–200	70	*Dreissena polymorpha* *Limnoperna fortunei* *Mytilus edulis*
Gastropods	~200	35	*Littorina littorea* *Aporrhais pespelicant* *Turitella communis* *Lamellaria perspicua*
Copepods	~1,000	24	*Acartia tonsa*
Barnacles	300–500	22	*Barnacle nauplii* *Cyprids*
Bryozoans	400–500	0.5	*Membranipora membranacea* *Electra pilosa*
Polychaetes	300–400	0.0	*Polychaete trochophores*
* Adjusted mortality is the incremental mortality due to turbulence above the background or control mortality rate.			

Some larvae, such as polychaete trochophores, had no mortality in response to turbulence regardless of intensity, suggesting that their carapace or coverings were not very sensitive to shear stresses and cross body flows. In contrast, larvae of freshwater bivalves were very sensitive to turbulence, with one study demonstrating maximum mortality of close to 70% of the population (Table 5-1).

5.1.3.3 Challenges and Application of Information from Literature Review

Two principal challenges were identified in terms of applying the information from the literature review to the assessment of environmental impacts for the discharge of brine into the ocean. One was that the studies in the literature review covered mainly freshwater larvae and, as such, were not representative of oceanic species. Moreover, species that are typically used for estimating the APF associated with intake (i.e., target species) include larvae of special status or commercially important fish and shellfish species (USEPA 1977, SWRCB 2015). Studies of turbulence impacts on such target species were not identified in this review.

A second challenge was that the reviewed mechanisms of generating turbulence did not include a jet stream, which is how the brine would be discharged into the ocean from a diffuser. The reason this may be important is that the mortality of organisms was found to vary depending on the mechanism used to generate the turbulence. For example, in one study with a Kolmogorov scale of ~0.19 mm, mortality varied by 50% depending on

whether the turbulence was generated by perforated plates versus wire grids (Figure 5-2A). In another study, the mortality varied several-fold depending on whether the paddles used to generate the turbulence had small holes, large holes, or no holes, even though the Kolmogorov length scale was constant at ~0.08 mm (Figure 5-2B). Results from these studies are counterintuitive because at the Kolmogorov scale, turbulence properties do not depend on how the turbulence is generated (i.e., they are isotropic) and therefore should give the same result in terms of mortalities. That this appears not to be the case in certain instances raises the possibility that part of organism mortality may be associated with damage from implements used to generate the turbulence rather than the turbulence itself. If so, this illustrates the importance of using a jet stream[30] to generate the turbulence to extrapolate results to what would happen with discharge of brine in the ocean.

Despite the two uncertainties described above, key information on the size spectrum of organisms most at risk for damage from turbulence was gained. Based on the literature review, it was demonstrated that mortality of small larval organisms increased sharply below a Kolmogorov length scale of 0.5 mm. Given that organisms suffer most damage when their size and diameter are similar to the Kolmogorov length scale, on the order of 1–2 for the ratio of length scales, it is recommended to focus attention on organisms smaller than 1 mm for estimating impacts. This 1 mm threshold is similar to a threshold arrived at when comparing the scales of turbulence produced naturally in the ocean by wind and waves versus to that produced by a jet stream (Roberts 2018). In the ocean, "background" turbulence produced by wind and waves typically manifests at Kolmogorov length scales greater than 1 mm (Walter et al. 2014). Turbulence associated with brine discharge will have length scales smaller and greater than 1 mm, but the turbulence that needs to be mitigated would be that which occurs at length scales less than 1 mm. This scale distinguishes the discharge-induced turbulence from natural, background turbulence and is also the scale that results in damage to organisms, based on the literature review.

[30] The turbulence in a brine diffuser discharge is caused by a free shear layer (i.e., fast-moving water next to slower moving water), and organisms would not be subject to impact from paddles or grids.

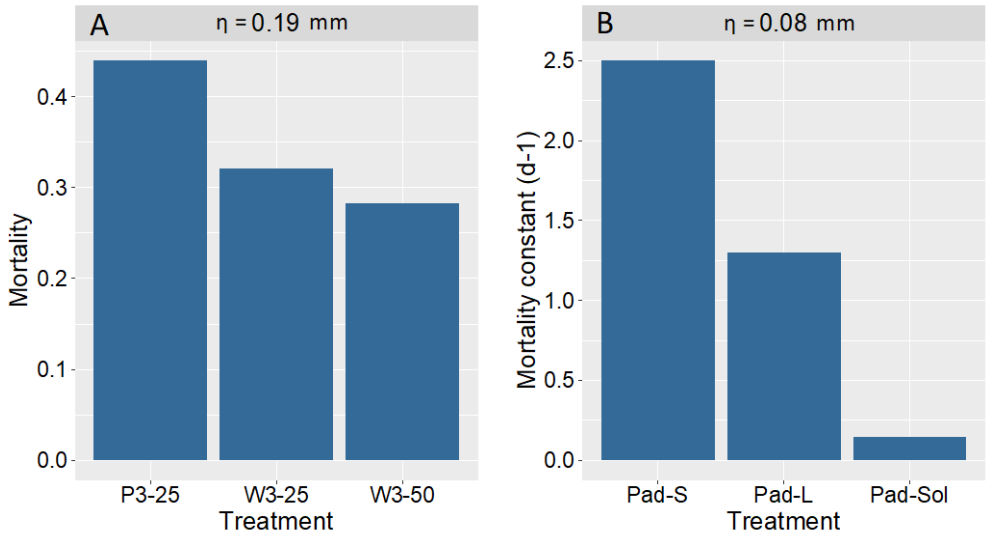

Figure 5-2. Dependence of mortality on turbulence generation mechanism. (A) Mortality fraction of golden mussels based on the use of perforated plates placed 25 cm apart (P3-25), wire grids spaced 25 cm (W3-25), or 50 cm (W3-50) apart in a tube at a Kolmogorov length scale (□) of 0.19 mm. Data from Zhang et al. (2017). (B) Mortality constant31 of zebra mussels measured using paddles with small holes (Pad-S), large holes (Pad-L), or no holes (Pad-Sol) at □=0.08 mm. Data based on Kozarek et al. (2018).

In summary, key elements gleaned from the literature review that can be applied to the estimation of damage to target planktonic larval species following exposure to turbulence include the following: (1) limiting the size of organisms to ≤ 1 mm, and (2) adjusting the mortality of organisms in this size spectrum to a level that is more comparable to turbulence conditions potentially present in a brine discharge plume. One such condition is a short period of exposure to turbulence. According to the data reviewed here, the maximum adjusted mortality in experiments where exposure was limited to less than 24 hours was ≤ 56% and ≤ 50% in a subset of the data where exposure was limited to 5 min or less. We recommend the use of a mortality level of 50% which is consistent with turbulence exposure durations below 5 min and does not include data from experiments where mortalities could potentially in part be due to mechanical damage. The recommended 50% mortality level could potentially be further refined in the future as more data become available on mortality levels generated using shorter turbulence exposure durations as well as data generated using target larval species.

[31] The mortality constant defines the rate at which the organisms die and is determined by fitting a first-order decay to the data.

5.2 Calculations of P_M and Scaling Factors

Following the literature review and CFD modeling, it is recommended that P_M for discharge is distinguished from the calculation of P_M for intake in the following manner:

1) Estimating the volume of water entrained by the jet plume up to the terminal rise height according to Eq. 5-1 above as described in Roberts (2018).
2) Limiting target species larvae that may sustain mortal damage following entrainment to the fraction of larvae ≤ 1 mm in size.
3) Adjusting the mortality of the ≤ 1 mm size target larvae to 50%, with the qualifier that further data are required to fully test this mortality threshold for target larvae used in P_M calculations.

The latter two points reflect the vulnerability of the larvae to damage by turbulence and will differ based on larval types. For example, limiting damage to the fraction that is ≤ 1 mm in size will require knowledge of larval sizes and will require a different factor to be applied to each group of larvae used for the P_M calculation (see Section 5.3 for examples). Based on their size range, some larvae are more vulnerable to damage when entrained than others. An example of a larva that is likely to escape damage due to turbulence when entrained is Silversides, which are typically 8 mm or longer in size (Tenera et al. 2008).

In addition, adjusting the mortality of the larvae from 100%, as for intake P_M calculations, to 50% reflects a lower vulnerability of larvae to damage by turbulence. However, as more data on turbulence-induced mortality become available with publication of future studies, varying mortalities could be applied for each target larval group used in the P_M calculation rather than a single mortality level across all groups.

Proportional mortality, P_M, calculated using ETM according to Appendix E of the Ocean Plan (SWRCB 2015), is principally a function of the proportion of larvae entrained (PE) and the proportion of the source water larvae (PS), as illustrated in Eq. 5-2 below:

$$P_M = 1 - \sum_{i=1}^{12} f_i (1 - PE \times P_S)^d \qquad \text{Eq. 5-2}$$

where:

f_i = the fraction of the total source water larval population present during any given monthly survey (i).

d = the estimated number of days of larval life for a given species.

PE = the proportion of larvae entrained, expressed as the fraction of larvae entrained over the source water larvae.

PS = the proportion of the source water larvae to the total larval population at risk of entrainment.

Because the central quantity of the P_M calculation reduces to the number of entrained larvae over the total larval population at risk of entrainment, any quantity that impacts the number of entrained larvae (such as concentration of larvae at the point of entrainment or the volume of water entrained) will directly impact P_M. As a result, P_M calculated for one project can easily be scaled by volume or larval fractions for subsequent projects in the same area. A comparison of P_M calculated using scaling factors with P_M calculated by changing target species concentrations and intake volumes is presented in Appendix B and demonstrates that simple scaling provides the same results.

5.2.1 Scaling Factors

Based upon the discussion above it is recommended that the following scaling factors be applied to the P_M calculated for an intake to obtain the P_M for a brine discharge:

- **F_V:** volume scaling factor = jet discharge entrainment volume as calculated according to Eq. 5-1 above (Roberts 2018) divided by the intake volume for which P_M has already been calculated[32].
- **F_S:** larval size scaling factor = abundance of target larval population $\leq$ 1 mm in size divided by the abundance of total target larval population. There would be a separate F_S for each type of larvae used in the P_M calculation, varying between 0 and 1. Calculation of this factor will require knowledge of larval sizes.
- **F_M:** larval mortality scaling factor = target larval population mortality limited to 50% based on results from Chapter 2, i.e., F_M = 0.5.

5.3 Case Studies

The methodology described above was applied to the West Basin OWDP and an alternative project to illustrate the approach.

[32] In the case where the P_M has been calculated for powerplant intake the powerplant intake volume should be used, and not the desalination plant intake volume.

5.3.1 Application to West Basin OWDP

Larval data (densities and sizes) for the West Basin OWDP were obtained from the Tenera and MBC (2008) 316(b) report prepared for the El Segundo Generating Station (ESGS) CWIS. Intake fractional larval population mortalities (P_M-in) published in this report were scaled with the three factors discussed above in Section 5.2.1, to generate two OWDP discharge fractional larval population mortalities (P_M-dis1 and P_M-dis2), as illustrated in Table 5-2.

For the OWDP, the two P_M-dis values calculated for comparison with the original, ESGS intake P_M (P_M-in) consisted of either applying only the F_V factor (i.e., P_M-dis1 = P_M-in × F_V), or applying all three factors (i.e., P_M-dis2 = P_M-in × F_V × F_S × F_M) (Table 5-2). As can be seen from P_M-in in Table 5-2, there is a loss from every larval population associated with the intake of seawater. In comparison, P_M-dis2 was zero for larger larvae (e.g., Combtooth blennies, CIQ gobies, Diamond turbot, Silversides, Queenfish, and English sole) and greatest for the smaller larvae such as Croakers and Sanddabs where 23% and 59%, respectively, of the population was ≤ 1 mm in size (Table 5-2).

Table 5-2. Scaling of original ESGS fractional larval mortalities for the intake (PM-in) by OWDP discharge entrainment volume (116 MGD) assuming 100% mortality of all target fish larval size classes (PM-dis1) and by using 50% mortality of the ≤ 1 mm size classes (PM-dis2). Target larval source water areas (ASW) are also noted. MGD=million gallons per day.

Target Larvae	**A_{SW}** (acres)	P_M-in	**F_V** (volume scaling factor)	**F_S** (size scaling factor)	**F_M** (mortality scaling factor)	P_M-dis1	P_M-dis2
Sea basses	30,305	5.00×10^{-3}	0.2985	0.07	0.5	1.49×10^{-3}	5.22×10^{-5}
Combtooth blennies	1,356	4.00×10^{-3}	0.2985	0	0.5	1.19×10^{-3}	0
CIQ goby complex	1,356	2.21×10^{-2}	0.2985	0	0.5	6.60×10^{-3}	0
Diamond turbot	1,356	3.09×10^{-2}	0.2985	0	0.5	9.23×10^{-3}	0
N. anchovies	292,775	2.20×10^{-3}	0.2985	0.01	0.5	6.57×10^{-4}	3.28×10^{-6}
Silversides	22,573	3.19×10^{-2}	0.2985	0	0.5	9.52×10^{-3}	0
White croaker	131,435	4.20×10^{-3}	0.2985	0.04	0.5	1.25×10^{-3}	2.51×10^{-5}
Queenfish	86,049	5.00×10^{-4}	0.2985	0	0.5	1.49×10^{-4}	0
Unid. croakers	52,114	6.80×10^{-3}	0.2985	0.23	0.5	2.03×10^{-3}	2.33×10^{-4}
Sanddabs	36,616	1.50×10^{-3}	0.2985	0.59	0.5	4.48×10^{-4}	1.32×10^{-4}
California halibut	65,246	2.40×10^{-3}	0.2985	0.025	0.5	7.17×10^{-4}	8.96×10^{-6}
English sole	55,964	1.10×10^{-3}	0.2985	0	0.5	3.28×10^{-4}	0

$F_V=OWDP_{entrain}/ESGS_{intake}=116$ MGD/398.6 MGD=0.2985
$F_S=Larvae_{<1mm}/Larvae_{ALL}$
$F_M=0.5$
P_M-dis1=P_M-in x F_V
P_M-dis2=P_M-in x F_V x F_S x F_M

5.3.2 Preliminary Application to an Alternative Project

A number of proposed desalination projects are in various stages of environmental review and permitting in California (e.g., Monterey Peninsula Water Supply Project, West Basin Ocean Desalination Project, Doheny Ocean Desalination Project[33], Huntington Beach Desalination Project). The Huntington Beach Desalination Plant (HBDP) Project, being developed by Poseidon Water, has obtained approval of its Environmental Impact Report (EIR) and is in the final stages of the project's permitting process. The HBDP Project, to be located in the vicinity of the Huntington Beach Generating Station (HBGS) at Huntington Beach in Orange County, has publicly available data on larval abundances and size distributions specific for their location that we used to estimate P_M values for brine discharge.

P_M values calculated previously (MBC and Tenera 2005) for the assessment of direct impacts of CWIS associated with HBGS were used to estimate scaled P_M values for the HBDP Project discharge (Table 5-3). The original HBGS P_M intake values (P_M-in) were modified by applying, discharge entrainment volume scaling factors (F_V), target species size fraction scaling factors (F_S), and a mortality factor (F_M) to generate discharge P_M values (Table 5-3). As with the example for the West Basin OWDP, two different discharge P_M values were calculated: the first by applying only the F_V factor (P_M-dis1), the second by applying all three factors (P_M-dis2). The target species size distributions used to generate each F_S were obtained from MBC and Tenera (2005). The P_M for sand crabs was generated by using zoea stage larval abundances, rather than the megalops stage typically used to estimate impacts, and applying alongshore distributions estimated for rock crabs (MBC and Tenera 2005). Similar to the example above for West Basin OWDP, P_M-dis2 was zero for the larger larvae and greatest for smaller larvae such as California halibut and sand crabs (Table 5-3).

[33] The Doheny Ocean Desalination Project would have a rising plume. The current methodology is developed based on a negatively buoyant (i.e., sinking) plume and would not be able to be applied directly to the Doheny Ocean Desalination Project. The method may be able to be adapted for rising plumes, but that is not within the current research scope.

Table 5-3. Scaling of original HBGS fractional larval mortalities for the intake (PM-in) by HBDP Project discharge entrainment volume (168 MGD) assuming 100% mortality of all target fish larval size classes (PM-dis1) and by using 50% mortality of the ≤ 1 mm size classes (PM-dis2). Target larval source water areas (ASW) are also noted. MGD=million gallons per day.

Target Larvae	**A_{SW} (acres)**	P_M-in	**F_V** (volume scaling factor)	**F_S** (size scaling factor)	**F_M** (mortality scaling factor)	P_M-dis1	P_M-dis2
Combtooth blennies	75,243	2.75×10^{-3}	0.2795	0	0.5	7.44×10^{-4}	0
CIQ goby complex	15,815	1.35×10^{-3}	0.2795	0	0.5	7.68×10^{-4}	0
Diamond turbot	20,880	1.01×10^{-3}	0.2795	0.17	0.5	2.83×10^{-4}	2.41×10^{-5}
Sand crabs	32,741	1.74×10^{-3}	0.2795	1.00	0.5	4.87×10^{-4}	2.43×10^{-4}
N. anchovies	88,958	2.25×10^{-3}	0.2795	0	0.5	6.28×10^{-4}	0
Spotfin croaker	20,880	5.21×10^{-4}	0.2795	0.11	0.5	1.46×10^{-4}	8.01×10^{-6}
White croaker	59,058	1.50×10^{-3}	0.2795	0.01	0.5	4.19×10^{-4}	2.09×10^{-6}
Queenfish	104,896	1.20×10^{-3}	0.2795	0	0.5	3.36×10^{-4}	0
California halibut	38,178	8.29×10^{-4}	0.2795	0.36	0.5	2.32×10^{-4}	4.17×10^{-5}

$F_V=HBDP_{entrain}/HBGS_{intake}=168$ MGD/601.1 MGD=0.2795
$F_S=Larvae_{<1mm}/Larvae_{ALL}$
$F_M=0.5$
P_M-dis1=P_M-in x F_V
P_M-dis2=P_M-in x F_V x F_S x F_M

5.3.3 Discharge APF Calculations

The P_M-dis2 values calculated using the three scaling factors described in Table 5-2 were used to revise the discharge APF (APF = $A_{sw} \times P_M$) for the West Basin OWDP. The discharge APF was calculated by scaling target fish larval population APFs according to their habitat dependence, followed by averaging of the APFs of target fishes with similar habitat requirements, and adding the different averaged habitat APFs, according to Raimondi (2011) as described in Appendix E of the Ocean Plan (SWRCB 2015). The fish larvae A_{SW} values used here are listed in Table 5-2. A comparison of the original APF for the (APF_{IN}) with the revised APF (APF_{DIS}) using the P_M-dis2 values is presented in Table 5-4. In a similar manner, P_M-dis2 values were used to calculate the APF_{DIS} for the HBDP Project (Table 5-4).

Table 5-4. Comparison of discharge APF using criteria for intake (APFIN) and new criteria for discharge (APFDIS) for the OWDP and the HBDP projects. MGD=million gallons per day.

Project	**Intake Volume** (MGD)	**Entrained Volume** (MGD)	**APF_{IN}** (acres)	**APF_{DIS}** (acres)
OWDP	41	116	47.5	1.6
HBDP	100	168	46.0	5.4

APF=A_{sw} x P_M
APF_{IN}=100% mortality of all entrained target species larval size classes
APF_{DIS}=50% mortality of ≤ 1 mm size entrained target larval species

5.4 Summary

A method for incorporating varying degrees of vulnerability of larval populations potentially entrained into a brine diffuser jet stream discharge was developed to aid calculations of larval population P_M values based on ETM. Key differences from seawater intake P_M calculations included:

- Using estimated volumes for entrainment into the rising portion of the discharge jet plume (i.e., up to the apex).
- Excluding larvae greater than 1 mm in size.
- Adjusting the mortality of the 1 mm and smaller larvae to 50% based on the available data for shorter duration turbulence exposures.

The method is applicable for negatively buoyant (i.e., sinking) discharges and was illustrated by applying it to the West Basin OWDP and the HBDP Project.

6. CONCLUSIONS

This project performed literature research and CFD calculations to develop a methodology to estimate mortality levels of small marine organisms from exposure to turbulence due to brine diffuser jet plume discharges from desalination projects. This was achieved by addressing each of the following three objectives;

1) Summarize the understanding of the relationship between turbulence characteristics and shear mortality of organism groups based on peer-reviewed literature,

2) Using CFD to improve the characterization of shear and turbulence properties in a negatively buoyant (i.e., sinking) brine discharge jet plume, and

3) Provide an approach for estimating larval population losses resulting from exposure to turbulence in a brine discharge plume.

The methodology developed is applicable for negatively buoyant (i.e., sinking) discharges and was illustrated by applying it to the West Basin OWDP and the HBDP Project.

The key findings pertaining to each of the above objectives are summarized in Section 6.1, with the key points in the developed methodology summarized in Section 6.1.3. Challenges and recommendations are provided in Section 6.2.

6.1 Key Findings

6.1.1 Objective 1: Relationship between discharge jet plume turbulence characteristics and shear mortality of organism groups

- Organism mortality is greatest when the size of the organism is comparable to that of the smallest turbulent eddies, i.e., eddies at the Kolmogorov length scale, η.

- Mortality increases sharply below Kolmogorov length scale of 0.5 mm for all taxonomic groups including copepods and larvae of bivalves, gastropods, bryozoans, polychaetes, and barnacles.

- Based on the available data, organism mortality increased from 9 to 70% with increasing energy dissipation rates that varied from 10^{-5} to 10^{-1} m^2/s^3.

- The maximum adjusted mortality of 70% was observed for mussel veligers exposed to intense turbulence for a duration of 24 hours. Mussel veliger mortality associated with experimental conditions where turbulence duration was more comparable to that expected to occur due to entrainment into a brine discharge plume was 56% and below.

- Experimental mortalities for exposure durations of less than 5 minutes were less than 50%.

6.1.2 Objective 2: Characterization of turbulence properties in a brine discharge jet plume

Microscale turbulence was characterized using computational fluid dynamics (CFD) modeling. Key insights from the CFD modeling for practically designed diffusers are that:

- The order of magnitude estimate of η developed by Roberts (2018) is appropriate for a neutrally buoyant jet and the rising portion of a negatively buoyant jet.

- Negative buoyancy moderates turbulence in the rising portion of the plume, resulting in larger values of η.

- This increase in η is relatively small, and values of η along the jet plume centerline up to the apex remain substantially less than 1 mm.

- The value of η throughout the entire rising portion of the plume is less than 1 mm.

6.1.3 Objective 3: Provide an approach for estimating larval population losses resulting from exposure to turbulence in brine discharge jet plume

The approach developed herein is based on applying scaling factors to the empirical transport modeling (ETM) method currently used to calculate mortality for seawater intakes. Key differences from the seawater intake calculations include scaling factors based upon:

- Using estimated volumes for entrainment into the rising portion of the discharge jet plume (i.e., up to the apex).

- Excluding larvae greater than 1 mm in size.

- Adjusting the mortality of the 1 mm and smaller larvae to 50% based on the available data for shorter duration turbulence exposures.

6.2 Challenges and Recommendations

Two principal challenges were identified in terms of applying the information from the literature review to the assessment of environmental impacts for the discharge of brine into the ocean. One was that the studies in the literature review covered mainly freshwater larvae and, as such, were not representative of oceanic species. Moreover, species typically used for estimating population losses (i.e., target species) such as larvae of special status or commercially important fish and shellfish species were not identified in this review.

The second challenge was that the mechanisms of generating turbulence in the literature were typically using grids or paddles. By contrast, the turbulence in a brine jet plume discharge is caused by the free shear layer at the edges of the jet stream. This distinction may be important as the mortality of organisms was found to partially vary depending on the mechanism used to generate the turbulence. In particular, it is likely that some of the mortality in the literature experiments may have been caused by mechanical damage due to physical contact with the grids or paddles.

For future experimental studies, it is recommended target species are used to test vulnerability of larvae to turbulence, and that turbulence is generated using a jet stream.

7. REFERENCES

Abessi O and Roberts PJW (2015) Effect of Nozzle Orientation on Dense Jets in Stagnant Environments. J Hydraulic Eng.

Abessi O and Roberts PJW (2015a) Dense Jet Discharges in Shallow Water. J Hydraulic Eng. 142(1).

Baum MJ and Gibbes B (2017) Improved Understanding of Dense Jet Dynamics to Guide Management of Desalination Outfalls. 22nd Int Congress on Modelling and Simulation, Hobart, Australia. December 2017.

Baum MJ and Gibbes B (2019) Field-scale Numerical Modeling of a Dense Multiport Diffuser Outfall in Crossflow. J Hydraulic Eng. 146(1).

Besalduch LA, Bada MG, Ferrari S, and Querzoli G (2013) Experimental Studies for the characterization of the mixing processes in negative buoyant jets. EPJ Web of Conferences 45, 01012. 2013.

Bickel SL, Malloy Hammond JD, and Tang KW (2011) Boat-generated turbulence as a potential source of mortality among copepods. J Exp Mar Biol 401: 105-109.

Boreman J, Goodyear CP, and Christensen SW (1981) An empirical methodology for estimating entrainment losses at power plants sited on estuaries. Trans Am Fish Soc 110: 253-260.

Cipollina A, Brucato A, Grisafi F, and Nicosia S (2005) Bench-scale investigation of inclined dense jets. J. of Hydraulic Eng., 131(11), pp 1017-1022.

Denny MW, Nelson EK, and Mead K (2002) Revised estimates of the effects of turbulence on fertilization in the purple sea urchin *Strongylocentrotus purpuratus*. Biol Bull 203: 275-277.

Ehrler CP, Steinbeck JR, Laman EA, Hedgepeth JB, Skalski JR, and Mayer DL (2002) A process for evaluating adverse environmental impacts by cooling-water system entrainment at a California power plant. The Scientific World JOURNAL 2(S1): 81-105.

Ferziger JH and Peric M (2002) Computational Methods for Fluid Dynamics, 3rd Edition. Springer, 2002.

Fischer HB, List EJ, Koh RCY, Imberger J, and Brooks NH (1979) Mixing in Inland and Coastal Waters. Academic Press. 1979.

Gaylord B and Gaines SD (2000) Temperature or transport? Range limits in marine species mediated solely by flow. Am Nat 155: 769-789.

Gaylord B, Hodin J, and Ferner MC (2013) Turbulent shear spurs settlement in larval sea urchins. PNAS 110: 6901-6906.

George R, Flick RE, Guza RT (1994) Observations of turbulence in the surf zone. J Geophys Res 99: 801-810.

Gildeh HK, Mohammadian A, and Nistor I (2014a) Numerical Modelling of Brine Discharges Using OpenFOAM. Proceedings of the Int Conf on New Trends in Transport Phenomena, Ottawa, Ontario, Canada. May 2014.

Gildeh HK, Mohammadian A, Nistor I, and Qiblawey H (2014b) Numerical modeling of 30° and 45° inclined dense turbulent jets in stationary ambient. Env Fluid Mech. July 2014.

Gildeh HK, Mohammadian A, Nistor I, Qiblawey H, and Yan X (2015) CFD modeling and analysis of the behavior of 30° and 45° inclined dense jets – new numerical insights. J Applied Water Eng and Research. October 2015.

Gopalakrishnan RN and Disimile PJ (2017) Effect of Turbulence Model in Numerical Simulation of Single Round Jet at Low Reynolds Number. Int J of Comp Eng Res, Volume 7(3), pp 29-44. March 2017.

Guadayol O, Peters F, Stiansen JE, Marrase C, and Lohrmann A (2009) Evaluation of oscillating grids and orbital shakers as means to generate isotropic and homogeneous small-scale turbulence in laboratory enclosures commonly used in plankton studies. Limnol Oceanogr: Methods 7: 287-303.

Haderlie E and Abbott D (1980) The Clams and Allies. In: R Morris, D Abbott, E Haderlie (eds). Intertidal Invertebrates of California. Stanford University Press, Stanford, California. Pp 355-411.

Horvath TG and Crane L (2010) Hydrodynamic forces affect larval zebra mussel (*Dreissena polymorpha*). Aquatic Invasions 5: 379-385.

Horvath TG and Lamberti GA (1999) Mortality of zebra mussel, Dreissena polymorpha, veligers during downstream transport. Freshwater Biology 42: 69-76.

Jessopp MJ (2007) The quick and the dead: larval mortality due to turbulent tidal transport. J Mar Biol Ass UK 87: 675-680.

Kaku VJ, Boufadel MC, and Venosa AD (2006) Evaluation of mixing energy in laboratory flasks used for dispersant effectiveness testing. J Envir Eng 132: 93-101.

Kikkert GA, Davidson MJ, and Nokes RI (2007) Inclined Negatively Buoyant Discharges. J Hydraulic Eng 133(5) pp 545 – 554.

Kozarek JL, Hondzo M, Kjelland ME, Piercy CD, and Swannack TM (2018) Effects of turbulence exposure on zebra mussel (*Dreissena polymorpha*) larval survival. Aquatic Sciences 80(12): https://doi.org/10.1007/s00027-017-0563-y.

Lai CCK and Lee JHW (2012) Mixing of inclined dense jets in stationary ambient. J Hydro-environ Res 6, pp 9 – 28.

Lazier JRN and Mann KH (1989) Turbulence and diffusive layers around small organisms. Deep-Sea Res 36: 1721-1733.

MBC Applied Environmental Sciences and Tenera Environmental (2005) AES Huntington Beach Generating Station Entrainment and Impingement Study Final Report. Prepared for AES Huntington Beach LLC and California Energy Commission, Sacramento, California. April 2005.

Mead KS and Denny MW (1995) The effects of hydrodynamic shear stress on fertilization and early development in the purple sea urchin, *Strongylocentrotus purpuratus*. Biol Bull 188: 46-56.

Morgan RP, Ulanowicz RE, Rasin VJ, Noe LA, and Gray GB (1976) Effect of shear on eggs and larvae of striped bass, *Morone saxatilis*, and white perch, *M. Americana*. Transactions of the American Fisheries Society 105: 149-154.

Nemlioglu S, and Roberts PJW (2006) Experiments on dense jets using three-dimensional laser-induced fluorescence (3DLIF). The 4th Int Conf on Marine Waste Water Disposal and Marine Env. Antalya, Turkey.

Oakey NS and Elliott JA (1982) Dissipation within the surface mixed layer. J Phys Oceanogr 12: 171-185.

Oliver CJ, Davidson MJ, and Nokes RI (2008) k-ε Predictions of the initial mixing of desalination discharges. Environ Fluid Mech, 8, pp 617-625. October 2008.

Oliver CJ, Davidson MJ, and Nokes RI (2013) Predicting the near-field mixing of desalination discharges in a stationary environment. Desalination 309, pp 148-155.

Palomar P, Losada IJ, and Lara JL (2015) PIV-PLIF experimental study of the spreading layer arisen from brine jet discharges. J Hydraulic Eng.

Peters F and Marrase (2000) Effects of turbulence on plankton: an overview of experimental evidence and some theoretical considerations. Mar Ecol Prog Ser 205: 291-306.

Prada AF, George AE, Stahlschmidt BJ, Chapman DC, and Tinoco RO (2020) Survival and drifting patterns of grass carp eggs and larvae in response to interactions with flow and sediment in a laboratory flume. PLoS ONE 13(12): https://doi.org/10.1371/journal.pone.0208326.

Raimondi P (2011) Variation in entrainment impact estimation based on different measures of acceptable uncertainty. California Energy Commission, PIER Energy-Related Environmental Research Program; CEC-500-2011-020.

Rehmann CR, Stoeckel JA, and Schneider DW (2003) Effect of turbulence on the mortality of zebra mussel veligers. Can J Zool 81: 1063-1069.

Roberts PJW (2018) Brine Diffusers and Shear Mortality. Final Report prepared for Eastern Research Group. April 18, 2018. https://www.waterboards.ca.gov/santaana/water_issues/programs/Wastewater/Poseidon/2018/4-18-18_HB_Analysis.pdf.

Roberts PJW (2019) Modeling Linear Diffusers for Brine Disposal from the West Basin Ocean Water Desalination Plant. Prepared for ESA Environmental Science Associates, San Francisco, California. May 10, 2019.

Roberts PJW, Ferrier A, and Daviero G (1997) Mixing in Inclined Dense Jets. J Hydraulic Eng. 123(8).

Robinson D, Wood M, Piggott M, and Gorman G (2016) CFD modelling of marine discharge mixing and dispersion. J Applied Water Eng and Research, 4:2, pp 152-162.

Seil G and Zhang Q (2010) CFD modeling of desalination plant brine discharges. Water. Pp 79 – 83, September 2010.

Sprung M (1989) Field and laboratory observations of *Dreissena polymorpha* larvae: abundance, growth, mortality, and food demands. Arch Hydrobiol 155: 537-561.

State Water Resources Control Board (SWRCB) (2015) California Ocean Plan, Water Quality Control Plan Ocean Waters of California. May 2015.

Tenera Environmental and MBC Applied Environmental Sciences (2008) El Segundo Generating Station Clean Water Act Section 316(b) Impingement Mortality and Entrainment Characterization Study. Prepared for El Segundo Power, LLC. January 2008.

Tennekes H and Lumley JL (1972) A First Course in Turbulence. The MIT Press, The Massachusetts Institute of Technology. 1972. ISBN 978-0-262-20019-6.

Terray EA et al. (1996) Estimates of kinetic energy dissipation under breaking waves. J Phys Oceanogr 26: 792-807.

United States Environmental Protection Agency (USEPA) (1977) Guidance for evaluating the adverse impact of cooling water intake structures on the aquatic environment: Section 316(b) P.L. 92-500, 58 p.

Vafeiadou P, Papakonstantis I, and Christodoulou G (2005) Numerical simulation of inclined negatively buoyant jets. Proc 9thInt Conf Environ Sci Tech. A, pp 1537-1542.

Walter RK, Squibb ME, Woodson CB, Koseff JR, and Monismith SG (2014) Stratified turbulence in the nearshore coastal ocean: dynamics and evolution in the presence of internal bores. JGR Oceans 119: 8709-8730.

Yan X, and Mohammadian A (2019) Numerical Modeling of Multiple Inclined Dense Jets Discharged from Moderately Spaced Ports. Water 2019, 11, 2077.

Zhang C, Xu M, Wang Z, Liu W, and Yu D (2017) Experimental study on the effect of turbulence in pipelines on the mortality of *Limnoperna fortunei* veligers. Ecological Engineering 109: 101-118.

Zhang S, Jiang B, Law AW, and Zhao B (2015) Large eddy simulations of 45° inclined dense jets. Environ Fluid Mech.

Zhang S, Law AW, and Jiang M (2017) Large eddy simulations of 45° and 60° inclined dense jets with bottom impact. J Hydro-environment Research 15: 54-66.

Zhu J, Han X, Qin B, Casenave C, and Yang (2016) Response of zooplankton community to turbulence in large, shallow Lake Taihu: a mesocosm experiment. Fundam Appl Limnol 187: 315-324.

Zirbel MJ, Veron F, and Latz MI (2002) The reversible effect of flow on the morphology of *Ceratocorys horrida* (Peridiniales, Dinophyta). J Phycol 36:46-58.

APPENDIX A

Dissipation Measurements and Estimates

Several of the references cited in this study did not provide a direct measurement nor calculation of the dissipation rate, ε, of the turbulent kinetic energy, and efforts were made to estimate or calculate them. These are briefly summarized here.

Table A-1 summarizes the experimental systems and sources of turbulence, and the dissipation measurement method (if applicable). Of the 11 studies, six directly calculated dissipation from measurements of turbulent velocity fluctuations using an acoustic Doppler velocimeter (ADV), micro-optical velocimeter (microV), or particle image velocimetry (PIV) techniques (Table A-1).

Of the remaining five studies, three use a Couette cell consisting of rotating cylinders that generate a shear flow and associated turbulence. Morgan et al. (1976) provided shear stress estimated within the cell but did not provide information to quantify turbulence. Additionally, while the cylinder diameters were provided, there is no information on the cylinder thickness so that the gap width could not be determined. It is possible that with additional information and sophisticated analyses (e.g., computational fluids dynamics simulations) that dissipation rates could be estimated, but this is beyond the scope of this study. Denny et al. (2002) determined the energy dissipation rate by measuring the rate of water temperature increase within a thermally insulated Couette cell (Table A-1). They pointed out that the previous work of Mead and Denny (1995) grossly underestimated the dissipation rate by assuming a laminar flow and using a simple molecular viscosity without accounting for the turbulent eddy viscosity.

Horvath and Lamberti (1999) did not provide an estimate for dissipation in their experiment conducted in a natural stream. Rehmann et al. (2003) used equations based on other fits to dissipations in streams assuming steady uniform flow to provide dissipation estimates for the Horvath and Lamberti (1999) study. However, turbulence conditions in the stream varied in both space and time, and it was difficult to estimate adjusted mortality from the information provided.

Horvath and Crane (2010) used 100 mL samples in 125 mL glass Erlenmeyer flasks to generate turbulence with an orbital shaker. Results were presented in terms of the rotation rate in revolutions per minute (rpm), rather than a direct measurement of turbulence. Specifically, results were provided for shaking at 100 rpm (f = 1.67 Hz) and 400 rpm (f = 6.67 Hz), where f is the shaker frequency. Additional literature research was conducted to determine methods to estimate dissipation for swirling flow in flasks.

Table A-1. Summary of methods used to measure or estimate dissipation for the references used in the current study.

Reference	Experimental System	Turbulence Source	Dissipation Measurement Method	Notes
Morgan et al. 1976	Couette cell	Opposing rotation of cylinders	N/A	Could not calculate dissipation. Only shear stress was provided.
Mead and Denny 1995	Couette cell	Opposing rotation of cylinders	See Denny et al. 2002	See Denny et al. 2002.
Horvath and Lamberti 1999	Natural stream	Stream flow	N/A	Estimated by Rehmann et al. 2003
Denny et al. 2002	Couette cell	Opposing rotation of cylinders	Measurement of increase in temperature of water in insulated cell	Rate of increase in water temperature was provided in W/m^3, that was converted to dissipation, ε, by dividing by density of water (ρ=1000 kg/m^3).
Rehmann et al. 2003	Glass beaker	Air flow	Measurement of turbulent velocity fluctuations (ADV) and correlation (R^2=0.995) with air flow rate	Paper provided $d^*$and d. Dissipation, ε, was estimated using Eqs. 2-1 and 2-2.
Jessopp 2007	Natural channel	Tidal flow	Measurement of turbulent velocity fluctuations (ADV)	
Horvath and Crane 2010	Glass flask	Orbital shaker	N/A	Estimated by correlation (R^2=0.94) with rotational frequency developed for current study
Bickel et al. 2011	Plexiglass container	Mixing paddle	Measurement of velocity fluctuations (ADV)	
Zhang et al. 2017	PVC pipe	Water flow through grid	Measurement of velocity fluctuations (ADV)	Paper provided $d^*$and d. Dissipation, ε, was estimated using Eqs. 2-1 and 2-2.
Kozarek et al. 2018	Plastic jar	Rotating paddles	Measurement of velocity fluctuations (microV)	
Prada et al. 2020	Plexiglass container	Vertically oscillating grid	Measurement of velocity fluctuations (PIV)	

Guadayol et al. (2009) developed relations for dissipation as a function of f, and optionally included other factors such as the orbital diameter and minor adjustments for different flask types. These relations were mostly based on experiments with flask sizes ranging from 1-L to 4-L, substantially larger than the flasks used by Horvath and Crane (2010). Guadayol et al. (2009) also cites and presents data points from Zirbel et al. (2002) and Kaku et al. (2006) that both use smaller flasks. These data were averaged and plotted in Figure A-1, together with a relation from Guadayol et al. (2009). The data points indicate a substantial departure at higher frequencies from the relationship that was developed for larger volume flasks.

A power relation was instead fitted to these data (Figure A-1) to better capture the relatively lower dissipation rates exhibited in the smaller flasks at the higher frequencies. This relation was used to estimate the dissipation rates for the experiments in Horvath and Crane (2010). This required extrapolation to a frequency of f = 6.67 Hz, and as such the results should be interpreted as an order of magnitude estimate, at best.

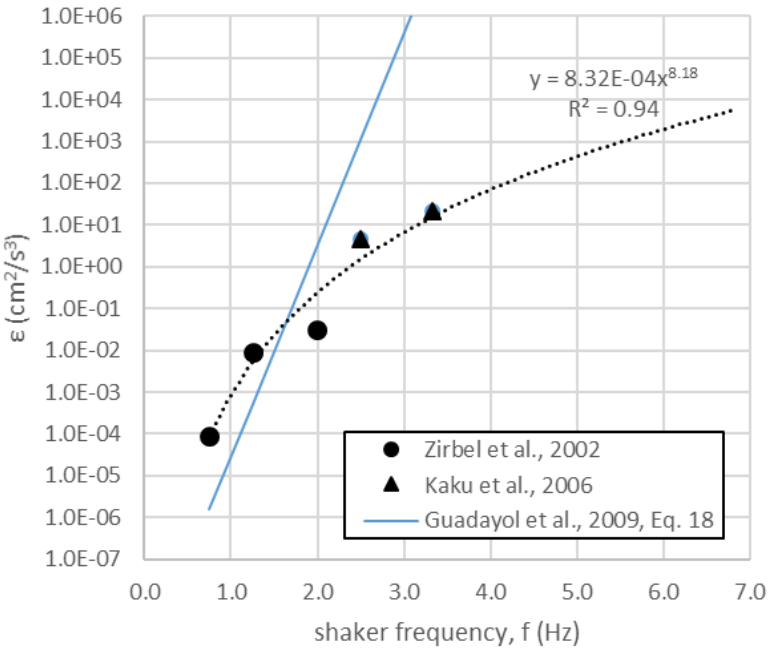

Figure A-1. Dissipation rate, ε, as a function of shaker frequency, f, for the experiments of Zirbel et al. (2002) and Kaku et al. (2006) and the relation developed by Guadayol et al. (2009) for larger volume flasks. A power relationship has been fitted to the data and is used for estimates in this study.

APPENDIX B
Comparison of P_M Values for Croaker Larvae

Scenario 1. Proportional mortality (P_M) of croaker larvae calculated from larval data collected by Tenera and MBC (2008) using the ESGS design intake volume of 398.6 MGD (1508864 m^3/d).

Survey Month	Vol_SW (m^3)	Vol_Intake (m^3/d)	Larvae_SW (Individuals/m^3)	Larvae_E (Individuals/m^3)	PE	Ps	fi	d	fi(1-PE*Ps)^d	P_M
Jan	735176994	1508864	1E-10pma	0	0	0.3904	0	9.7	0	0.00613217
Feb	735176994	1508864	0.00146365	0.02481608	0.03479803	0.3904	0.0016	9.7	0.001401194	
Mar	735176994	1508864	0.02738378	0.04657027	0.00349039	0.3904	0.04913	9.7	0.048484451	
Apr	735176994	1508864	0.03064786	0.04754125	0.00318368	0.3904	0.0458	9.7	0.045250802	
May	735176994	1508864	0.0147685	0	0	0.3904	0.01019	9.7	0.01019	
Jun	735176994	1508864	0.29276297	0.21254951	0.00149005	0.3904	0.36882	9.7	0.366744133	
Jul	735176994	1508864	0.14032054	0.08565693	0.00125285	0.3904	0.30586	9.7	0.304411962	
Aug	735176994	1508864	0.06883823	0.1125597	0.00335592	0.3904	0.07863	9.7	0.077636409	
Sep	735176994	1508864	0.02368634	0	0	0.3904	0.03088	9.7	0.03088	
Oct	735176994	1508864	0.00572678	0	0	0.3904	0.00347	9.7	0.00347	
Nov	735176994	1508864	0.02381797	0	0	0.3904	0.05443	9.7	0.05443	
Dec	735176994	1508864	0.03389204	0.01887347	0.00114291	0.3904	0.05119	9.7	0.050968876	

Scenario 2. Proportional mortality (P_M) of croaker larvae calculated from larval data collected by Tenera and MBC (2008) using the WB ODP discharge entrainment volume of 119 MGD (450464 m^3/d).

Survey Month	Vol_SW (m^3)	Vol_Intake (m^3/d)	Larvae_SW (Individuals/m^3)	Larvae_E (Individuals/m^3)	PE	Ps	fi	d	fi(1-PE*Ps)^d	P_M
Jan	735176994	450464	1E-10	0	0	0.3904	0	9.7	0	0.00183767
Feb	735176994	450464	0.00146365	0.02481608	0.01038878	0.3904	0.0016	9.7	0.001538153	
Mar	735176994	450464	0.02738378	0.04657027	0.00104204	0.3904	0.04913	9.7	0.048936472	
Apr	735176994	450464	0.03064786	0.04754125	0.00095047	0.3904	0.0458	9.7	0.045635417	
May	735176994	450464	0.0147685	0	0	0.3904	0.01019	9.7	0.01019	
Jun	735176994	450464	0.29276297	0.21254951	0.00044485	0.3904	0.36882	9.7	0.368199159	
Jul	735176994	450464	0.14032054	0.08565693	0.00037403	0.3904	0.30586	9.7	0.30542705	
Aug	735176994	450464	0.06883823	0.1125597	0.00100189	0.3904	0.07863	9.7	0.078332181	
Sep	735176994	450464	0.02368634	0	0	0.3904	0.03088	9.7	0.03088	
Oct	735176994	450464	0.00572678	0	0	0.3904	0.00347	9.7	0.00347	
Nov	735176994	450464	0.02381797	0	0	0.3904	0.05443	9.7	0.05443	
Dec	735176994	450464	0.03389204	0.01887347	0.00034121	0.3904	0.05119	9.7	0.051123895	

Scenario 3. Proportional mortality (P_M) of croaker larvae calculated from larval data collected by Tenera and MBC (2008) using the WB ODP discharge entrainment volume of 119 MGD (450464 m^3/d) and fraction of croaker larvae ≤ 1 mm in size (23% of larvae).

Survey Month	Vol_SW (m^3)	Vol_Intake (m^3/d)	Larvae_SW (Individuals/m^3)	Larvae_E (Individuals/m^3)	PE	Ps	fi	d	fi(1-PE*Ps)^d	P_M
Jan	735176994	450464	1E-10	0	0	0.3904	0	9.7	0	0.00042319
Feb	735176994	450464	0.00146365	0.0057077	0.00238942	0.3904	0.0016	9.7	0.001585581	
Mar	735176994	450464	0.02738378	0.01071116	0.00023967	0.3904	0.04913	9.7	0.049085428	
Apr	735176994	450464	0.03064786	0.01093449	0.00021861	0.3904	0.0458	9.7	0.045762099	
May	735176994	450464	0.0147685	0	0	0.3904	0.01019	9.7	0.01019	
Jun	735176994	450464	0.29276297	0.04888639	0.00010232	0.3904	0.36882	9.7	0.368677124	
Jul	735176994	450464	0.14032054	0.01970109	8.6027E-05	0.3904	0.30586	9.7	0.305760373	
Aug	735176994	450464	0.06883823	0.02588873	0.00023044	0.3904	0.07863	9.7	0.078561412	
Sep	735176994	450464	0.02368634	0	0	0.3904	0.03088	9.7	0.03088	
Oct	735176994	450464	0.00572678	0	0	0.3904	0.00347	9.7	0.00347	
Nov	735176994	450464	0.02381797	0	0	0.3904	0.05443	9.7	0.05443	
Dec	735176994	450464	0.03389204	0.0043409	7.8478E-05	0.3904	0.05119	9.7	0.051174789	

Scenario 4. Proportional mortality (P_M) of croaker larvae calculated from larval data collected by Tenera and MBC (2008) using the WB ODP discharge entrainment volume of 119 MGD (450464 m^3/d), fraction of croaker larvae ≤ 1 mm in size (23% of larvae), and 50% survival of the larvae (50% mortality).

Survey Month	Vol_SW (m^3)	Vol_Intake (m^3/d)	Larvae_SW (Individuals/m^3)	Larvae_E (Individuals/m^3)	PE	Ps	fi	d	fi(1-PE*Ps)^d	P_M
Jan	735176994	450464	1E-10	0	0	0.3904	0	9.7	0	0.00021164
Feb	735176994	450464	0.00146365	0.00285385	0.00119471	0.3904	0.0016	9.7	0.001592776	
Mar	735176994	450464	0.02738378	0.00535558	0.00011983	0.3904	0.04913	9.7	0.049107709	
Apr	735176994	450464	0.03064786	0.00546724	0.0001093	0.3904	0.0458	9.7	0.045781046	
May	735176994	450464	0.0147685	0	0	0.3904	0.01019	9.7	0.01019	
Jun	735176994	450464	0.29276297	0.02444319	5.1158E-05	0.3904	0.36882	9.7	0.368748556	
Jul	735176994	450464	0.14032054	0.00985055	4.3014E-05	0.3904	0.30586	9.7	0.305810183	
Aug	735176994	450464	0.06883823	0.01294437	0.00011522	0.3904	0.07863	9.7	0.078595699	
Sep	735176994	450464	0.02368634	0	0	0.3904	0.03088	9.7	0.03088	
Oct	735176994	450464	0.00572678	0	0	0.3904	0.00347	9.7	0.00347	
Nov	735176994	450464	0.02381797	0	0	0.3904	0.05443	9.7	0.05443	
Dec	735176994	450464	0.03389204	0.00217045	3.9239E-05	0.3904	0.05119	9.7	0.051182394	

Column Headings:
Vol_SW=Source water volume (m^3)
Vol_Intake=entrained volume (m^3/d)
Larvae_E= Entrainment station larvae (Individuals/m^3)
Larvae_SW= Source water larvae (individuals/m^3)
PE=Proportion of source water larvae entrained by intake
Ps=Proportion of total larval population in source water
fi=fraction available to be entrained in given survey month
d=days in larval stage
fi(1-PE*Ps)^d=fraction of larvae escaping entrainment
P_M=larval population mortality constant

Comparison of proportional mortality (P_M) of croaker larvae calculated in scenarios 2-4 above based on ETM (P_M -ETM) with P_M calculated by applying scaling factors to ESGS intake P_M values (P_M -Scaling).

Scenario	P_M - ESGS Intake	Scaling Factors	P_M - ETM	P_M - Scaling
2		Fv=0.2985	0.001838	0.001831
	0.00613217			
3		Fv=0.2985	0.0004232	0.0004211
		Fs=0.23		
	0.00613217			
4		Fv=0.2985	0.0002116	0.0002105
		Fs=0.23		
	0.00613217	Fm=0.50		

Attachment B

Cost Information

West Basin has submitted to MWD all invoice packages for the work performed between January 23, 2020, through October 31, 2021. Overall, the Study is within the established budget. The following table outlines the cost incurred during this period, the total amount awarded, and the cost breakdown per funding agency.

Table 1 – Share Cost

Cost Category		Total Award Updated Amount	Sharing Cost		Total Cost Paid to Date (01/23/20 – 10/31/21)	Cost To date Breakdown	
			Non-MWD Share	MWD Funding Share Awarded		West Basin and USBR	MWD Reimbursable cost
1	PM and Meetings	$70,902	$73,899	$40,985	$73,899	$33,040	$40,858
2	Literature Review of Mortality	$43,349	$46,901	$18,583	$46,901	$28,318	$18,583
3	CFD Simulations	$182,523	$190,944	$98,129	$190,944	$93,547	$97,397
4	Case Study: West Basin and Alternative Project	$54,760	$21,616	$11,730	$21,616	$11,413	$10,203.00
5	Reporting	$41,258	$30,886	$20,573	$30,886	$15,938	$14,948
Grand Total		**$392,792**	**$202,792**	**$190,000**	**$364,246**	**$182,256**	**$181,990**

Schedule Information

Table 2 presents a detailed and updated Study schedule, anticipated completion date, and status for each Task completed to date. Reporting schedule from Task 5 has been revised based upon the current Study progressive schedule. Extensive effort in reviewing additional data for Task 4.2 and 4.3 was conducted. This effort is reflected in the time it took to complete each Task. A Draft Final Report was submitted to MWD on October 9, 2021. Due to these updates, the Final Report is submitted to MWD on December 21, 2021. Results of the Study and conclusions have been scheduled to be presented to MWD during the CalDesal Conference, which will be held in February 2022.

Table 2 – Schedule Information Table

Task	Description	Anticipated Completion Date	Updated Dates	Status
1.	*Project Management and Meetings*			
1.1	Preparation and Kick-off meeting	February 10, 2020	February 10, 2020	Complete
1.2	Conference calls	October 15, 2021	October 15, 2021	Complete
1.3	General coordinating and QA/QC	September 15, 2021	March 15, 2022	On-going
1.4	Progress update and invoices**	October 30, 2021	May 30, 2022	On-going
2.	*Literature Review of Mortality Studies*			
2.1	Literature Search	March 12, 2020	March 12, 2020	Complete
2.2	Literature review	May 21, 2020	May 21, 2020	Complete
2.3	Draft Summary Memorandum**	July 30, 2020	July 30, 2020	Complete
3.	*CFD Simulations*			
3.1	Develop CFD simulation and validate	August 31, 2020	August 31, 2020	Complete
3.2	Draft Validation Report**	October 30, 2020	October 30, 2020	Complete
3.3	CFD Simulations	November 30, 2020	November 30, 2020	Complete
3.4	Parameterization of simulations	February 18, 2021	February 18, 2021	Complete
3.5	Draft CFD Results Report**	March 22, 2021	March 22, 2021	Complete
3.6	Develop revised Calculation methodology	May 20, 2021	May 20, 2021	Complete
4.	*Case Studies: Ocean Water Desalination and Alternative Projects*			
4.1	Apply methodology to Ocean Water Desalination	May 31, 2021	May 31, 2021	Complete
4.2	Calculation package**	June 15, 2021	June 22, 2021	Complete
4.3	Preliminary application to alternative project	May 31, 2021	August 23, 2021	Complete
5.	*Reporting*			
5.1	Draft Final Report**	June 30, 2021	October 9, 2021	Complete
5.2	Final Report**	August 31, 2021	December 20, 2021	Complete
5.3	Seminar/Webinar** [1]	September 30, 2021	February 10, 2022	In Progress

**Deliverables to be submitted to MWD

[1] Study results have been scheduled to be presented at the 2022 CalDesal conference.